Ocean Mesoscale and Frontal-scale Ocean-Atmosphere Interactions and Influence on Large-scale Climate: A Review

US CLIVAR Ocean Mesoscale Air-Sea Interaction Working Group

Hyodae Seo* (Woods Hole Oceanographic Institution, Woods Hole, MA, USA)
Larry W. O'Neill (Oregon State University, Corvallis, OR, USA)
Mark A. Bourassa (Florida State University, Tallahassee, FL, USA)
Arnaud Czaja (Imperial College London, London, United Kingdom)
Kyla Drushka (Applied Physics Laboratory, University of Washington, Seattle, WA, USA)
James B. Edson (Woods Hole Oceanographic Institution, Woods Hole, MA, USA)
Baylor Fox-Kemper (Brown University, Providence, RI, USA)
Ivy Frenger (GEOMAR Helmholtz Centre for Ocean Research Kiel, Germany)
Sarah T. Gille (Scripps Institution of Oceanography, University of California San Diego, La Jolla, CA, USA)
Benjamin P. Kirtman (University of Miami, Miami, FL, USA)
Shoshiro Minobe (Hokkaido University, Sapporo, Japan)
Angeline G. Pendergrass (Cornell University, Ithaca, NY, USA)
Lionel Renault (LEGOS, Université de Toulouse, CNES-CNRS-IRD-UPS, Toulouse, France)
Malcolm J. Roberts (Met Office Hadley Centre, Exeter, United Kingdom)
Niklas Schneider (University of Hawai'i at Manoa, Honolulu, HI, USA)
R. Justin Small (National Center for Atmospheric Research, Boulder, CO, USA)
Ad Stoffelen (Royal Netherlands Meteorological Institute, Utrecht, the Netherlands)
Qing Wang (Naval Postgraduate School, Monterey, CA, USA)

Revision submitted on July 12, 2022

*Corresponding author: Hyodae Seo (hseo@whoi.edu)

Abstract

Two decades of high-resolution satellite observations and climate modeling studies have indicated strong ocean-atmosphere coupled feedback mediated by ocean mesoscale processes, including semi-permanent and meandrous SST fronts, mesoscale eddies, and filaments. The air-sea exchanges in latent heat, sensible heat, momentum, and carbon dioxide associated with this so-called mesoscale air-sea interaction are robust near the major western boundary currents, Southern Ocean fronts, and equatorial and coastal upwelling zones, but they are also ubiquitous over the global oceans wherever ocean mesoscale processes are active. Current theories, informed by rapidly advancing observational and modeling capabilities, have established the importance of mesoscale and frontal-scale air-sea interaction processes for understanding large-scale ocean circulation, biogeochemistry, and weather and climate variability. However, numerous challenges remain to accurately diagnose, observe, and simulate mesoscale air-sea interaction to quantify its impacts on large-scale processes. This article provides a comprehensive review of key aspects pertinent to mesoscale air-sea interaction, synthesizes current understanding with remaining gaps and uncertainties, and provides recommendations on theoretical, observational, and modeling strategies for future air-sea interaction research.

Significance Statement

Recent high-resolution satellite observations and climate models have shown a significant impact of coupled ocean-atmosphere interactions mediated by small-scale (mesoscale) ocean processes, including ocean eddies and fronts, on Earth's climate. Ocean mesoscale-induced spatial temperature and current variability modulate the air-sea exchanges in heat, momentum, and mass (e.g., gases such as water vapor and carbon dioxide), altering coupled boundary layer processes. Studies suggest that skillful simulations and predictions of ocean circulation, biogeochemistry, and weather events and climate variability depend on accurate representation of the eddy-mediated air-sea interaction. However, numerous challenges remain in accurately diagnosing, observing, and simulating mesoscale air-sea interaction to quantify its large-scale impacts. This article synthesizes the latest understanding of mesoscale air-sea interaction, identifies remaining gaps and uncertainties, and provides recommendations on strategies for future ocean-weather-climate research.

1. Introduction

Decades of observational and modeling analysis have broadly identified two fundamental regimes of ocean-atmosphere coupling dependent on the spatial scale of ocean surface variability. The first regime involves the ocean response to large-scale (>1000 km) internal atmospheric variability, which drives a response in sea surface temperature (SST) through the mediation of surface turbulent heat fluxes and upper-ocean turbulent mixing (e.g., Frankignoul et al. 1985; Alexander and Scott 1997). The large-scale ocean response feeds back onto the incipient atmospheric circulation anomaly to reinforce or erode it (e.g., Bladé 1997). In this framework, the ocean is viewed as relatively passive, mainly advecting anomalies, storing heat, and integrating white noise atmospheric forcing.

The second regime, the focus of this paper, involves an atmospheric response driven by ocean mesoscale eddy-induced spatial SST and current variability. Here, the term "mesoscale eddies and fronts" broadly refers to all forms of oceanic processes with horizontal length-scales smaller than the first regime of air-sea interaction (>1000 km) but larger than oceanic submesoscale (~1-10 km). These processes include coherent, swirling, and transient ocean circulations with length-scales near the Rossby radius of deformation (Chelton et al. 2011), filamentary eddy structures that are widely observed in coastal upwelling systems, and semi-permanent fronts and undulations near the midlatitude western boundary currents (WBCs) and their extensions, and SST fronts along the equatorial tongue in the Pacific and Atlantic oceans.

The SST signature from these ocean mesoscale processes modifies surface turbulent heat and momentum fluxes, driving local responses in marine atmospheric boundary layer (MABL) processes (Small et al. 2008), inducing responses in winds, clouds, and rainfall (e.g., Deser et al. 1993; Tokinaga et al. 2009; Frenger et al. 2013; Miyamoto et al. 2018; 2022; Takahashi et al. 2020, 2021). The MABL responses then drive non-local responses in the path and activity of storm tracks in the extratropics (e.g., Czaja et al. 2019) and deep moist convection in the tropics (e.g., Li and Carbone 2012; Skyllingstad et al. 2019; de Szoeke and Maloney 2020). The atmospheric response to ocean mesoscales feeds back onto eddy activity and SST, altering the large-scale ocean circulation, further influencing these atmospheric processes (e.g., Nakamura et al. 2008; Hogg et al. 2009; Frankignoul et al. 2011; Taguchi et al. 2012). Mesoscale ocean

107 surface currents also affect the wind stress and heat fluxes as well as the kinematic profiles in the
108 MABL, which influence ocean circulation, including the stability and strength of the WBCs and
109 their meanders (Renault et al. 2016b, 2019b) and the basin-scale coupled climate variability such
110 as ENSO (e.g., Luo et al. 2005). The ocean drives the SST variability more strongly than the
111 atmosphere at longer time-scales and shorter spatial-scales (Bishop et al. 2017), suggesting the
112 need to include rectified coupled effects of ocean mesoscale eddies in high-resolution coupled
113 climate model simulations (e.g., Bryan et al. 2010; Kirtman et al. 2012; Roberts et al. 2016;
114 Hewitt et al. 2020).
115
116 Aside from earlier limited observational studies showing evidence of the MABL response to
117 mesoscale SSTs (e.g., Sweet et al. 1981), the first observational global-scale surveys of the
118 MABL and surface wind responses based on satellite observations were provided by Chelton et
119 al. (2004) and Xie (2004), followed by comprehensive review papers by Small et al. (2008) and
120 Kelly et al. (2010). The number of publications that include aspects of mesoscale air-sea
121 interaction has grown exponentially in the last decade or so (see Robinson et al. 2018, 2020),
122 which also emphasizes a strong cross-disciplinary nature of the research subject (e.g., AMS
123 Special Collection on *Climate Implications of Frontal Scale Air-Sea Interaction*, and the *J.*
124 *Oceanography* Special Collection on "Hot Spots" in the climate system, Nakamura et al. 2015).
125 Notwithstanding the existing review papers, no comprehensive synthesis papers exist that
126 consolidate the exponential increase in scientific understanding of mesoscale air-sea interaction.
127 This forms the key motivation of this review, which mainly focuses on a synthesis of the studies
128 since Small et al. (2008).
129
130 The paper is organized in the following logical order. Section 2 discusses the air-sea flux
131 responses to mesoscale SST and surface currents, along with theories and analytical studies of
132 MABL dynamics describing the flux responses. The subsequent two sections review critical
133 aspects of large-scale atmospheric and ocean circulation responses resulting from the
134 atmospheric boundary layer processes. That is, Section 3 discusses the tropospheric responses
135 emphasizing the modulation of local and downstream adjustments of extratropical weather
136 systems and their aspects related to climate change. Section 4 probes into the oceanic responses
137 due to thermal and mechanical feedback processes. The chapter emphasizes the need to develop

new theories and parameterizations to account for rectified effects of eddy-atmosphere interaction. Section 5 explores the emerging observational platforms critical for accurate in situ and remote-sensing characterization of air-sea interaction at small spatial scales in the coming decade. Section 6 provides a summary and synthesis.

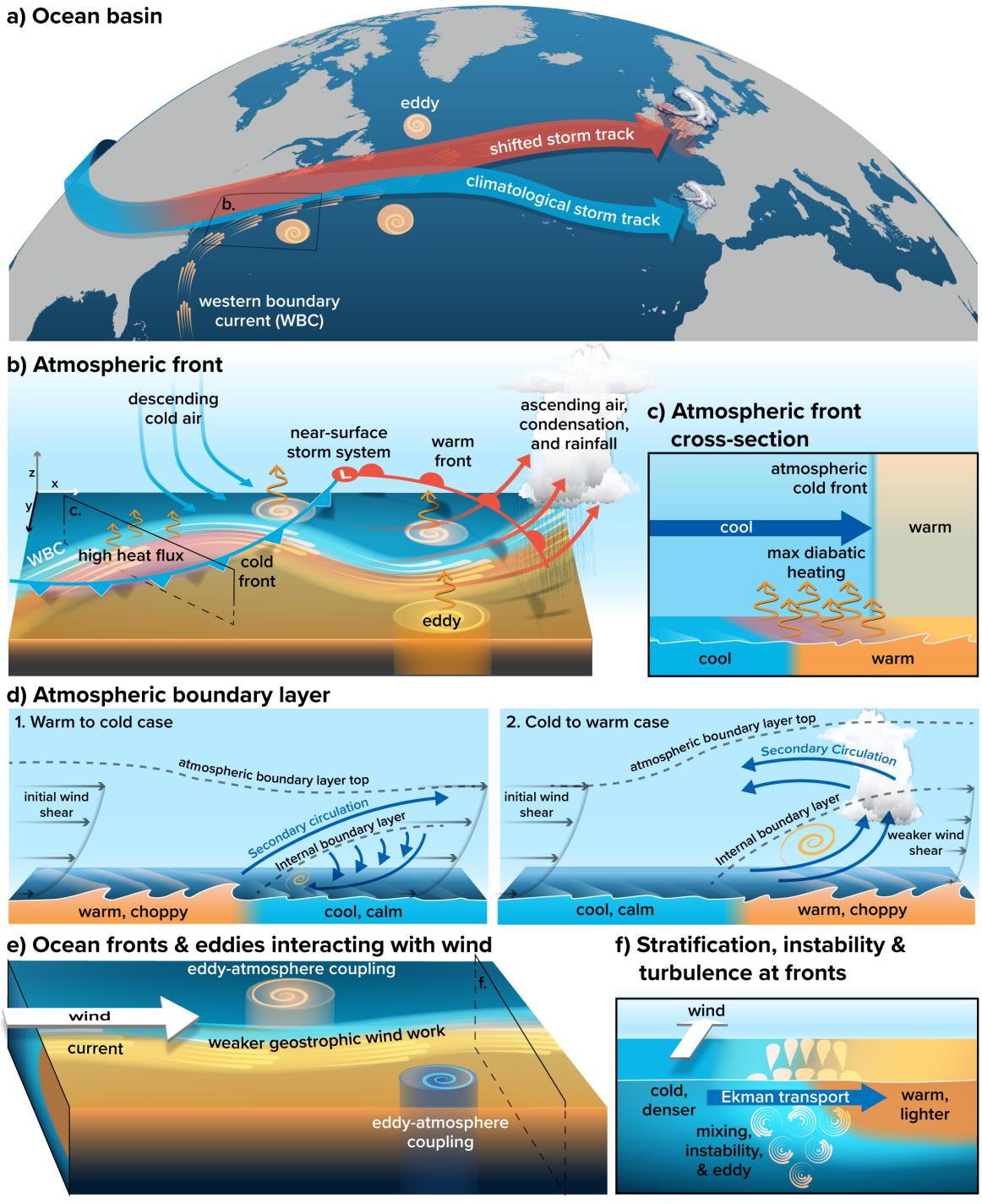

Figure 1: Schematic illustrations of the coupled ocean-atmosphere feedback processes in the Northern Hemisphere. (a) On the basin scale, the storm track affected by the WBCs leads to anomalous rainfall patterns downstream. (b) A zoom-in view over the black box in (a) illustrates cold and warm fronts within a low-pressure system traversing the semi-permanent SST front. On the trailing edge of the cold front (purple), the cold/dry air mass over the warm ocean water induces large diabatic heating of the storms, strengthening the storm. A similar process might occur over the transient mesoscale eddies. The modified air mass ascends over the warm front, leading to deep cumulus clouds and heavy precipitation. (c) A 2-D view of the cross-section in (b), where the cold front translates eastward over the SST front. When the cold front is east of the SST front, the large air-sea temperature and humidity differences (purple) cause the maximum upward turbulent heat flux, facilitating the diabatic frontogenesis. This strengthening of the atmospheric front can be inferred from the sign of a cross-frontal sensible heat flux gradient, which in this case, is negative. The reverse is true when the cold front is west of the SST front (not shown). (d) A 2-D view of the MABL with the cross-frontal winds. For the warm-to-cold case, the warm air blowing over cold water downwind of the SST front leads to a stable internal boundary layer with a capping inversion and a shallow clockwise secondary circulation. Due to weaker vertical mixing, the surface wind slows down, reinforcing the initial wind shear. The weak wind over cold SST yields a reduced surface drag. For the cold-to-warm case, MABL and internal boundary layers deepen quickly, with the counter-clockwise secondary circulation developing downstream. The increased turbulent mixing accelerates the surface wind, leading to a well-mixed wind profile. The choppier surface waves on the warm side due to higher winds enhance surface drag. Wind direction also changes across the front as wind speed adjusts to local stability (not featured in this schematic). The surface currents near the ocean front (also not shown) modulate the wave slopes and surface roughness via wave-current interaction and the wind stress via current-wind interaction. (e) Meandering eastward currents and mesoscale eddies under a uniform westerly wind. On a large scale, because surface currents are oriented downwind, the relative wind leads to weaker geostrophic wind work than the absolute wind, stabilizing the large-scale circulation but stimulating submesoscale instabilities. Over the eddies, eddy-atmosphere coupling induces the diabatic dissipation of eddy potential energy (thermal feedback) and the negative geostrophic eddy wind work via current-wind interaction (mechanical feedback), weakening the eddy energy. The eddies' swirling currents manifest reversely in the wind stress, leading to current-induced wind stress curls and the up/downwelling in the ocean. (f) The cross-section across the front/jet in (e). The down-front wind drives an eastward Ekman transport of cold/dense water over warm/light water, reducing stratification near the front. The unstable front leads to enhanced turbulence and submesoscale activity, with the induced secondary circulation accelerating the jet. The oceanic frontogenesis influenced by the surface waves is not featured in this schematic but illustrated in Figure 9.

The readers might find it helpful to visualize key feedback mechanisms discussed throughout the paper by referring to the schematic illustrations in Figure 1, which are organized at different characteristic length scales and by processes. The MABL response to a mesoscale SST front (Figure 1d) corresponds to Section 2. The diabatic heat exchanges between the atmospheric fronts and the SST fronts (Figure 1b-c) are elaborated in Section 3b, while a broader view of modulation of the midlatitude storm track by the WBCs and the subsequent downstream rainfall patterns (Figure 1a) is discussed in detail in Sections 3a-c. The discussion about the modulation of wind stress and heat fluxes by the mean and eddy currents and their feedback to oceans (Figure 1e) jibes with Section 4a. The resulting fine-scale near-surface instability and turbulence (Figure 1d) are touched upon in Section 4b-c.

It is not possible to cover all relevant aspects of mesoscale air-sea interaction with sufficient details. There exist many review articles that might be helpful for readers interested in gaining a more in-depth understanding of specific topics. For Section 2, such papers include Bourassa et al. (2013) on challenges/needs for accurate air-sea flux measurements in high-latitude oceans; Swart et al. (2019) on observational strategies to improve Southern Ocean heat and gas flux estimates; Cronin et al. (2019) on global air-sea flux accuracy requirements; Bourassa et al. (2019) on satellite remote sensing of wind and winds stress; and Deskos et al. (2021) on sea state impacts on surface winds from a wind energy perspective. For Section 3, Kushnir et al. (2002) reviewed the atmospheric responses to extratropical SST anomalies in climate models. Czaja et al. (2019) updated the extratropical air-sea interaction based on high-resolution climate modeling studies, while Kwon et al. (2010) and Kelly et al. (2010) reviewed the impacts of WBC SST anomalies on seasonal to decadal climate variability. For Section 4, more detailed accounts of surface waves, upper ocean mixing, and submesoscale dynamics are provided by Sullivan and McWilliams (2010), D'Asaro (2014), and McWilliams (2016). McGillicuddy et al. (2016) offer a comprehensive review of mechanisms of physical-biological-biogeochemical interactions on the oceanic mesoscale. For Section 5, helpful review papers include Ardhuin et al. (2019) on observing sea state information; Villas Bôas et al. (2019) on wind-wave-current interaction; Centurioni et al. (2019) on global ocean surface observation networks; and Wanninkhof et al. (2019) on global CO_2 flux measurements. The observational needs for data assimilation, coupled reanalyses, and short-term and extended-range predictions have been discussed by Penny et al. (2019), Domingues et al. (2019), and Subramanian et al. (2019).

2. Boundary layer and surface heat, momentum, and gas flux responses

Surface fluxes communicate mass and energy between the ocean and atmosphere and are thus vital processes in Earth's climate system. The ocean is a major reservoir of heat and carbon in the Earth system, and it is increasingly clear that exchanges with the atmosphere occurring on the oceanic mesoscale are significant in shaping Earth's climate. Recent assessments on projected trends in surface air temperature (SAT) and SST have indicated a need to better understand surface heat fluxes to reconcile conflicting lines of evidence on the projected trends in SAT and SST (e.g., Box TS.1, IPCC 2021). The surface turbulent heat fluxes are composed of sensible

and latent heat fluxes, while the surface wind stress represents the turbulent momentum flux between the atmosphere and ocean mediated by surface waves. This section discusses air-sea heat, momentum, and gas flux responses to spatially heterogeneous fields of SST, surface currents, and sea state. We also discuss the local MABL response to ocean-induced mesoscale forcing, given its strong relationship with the surface fluxes. These processes are illustrated in Figure 1d.

Spatially heterogeneous SST and surface currents generate localized anomalies in the surface heat and momentum fluxes. The atmospheric and oceanic responses to these flux anomalies are initially confined to the MABL and ocean mixed layer, but the responses to this coupling may spread to the free atmosphere above (Section 3) or the ocean thermocline below (Section 4). The atmospheric boundary layer and the oceanic mixed layer directly mediate responses of the large-scale oceanic and atmospheric circulation to the mesoscale and frontal-scale air-sea coupling.

Figure 2 shows the strong correlation between monthly mesoscale surface fluxes and ocean mesoscale variability from the ERA5 reanalysis (Hersbach et al. 2020). Here, the turbulent heat flux is defined as positive downward (ocean warming). When the local point-by-point correlation between the turbulent fluxes and SST is strongly negative, the SST variability can be viewed as the ocean forcing the atmosphere (e.g., the warm ocean heats the atmosphere). Similarly, when the correlation between turbulent heat flux and SST *tendency* is positive, the atmosphere is considered to drive ocean variability. Over mesoscale, the wind stress and upward heat fluxes are enhanced over warm SST anomalies (SSTA) and reduced over cool SSTA. The correlations are much stronger for sensible and latent heat flux responses, while the surface stress response on this spatial scale is much more apparent in oceanic frontal boundary regions where mesoscale SST variability is most pronounced. However, it should be noted that the amplitude of correlation represents empirical estimates of the strength of covariability since the atmospheric response to an ocean anomaly modifies the turbulent fluxes and would obscure this simple rule (e.g., Sutton and Mathieu, 2002). The effect of the surface flux on the ocean is discussed in Section 4.

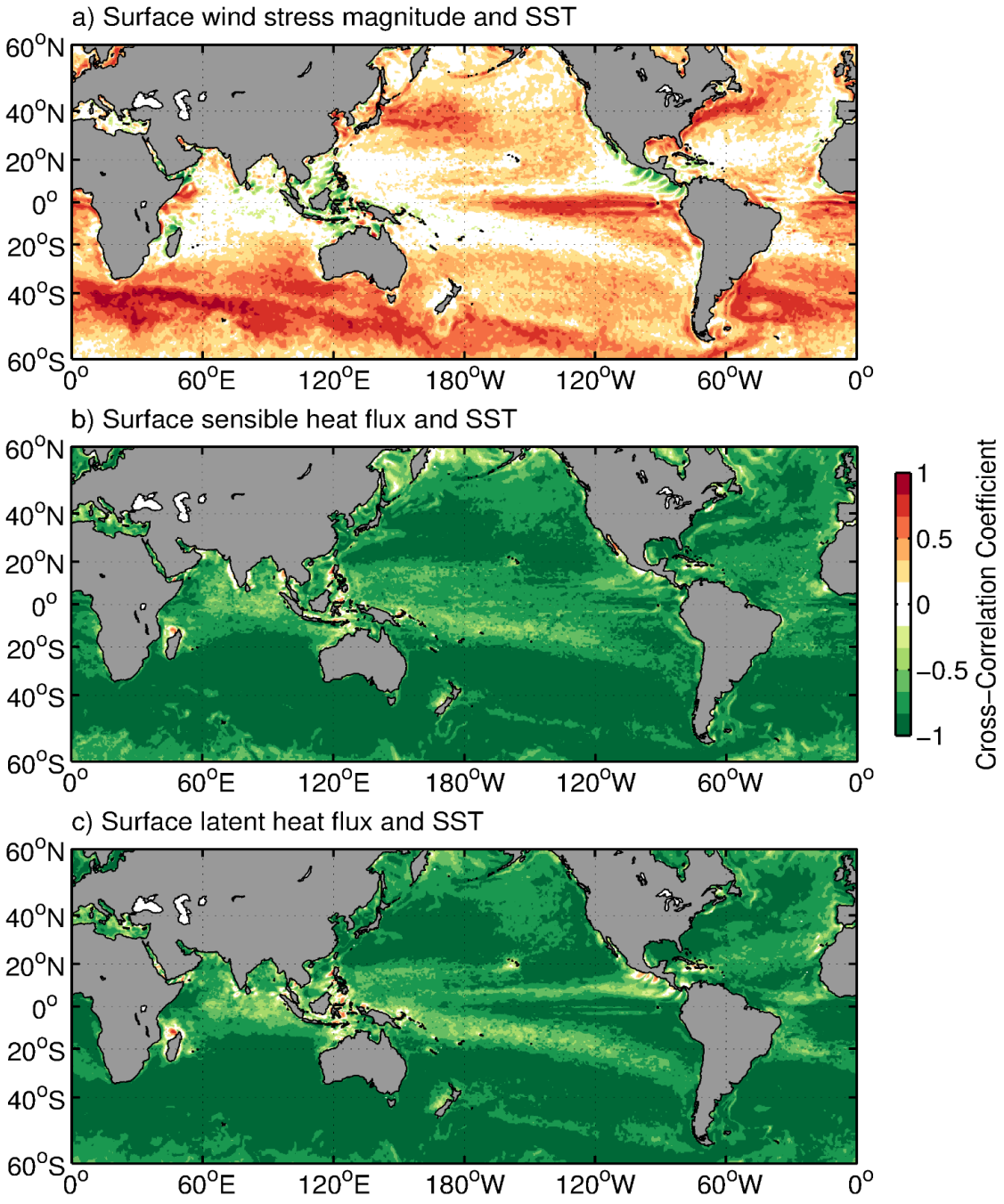

Figure 2: Maps of the cross-correlation coefficients between ERA5 monthly spatially high-pass filtered SST and (a) wind stress magnitude, (b) surface sensible heat flux, and (c) surface latent heat flux. The spatial high-pass filter removed variability with spatial scales greater than 1000 km. These maps were averaged over the 30-year period 1991-2020. The ERA5 reanalysis time period used here was 1991-2020. The standard sign convention for ERA5 surface fluxes is used: positive fluxes mean energy entering the ocean. The high correlations in these maps correspond to regions of strong mesoscale SST variability, such as in the WBCs and their extension regions (Kuroshio, Gulf Stream, Brazil Current, and Agulhas Current), along the Antarctic Circumpolar Current and equatorial fronts, and near the Somali Current. A similar plot to Figure 2(a) can be found in Small et al. (2008) and Seo (2017).

a. Turbulent heat flux response

On smaller scales encompassed by the oceanic mesoscale and on time-scales longer than synoptic time-scales in the atmosphere (e.g., 2-8 days), spatial variations in the surface turbulent heat fluxes are driven primarily by spatial perturbations of SST, such that negative heat flux anomalies (i.e., atmosphere heat gain) occur over warm SST perturbations and positive heat flux anomalies (i.e., atmosphere heat loss) occur over cool SST perturbations (Figure 2b-c). Over these scales, the ocean forces a response of the atmosphere driven by the surface heat exchange, which is fundamentally distinct from the response over larger spatial scales. Near-surface air temperature and specific humidity adjust slowly to spatially heterogeneous SST as air flows across SST gradients. Ocean mesoscale eddies and SST fronts near the semi-permanent WBCs often generate large air-sea temperature and humidity differences (Figure 1b-c). A dramatic example was observed during the CLIMODE experiment near the Gulf Stream during wintertime, when air-sea temperature differences exceeded 10 °C over 200 km, yielding >1000 W/m^2 surface turbulent heat fluxes into the atmosphere (Marshall et al. 2009).

Past field experiments captured less extreme but nonetheless strong responses of turbulent heat fluxes and MABL convective turbulence to mesoscale and frontal-scale SSTs. Examples can be found from the Sargasso Sea during the FASINEX experiment (e.g., Friehe et al. 1991), Gulf Stream (e.g., Plagge et al. 2016), Kuroshio (e.g., Tokinaga et al. 2009); Pacific Tropical Instability Waves (Thum et al. 2002), Brazil-Malvinas Confluence system (e.g., Pezzi et al. 2005; Villas Bôas et al. 2015; Souza et al. 2021), Agulhas Current (e.g., Jury and Courtney 1991; Messager and Swart 2016), and the western Arabian Sea (e.g., Vecchi et al. 2004).

The scale dependence of turbulent flux responses to mesoscale SST variations has been quantified primarily from reanalysis-based surface flux and SST datasets (e.g., Li et al. 2017; Sun and Wu 2022). Bishop et al. (2017), in particular, showed that on time-scales longer than one month, the turbulent heat fluxes on the ocean mesoscale and frontal scale are driven by SST variability associated with oceanic internal processes. On shorter time-scales, the variability is driven more by synoptic-scale weather variability, particularly along the storm tracks overlying the WBCs. Based on this simple diagnostic, Kirtman et al. (2012) concluded that eddy-parameterized models grossly underestimate the ocean forcing of the atmosphere in eddy-rich

290 regions (e.g., WBCs and the Southern Ocean) and overestimate the atmospheric forcing of the
291 ocean throughout much of the mid-latitudes compared to the ocean eddy-resolving simulations.
292
293 *b. Turbulent momentum flux and MABL wind responses*
294 The turbulent heat flux response to SST is a crucial process that drives the responses in turbulent
295 momentum flux to SST. The variability in ocean surface currents at mesoscales also affects the
296 wind stress through the relative motion of the surface winds and currents. The most immediate
297 local atmospheric response to SST and surface currents is initially confined to the MABL. The
298 wind and wind stress responses mainly result from a dynamical adjustment of the MABL
299 pressure and vertical turbulent stress profile distinct from simple adjustments of the surface layer
300 logarithmic wind profile (Small et al. 2008; O'Neill 2012; Renault et al. 2016a), the relative
301 importance of which strongly depends upon background wind condition (e.g, Schneider and Qiu
302 2015; Byrne et al. 2015; Section 2c).
303
304 1) Mesoscale SST effects
305 Traditionally, local atmospheric responses to the mesoscale SST have been characterized
306 empirically by linear regressions between collocated mesoscale SSTs and surface winds and
307 surface wind stress, all spatially high-pass filtered to isolate the coupling on scales smaller than
308 about O(1000 km). Linear regression coefficients, also called coupling coefficients, obtained
309 from satellite-observed wind speed and wind stress indicates ubiquitous increases in their
310 magnitudes over warm SSTs, increases of wind divergence and wind stress divergence co-
311 located with the downwind component of the SST gradient, and wind curl and wind stress curl
312 that scale with crosswind components of SST gradients (Chelton et al. 2001; O'Neill et al. 2003,
313 2012). The SST-induced curl and divergence responses provide further constraints on spatial
314 scales of the SST-induced MABL response. These simple but powerful diagnostic metrics have
315 been broadly used to diagnose the simulated air-sea interaction over a range of scales in
316 numerical models (Bellucci et al. 2021), leading to refinements in the SST resolution (Chelton
317 2005) and the PBL parameterizations in NWP models (Song et al. 2017). However, the coupling
318 coefficients include contributions from broad scales represented in the high-pass filtered input
319 fields. Hence, other than the gross separation of small scales from large scales, it is difficult to
320 extract useful information about the scale dependence from such calculations. Alternative

statistical and analytical approaches exist, including cross-spectral analysis (e.g., Small et al. 2005b; O'Neill et al. 2012; Laurindo et al. 2019; Samelson et al. 2020), cross-covariance and correlation functions between SST (and its tendency), wind and turbulent heat fluxes (e.g., Frankignoul and Hasselmann 1977; Wu et al. 2006; Bishop et al. 2017; Small et al. 2019), and an analytical model for MABL heat and momentum budgets (Schneider and Qiu 2015; Schneider 2020). The analytical model for MABL is explored in detail in Section 2c.

2) Mesoscale current effects

Regions of strong SST gradients are also regions of substantial variability in ocean surface current. The current feedback (CFB) mechanism directly modifies wind stress through the relative motion of surface winds and currents, which in turn alters the low-level wind shear and wind. That is, a negative current anomaly induces a positive stress anomaly acting on the atmosphere, which causes a negative wind anomaly (Renault et al. 2016a). At the mesoscale, CFB primarily impacts the surface wind stress curl but not its divergence due to the quasi-geostrophic nature of ocean currents (Chelton et al. 2004). The wind stress and wind responses to CFB can also be diagnosed using empirical relationships based on satellite and numerical simulations. Renault et al. (2016a; 2019a) defined two coupling coefficients related to CFB: s_w is the regression slope between mesoscale surface currents and 10 m wind and s_τ is the linear regression coefficient linking mesoscale surface current and surface stress. The coefficient s_τ can be interpreted as a measure of the damping efficiency of CFB to ocean eddy energy, as discussed in greater detail in Section 4.

The SST and current-induced stress responses are challenging to separate since mesoscale SST and current variations co-vary strongly near ocean fronts and eddies. Nonetheless, estimates of the contributions of the current-induced wind stress response via the linear coupling coefficients indicate that the current-induced stress anomalies exceed the SST-induced response over strong WBCs and within isolated ocean eddies (e.g., Gaube et al. 2015; Renault et al. 2019a). The current-induced stress response exists in scatterometer and direct air-sea flux observations and coupled ocean-atmosphere simulations, but it is not directly apparent in atmosphere-only simulations and reanalyses, such as the ERA5 wind stress anomalies used in Figure 2. Including

both current and SST-induced stress anomalies strongly impacts the mesoscale wind stress curl field (e.g., Renault et al. 2019a).

c. Analytic framework for SST-induced boundary layer response

The MABL response to ocean mesoscale current must incorporate coupling between the MABL thermodynamics and dynamics to adequately represent the influence of SST and surface current on the surface wind stress and sensible and latent heat fluxes. An analytical framework for SST impacts was recently proposed, which incorporates MABL heat and momentum budgets that capture the first-order response of the MABL to SST forcing (Schneider and Qiu 2015; Schneider 2020) and includes a representation of the processes shown in the literature to be of primary importance. This framework considers an MABL capped by an inversion (Battisti et al. 1999). Within this layer, air temperature is assumed to be well mixed and vertically constant, and subject to horizontal advection and air-sea heat exchanges. The system is driven by winds with horizontal scales far larger than the ocean mesoscale that satisfy a drag law at the sea surface and experience zero vertical momentum flux at the inversion. The large-scale winds $\vec{U}$ form a modified Ekman spiral (Holton 1965a,b), which is considered horizontally homogeneous on scales commensurate with the ocean mesoscale.

SST T enters the heat budget of the layer via the air-sea heat exchanges due to the air-sea temperature difference with a rate γ. Air temperature Θ results, to first order, from a steady balance of surface sensible heat fluxes with advection by large-scale winds (e.g., Small et al. 2005a),

$$\vec{U} \cdot \nabla\Theta = \gamma(T - \Theta) \qquad (1).$$

The MABL air temperatures Θ adjust to T over a length-scale of U/γ, forming a wake of elevated values of the air-sea temperature differences in the lee of spatial SST variations. Thermal adjustment rates of the boundary layer γ correspond to adjustment times of a few hours to half a day (Schubert et al. 1979), yielding length scales of O(100 km). The momentum equations govern the wind response to the ocean mesoscale SST-induced acceleration $\vec{F}$,

$$\vec{U} \cdot \nabla \vec{u} + \frac{w^\star}{H} \partial_s \vec{U} + f \hat{e_3} \times \vec{u} - \frac{1}{H^2} \partial_s A \partial_s \vec{u} + g' \nabla h = \vec{F}, \qquad (2)$$

which include, on the left-hand side, horizontal advection by large-scale winds $\vec{U}$ of SST induced winds $\vec{u}$ and vertical advection $w^\star$ of the large-scale shear, the Coriolis acceleration with Coriolis frequency f, the divergence of vertical fluxes of horizontal momentum due to large-scale mixing with eddy coefficient A, and hydrostatic pressure gradient forces, including the so-called back pressure effect (e.g., Hashizume et al. 2002) due to ocean mesoscale-induced changes of inversion height H, and $\hat{e}_3$ is the upward unit vector. Together with the continuity equation and boundary conditions of a drag law at the sea surface, and a material inversion with no flux of momentum, these equations provide a complete analytical solution for the wind response to ocean mesoscale SSTs.

Changes in Θ impact accelerations $\vec{F}$ to the horizontal momentum on the right-hand side through the hydrostatic pressure term, which couples the MABL thermodynamics with the dynamics:

$$\vec{F} \;=\; \frac{gH}{\Theta_0}(1-s)\nabla\Theta \;+\; \frac{1}{H^2}\partial_s\left(\dot{A}\;\partial_s\vec{U}\right) \qquad (3)$$

through the modulation of the hydrostatic pressure gradients (the first term on the right), and the sensitivity of the vertical mixing to the fluxes at the air-sea interface (the second term on the right). The sigma vertical coordinate s measures the height relative to the mean inversion height H, Θ_0 is a reference temperature, g the earth's gravitational acceleration, and $\dot{A}$ is the sensitivity of vertical mixing A to SST.

The vertical mixing effect, the second term on the right in Eq. (3), is a linearization of the 'nonlinear' term envisioned by Wallace et al. (1989) and Hayes et al. (1989) that captures the modulations of the vertical mixing acting on the large-scale wind profile. The dynamics, amplitude, and vertical structure of $\dot{A}$ determine the character of mixing sensitivity. Mixing can intensify and change its vertical scale. The dependence of vertical mixing on the non-equilibrium air-sea temperature difference is but one possibility. Alternatively, SST induces convective adjustment of the lapse rate and permanently deepens the boundary layer over warmer waters

(Samelson et al. 2006). These diagnostic formulations for $\dot{A}$ are endpoints of the non-equilibrium evolution of vertical mixing simulated by Large Eddy Simulations (LES, e.g., de Szoeke and Bretherton 2004; Skyllingstad et al. 2007; Sullivan et al. 2020), which allow for changes in the vertical mixing that lag modulations of boundary layer stability (Wenegrat and Arthur 2018). As such, the coupling between surface winds and SST is sensitive to the MABL turbulence closure schemes (e.g., Song et al. 2009, 2017; Perlin et al. 2014; Samelson et al. 2020). The MABL turbulence subsequently affects the SST by altering mixing and entrainment in the ocean surface boundary layer, indicating co-dependence of the turbulent boundary layer schemes in the atmosphere and oceans (Fox-Kemper et al. 2022).

Advection by large-scale winds allows for disequilibrium in air-sea temperature and shifts responses of winds or stress as a function of the SST spatial scales and the large-scale wind direction and speed (e.g., Small et al. 2005a, 2008). Spectral transfer functions, or their corresponding physical-space impulse response functions, capture these non-local relationships and generalize the widely used coupling coefficients to include spatial lags. Estimates from satellite observed winds and SST of spectral transfer functions suggest scale-dependent, lagged dynamics as a function of the Rossby number determined by large-scale winds, the wavenumbers of ocean mesoscale SST, and the Coriolis frequency f, or thermal or frictional adjustment rates γ or A/H^2 (Schneider 2020; Masunaga and Schneider 2022). For small Rossby numbers, the pressure effect dominates, while large Rossby numbers favor the vertical mixing effect, and order one Rossby numbers combine both with rotational effects, consistent with modeling studies of boundary layer responses to prototype SST fronts (Spall 2007a; Kilpatrick et al. 2014, 2016) and ocean eddy fields (Foussard et al. 2019a) in the presence of large-scale winds.

The analytical model described above considers a dry MABL without incorporating MABL moisture or latent heat fluxes. The contribution of moisture to buoyancy fluxes, latent heating/cooling, and overall MABL structure has not been investigated in as much detail within the context of the mesoscale MABL response. However, it is anticipated to have a non-negligible impact on the MABL dynamical response to mesoscale SSTA (Skyllingstad and Edson 2009). For instance, during CLIMODE, the buoyancy heat flux was approximately 20% larger than the sensible heat flux due to moisture, and the average magnitude of the latent heat flux was ~2.5

times greater than the sensible heat flux (Marshall et al. 2009). In the tropics, the ratio of latent to sensible heat flux is even larger (e.g., de Szoeke et al. 2015), so the moisture contribution is often an order of magnitude greater than the sensible heat contribution. The impact of moist convection during a cold air outbreak over the Gulf Stream was investigated with an LES (Skyllingstad and Edson 2009), showing that the latent and sensible heat fluxes are enhanced over a simulated SST front resulting in stronger turbulent mixing and precipitation compared to a constant SST simulation. The simulation across the SST front shows that relatively low humidity values near the surface are maintained by the continual expansion of the boundary layer in the entrainment layer, which mixes dry air from aloft into the MABL. This maintains the large air-sea specific humidity and temperature differences necessary for strong latent and sensible heat fluxes in the surface layer. Additional simulations and measurements are required to investigate the role of moisture in response to mesoscale SST. For example, the analytical model could provide insight by using the virtual temperature at both the sea surface and aloft.

d. Modulation of air-sea fluxes of tracers

Air-sea gas fluxes of tracers depend on the air-sea disequilibrium and processes driving exchange, such as winds and breaking waves. From the ocean perspective, the disequilibrium can be understood as the difference of the concentrations of a gas in the seawater, C, relative to the concentration the gas would have at equilibrium with the atmosphere, C_{eq}, which, in turn, is determined by the solubility of the gas in seawater. The air-sea flux F then is estimated as $F = k(C - C_{eq})$, where k is the gas transfer velocity (e.g., Woolf 1993; McGillis et al. 2001; Wanninkhof et al. 2009; Dong et al. 2021). Impacts of ocean mesoscale features on the net F may be introduced via k or C_{eq}, each of which varies nonlinearly with wind speed and depends on sea state. The mesoscale may also affect C by impacting biological sources and sinks of tracers (Section 4d). Indeed, studies find local modulations of air-sea CO_2 fluxes due to the effects of mesoscale eddies on solubility, productivity, or winds (Jones et al. 2015; Song et al. 2015, 2016; Olivier et al. 2021). One such study in the Southwest Atlantic Ocean detected clear spatial covariations of CO_2 flux with the MABL stability over a warm-core eddy (Figure 3; Pezzi et al. 2021). Yet, on the basin-to-global scales, positive and negative mesoscale anomalies of CO_2 fluxes appear to essentially cancel (Wanninkhof et al. 2011; Song et al. 2015). Clear separation and quantification of the individual and rectified effects of mesoscale phenomena on

k, C, and C_{eq} from observations and models remain challenging, given the difficulty of capturing transient mesoscale variations in the ocean and atmosphere, including the concentration of tracers such as carbon.

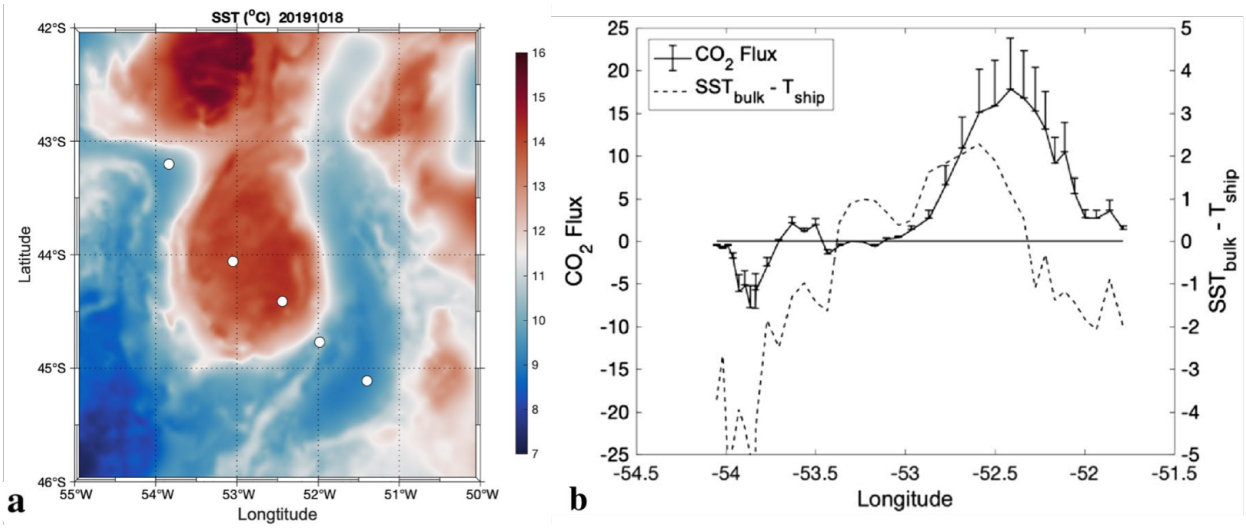

Figure 3: (a) Observed SST (°C) in the Southwestern Atlantic Ocean on 18 October 2019. The white circles denote the Po/V *Almirante Maximiano* trajectory. (b) In situ CO_2 fluxes (μmol $m^{-2}s^{-1}$) measured by Eddy Covariance method (solid) and atmospheric stability parameter SST-Tair (°C) (dotted). The error bars denote the standard error representing a 95% confidence interval. Figures adapted from Pezzi et al. (2021). The figure needs permission to reproduce.

3. Free-tropospheric, extratropical atmospheric circulation responses

This section investigates atmospheric response beyond the MABL (Section 2) by focusing on local and non-local circulation responses in the extratropics to SSTA patterns observed in the WBC regions, including the semi-permanent SST fronts and transient mesoscale eddies. Some aspects of deep convective response in the tropical atmosphere have also been attributed to MABL adjustments to the mesoscale SST fields (Li and Carbone 2012; Skyllingstad et al. 2019; de Szoeke and Maloney 2020), although much of the studies on deep atmospheric responses published to date is based on the extratropics. We start with a summary of previous studies on the role of extratropical SSTA in quasi-equilibrium atmospheric circulation and storm tracks. We then revisit the debates about the observed near-surface wind convergence and precipitation in WBC regions diagnosed as a response to either SST variations or extratropical storms. Finally, we will consider whether these processes may be important to future climate, focusing on the

difference between projections at high and low resolution in the oceans. The feedback processes examined in this section are schematically illustrated in Figure 1a-c.

a. Time-mean general circulation responses

The question of how the extratropical atmosphere responds to variability in ocean fronts and/or extratropical SSTA has been addressed over many decades. Early studies considered the linear response (Hoskins and Karoly 1981; Frankignoul 1985), which predicted a shallow heating response characterized by a downstream trough with a baroclinic structure. This was argued against by Palmer and Sun (1985), who found a downstream ridge, with an advection of temperature anomalies by mean flow acting against anomalous advection of mean temperature gradients. Later, Peng et al. (1997) showed that the transient eddy response was important in forming an equivalent barotropic high. More recent observational analyses find a weak low-pressure response east of warm SSTA near the Gulf Stream (Wills et al. 2016) and Kuroshio (Frankignoul et al. 2011; Wills and Thompson 2018). Deser et al. (2007) demonstrated that the initial linear, baroclinic response is quickly (within 2 weeks) replaced with the equilibrium barotropic response with a much broader spatial extent and magnitude (Ferreira and Frankignoul 2005, 2008; Seo et al. 2014). The adjustment time is shorter near WBC regions (Smirnov et al. 2015). This literature is well summarized in existing review papers (Kushnir et al. 2002; Small et al. 2008; Kwon et al. 2010; Czaja et al. 2019).

Recent studies also indicated a strong sensitivity to the spatial resolution of the atmospheric dynamics governing the large-scale circulation response. For example, Smirnov et al. (2015) show that a low-resolution (1°) model induces a weak response resulting from shallow anomalous heating balanced by equatorward cold air advection, consistent with the results from steady linear dynamics. This contrasts with the higher resolution (1/4°) model showing that the anomalous diabatic heating is balanced by a deep vertical motion mediated by the transient eddies (Hand et al. 2014; Wills et al. 2016; Lee et al. 2018). The anomalous diabatic heating and the induced vertical motions maintain the climatological circulation pattern over the WBCs.

b. Synoptic storms and storm track responses

Storm tracks typically occur in the 30-50° latitude band coincident with the climatological SST fronts (Figure 4) and are associated with strong and frequent precipitation, particularly via atmospheric fronts. Midlatitude storm tracks can be primarily defined in two ways (Chang et al. 2002; Hoskins and Hodges 2002): either using distributions of the tracks and intensity of synoptic cyclones (the Lagrangian view) or as regions of strong variability or co-variability of winds, geopotential height, temperature, and humidity in the lower to upper troposphere (the Eulerian perspective). To better elucidate the forcing of near-surface weather by the oceans, other studies also use the surface-based storm track, defined as the variance of near-surface meridional winds (Booth et al. 2010, 2017; O'Neill et al. 2017; Small et al. 2019). The concept of the surface storm track stems from earlier scatterometer measurements illustrating strong imprints of the free-tropospheric storm tracks in the surface wind fields over the warm WBCs (Sampe and Xie 2007; Bourassa et al. 2013). The reduced static stability and the enhanced vertical mixing within the MABL (Figure 1d) synchronize the locations of the surface storm track with the warm currents (Figure 4). The surface and free-tropospheric storm tracks are, thus, dynamically coupled via deep moist convection (Czaja and Blunt 2011).

One possible mechanism of midlatitude oceanic influence on the storm track was suggested by Hoskins and Valdes (1990), which found that enhanced diabatic heating by surface fluxes over WBCs supports atmospheric baroclinicity, a vital element in setting the location of the storm track (Hawcroft et al. 2012; Kaspi and Schneider 2013). Nakamura and Shimpo (2004) and Nakamura et al. (2004) further argued that SST gradients directly influence low-level air temperature gradients via cross-frontal gradients in sensible heat flux (Nakayama et al. 2021). The baroclinicity is measured as the atmospheric maximum Eady growth rate (Charney 1947; Eady 1949; Lindzen and Farrell 1980), such that stronger low-tropospheric baroclinicity is associated with weaker static stability and a stronger meridional air temperature gradient (see Figure 4 caption). Both conditions are observed over WBCs. Hence, the anchoring effect by cross-frontal differential heat supply from the ocean is consistent with the formation of a storm track over the WBC SST fronts (Nonaka et al. 2009; Hotta and Nakamura 2011), while diabatic heating over the warm portion of the WBC SST fronts to the warm and cold sectors of the

cyclones supports the growth of transient baroclinic waves (Booth et al. 2012; Willison et al. 2013; Hirata and Nonaka 2021; Figure 1b,c).

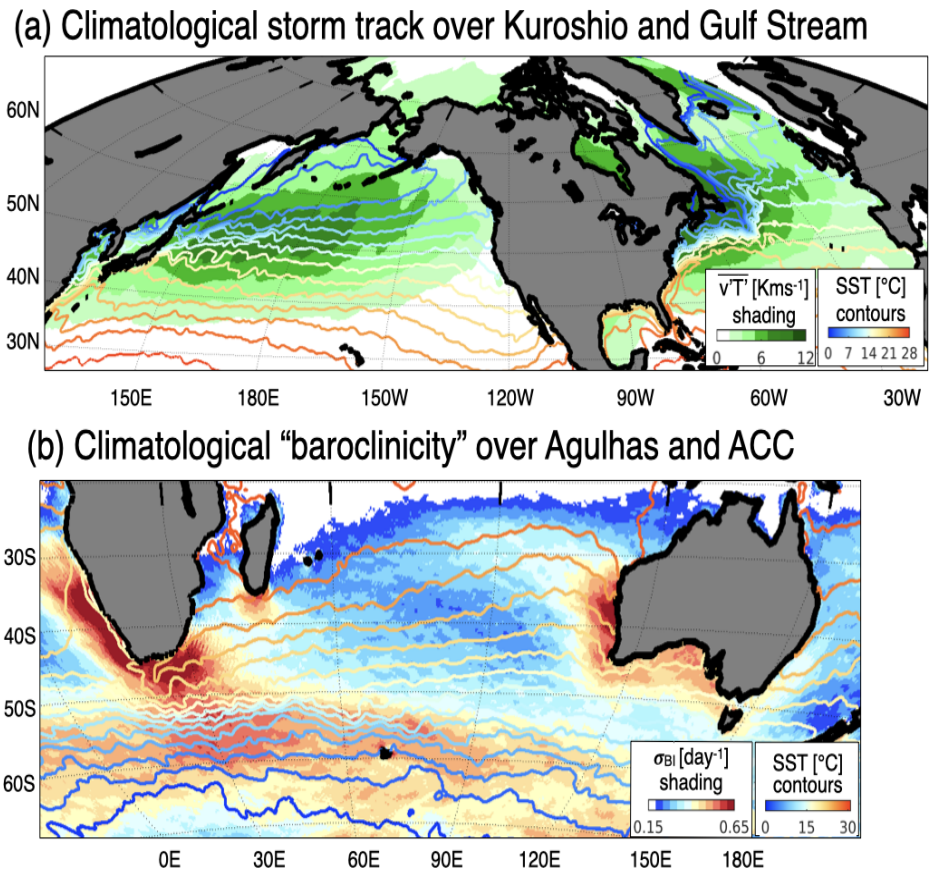

Figure 4: The climatological relationship of the extratropical storm tracks with the SST fields in (a) Kuroshio-Oyashio Extension and Gulf Stream in the Northern Hemisphere and (b) Agulhas Current and the Antarctic Circumpolar Current systems in the south Indian Ocean. The atmospheric storm track is estimated in (a) as the time-mean meridional heat transport by atmospheric transient eddies, $\overline{v'T'}$ at 850 hPa (low troposphere), where primes denote the 2-8-day bandpass filtered fields and the over-bar indicates the time-mean, and in (b) as the atmospheric maximum Eady growth rate, defined as the most unstable baroclinic mode whose growth rate is scaled as the magnitude of the baroclinicity vector, $|\sigma_{BI}| = 0.31 \left(\frac{g}{N\theta}\right) \left|-\frac{\partial\theta}{\partial y}, \frac{\partial\theta}{\partial x}\right|$, at 850 hPa, where g is the gravitational acceleration, N is the buoyancy, and θ is the potential temperature. These storm track quantities are derived from ERA5. The SST climatology is obtained from the NOAA daily Optimum Interpolation dataset. The climatologies are calculated from 2010 to 2015.

A standard method to diagnose the SST forcing mechanism of the storm track is to run a pair of AGCM simulations, one using observed SSTs (CONTROL), and another using a spatially-smoothed SST field with weaker gradients (SMOOTH), which also alters absolute SST (Figure 5). Alternatively, AGCMs are forced by shifting the latitude of the SST fronts or filtering mesoscale eddy SSTs (Seo et al. 2017). Such AGCM simulations indicate a strengthening of the

storm track near the Kuroshio-Oyashio Extension (KOE) (Kuwano-Yoshida and Minobe 2017) and the Gulf Stream (O'Reilly et al. 2017) in CONTROL near the climatological maximum cyclogenesis (Figure 5). Altered storm activity over the WBC regions influences the intensity of the coastal storms, and, thereby, inland weather near the Kuroshio (Nakamura et al. 2012; Hayasaki et al. 2013; Sugimoto et al. 2021), Gulf Stream (Infanti and Kirtman 2019; Hirata et al. 2019; Liu et al. 2020), and the Agulhas Current (Singleton and Reason 2006; Nkwinkwa Njouodo et al. 2018).

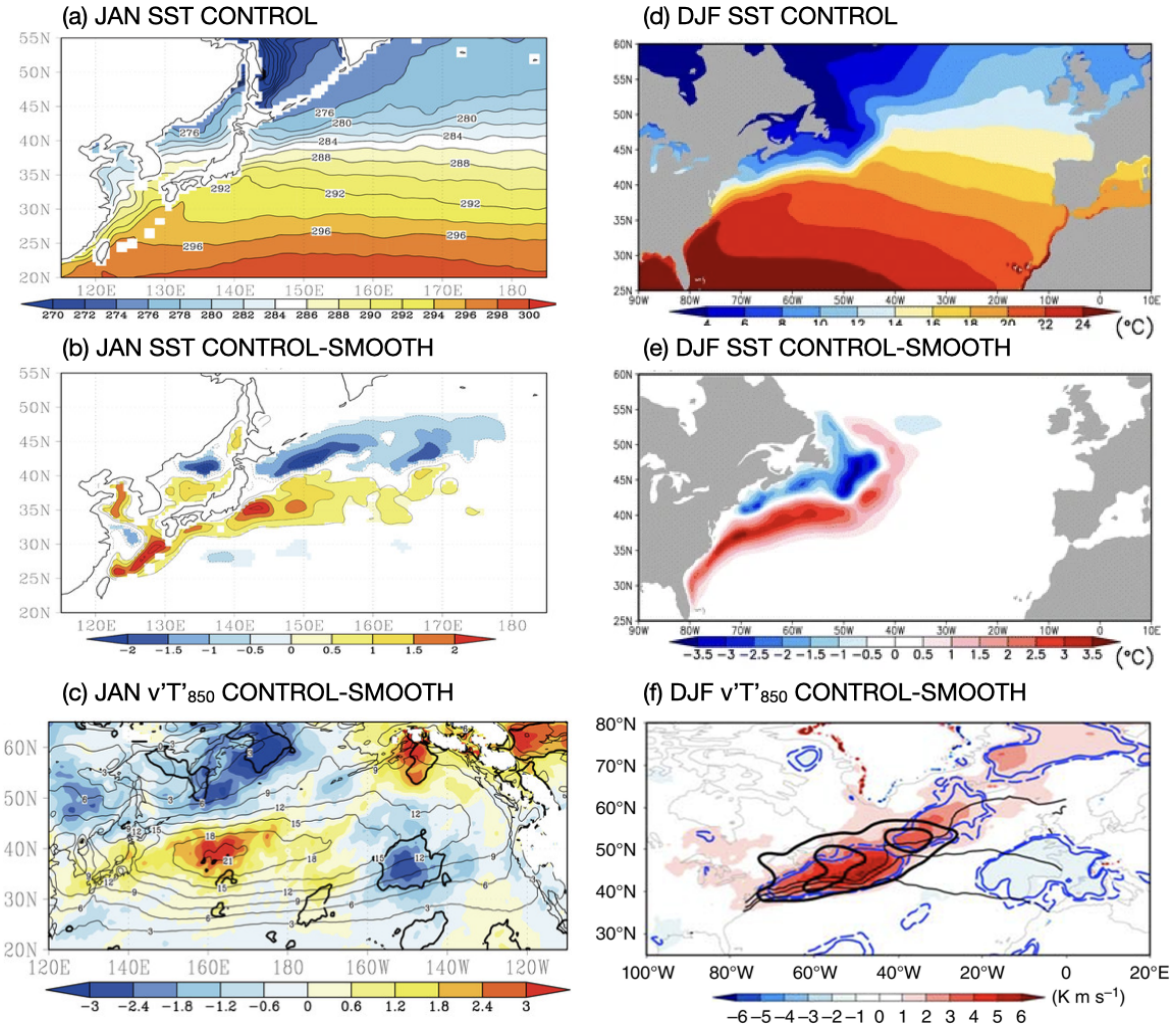

Figure 5: (Left) January observed SST, its difference (CONTROL-SMOOTH), and the difference (CONTROL-SMOOTH) in storm tracks over the North Pacific Ocean. The thin black contours show $\overline{v'T'}$ from the CONTROL case. Thick contours denote the 95% confidence level. (Right) As in (left) but for over the North Atlantic. Black contours in (f) denote atmospheric Eady growth rate at 775 hPa. The dashed and solid blue contours indicate significant differences at the 10 and 5% levels, respectively. Figures adapted from Kuwano-Yoshida and Minobe (2017) and O'Reilly et al. (2016, 2017). The figure needs permission to reproduce.

Recent studies indicate that atmospheric mesoscale phenomena within the storm tracks, such as atmospheric fronts, directly interact with the WBC fronts. Parfitt and Czaja (2016) used reanalysis data over the Gulf Stream, and Parfitt et al. (2016) used AGCM simulations over the KOE to argue that the cross-frontal sensible heat flux gradients across the SST fronts exert "thermal damping or strengthening" of atmospheric fronts depending on the space-time alignment between the SST gradients and atmospheric fronts with shared cross-frontal length-scales (Figure 1b-c). The most significant diabatic heating by surface fluxes is concentrated on the narrow space-time scales at which the cold sectors of the atmospheric front coincide with the warm sector of the SST fronts (Figure 1c), significantly enhancing precipitation associated with the atmospheric fronts and often facilitating explosive cyclogenesis (Hirata and Nonaka 2021 and references therein).

In contrast, other studies emphasize the limited role of SST fronts on extreme cyclones. AGCM experiments by Tsopouridis et al. (2021) indicated that the direct impacts of sharp SST fronts on individual cyclones over the Gulf Stream and KOE are weak, although SST fronts induce significant indirect responses in large-scale environments in which such storms form. Using an analytic model, Reeder et al. (2021) showed that diabatic frontogenesis over the WBCs intensifies atmosphere fronts only when strong and rapidly propagating synoptic systems are not already in the environment.

Much uncertainty remains in model simulations and observational analysis regarding the relative importance of SST gradients causing cross-atmospheric frontal sensible heat flux gradients *vs.* absolute SST affecting the large-scale condensational heating over warm currents. Another critical issue is that since the SST contributions to the precipitation from the warm and cold sectors of extratropical cyclones differ in terms of magnitude and spatial distribution (i.e., larger and broader for the warm sectors and weaker and more "anchored" to the SST fronts for the cold sectors, e.g., Vannière et al. 2017), the cold sector contribution might have been dominating the sensitivity of relatively high-resolution (~50 km) AGCM simulations to SST smoothing. It remains an open question whether even higher resolution AGCMs might amplify a sensitivity from the dynamics of the warm sectors, including atmospheric mesoscale instabilities developing on the warm conveyor belt (Czaja and Blunt 2011; Sheldon et al. 2017).

c. Near-surface wind convergence and vertical motion over the WBCs

A crucial part of the storm track response to SST is precipitation, which tends to cluster around the WBCs and is associated with high near-surface wind convergence (NSWC) and substantial vertical ascent. The climatological NSWC coincides with the ocean fronts and the Laplacians of SST and SLP, which indicates that the boundary layer process depicted by linear Ekman dynamics is germane to the observed NSWC and precipitation responses (Feliks et al. 2004; Minobe et al. 2008, 2010). However, the unambiguous attribution of NSWC to the steady Ekman-balanced mass adjustment mechanism remains difficult due to the coexistence of extratropical storm tracks with the WBC currents, which also induce minima in the time-mean SLP Laplacian over the SST fronts (O'Neill et al. 2017).

O'Neill et al. (2015) show from QuikSCAT observations and a regional atmospheric model that linear boundary layer dynamics cannot explain the daily time-scale occurrence of NSWC since, on rain-free days, surface divergence dominates even though the SST Laplacian would indicate convergence (Figure 6). Using an extreme value filter, O'Neill et al. (2017) further show that NSWC and vertical motion over the Gulf Stream are highly skewed and consist of infrequent yet extreme surface convergence events and more frequent but weak, divergent events, such that the median surface flow field is weakly divergent or nearly non-convergent (Figure 6). Parfitt and Czaja (2016) and Parfitt and Seo (2018) argue that much of the precipitation and NSWC are associated with atmospheric fronts, given that only a weak near-surface divergence remains when the contribution from atmospheric fronts is removed (Rousseau et al. 2021). In contrast, Masunaga et al. (2020a,b) showed that storms and fronts of moderate intensity are significant contributors to the time-mean convergence observed over the Gulf Stream and KOE.

Current research emphasizes identifying how and why atmospheric fronts align with and linger over ocean fronts in all major WBCs and whether there is an additional underlying, steady, small-scale boundary layer effect. There might exist a distinct temporal dependence of the NSWC over WBC SSTs, where atmospheric fronts govern its day-to-day variability, while the pressure adjustment and vertical mixing mechanisms provide lower frequency modulations (e.g., Brachet et al. 2012; Small et al. 2022).

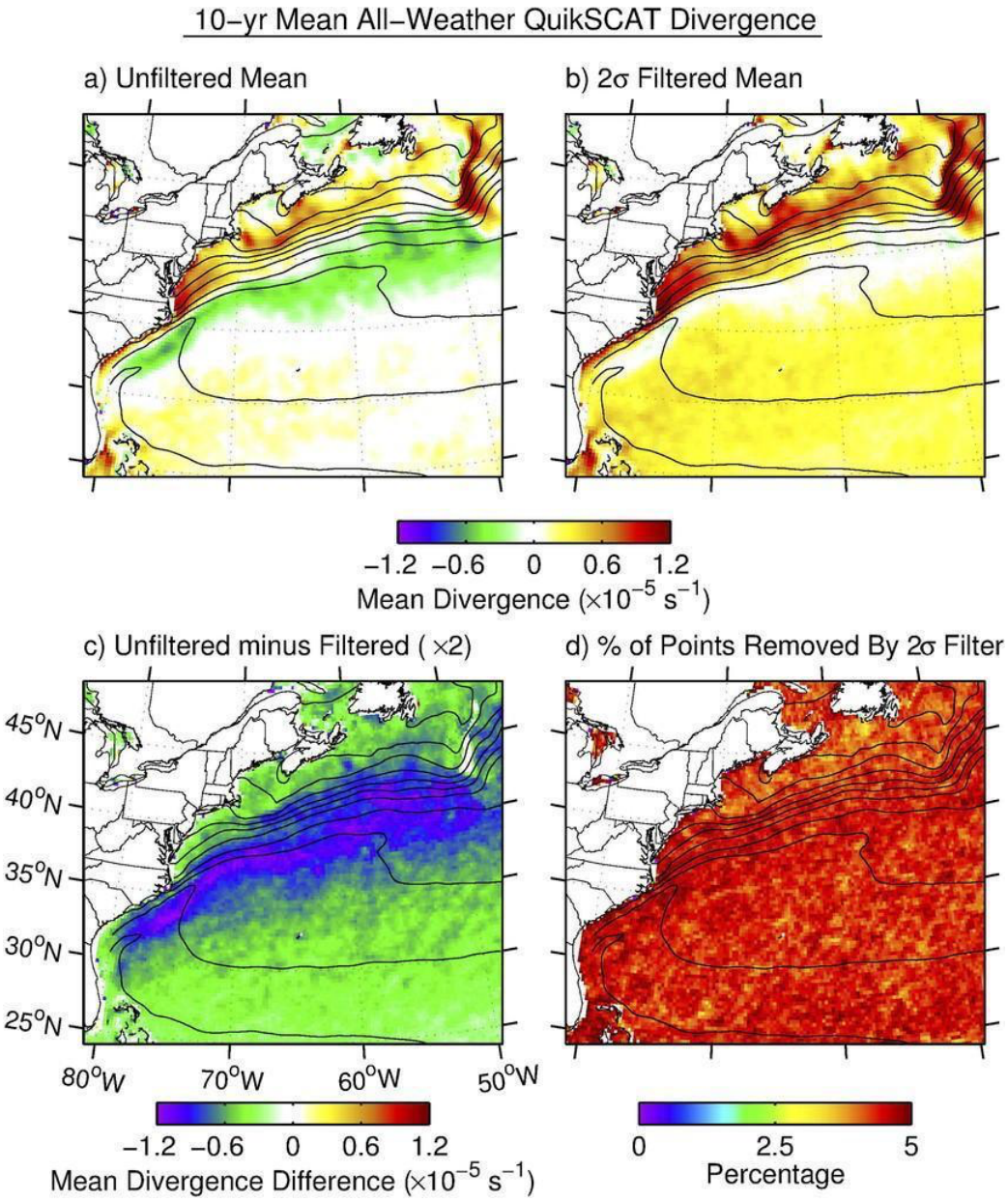

Figure 6: Maps of the 10-yr-mean QuikSCAT all-weather divergence (a) consisting of all points; (b) after application of the 2σ temporal extreme-value filter; (c) difference between (a) and (b); and (d) the percentage of divergence points removed by the 2σ extreme-value filter. The contours in each panel are of the 10-yr-mean Reynolds SST with a contour interval of 2ºC. From O'Neill et al. (2017). The figure needs permission to reproduce.

d. Non-local downstream atmospheric circulation responses

The upstream storm track variability leading to downstream development of the storm track is an essential characteristic of midlatitude baroclinic waves (Chang 1993). The altered synoptic-scale disturbances over the baroclinically unstable western basins (Section 3b) radiate energy downstream, influencing the growth of a subsequent baroclinic wave toward the eastern basins

(e.g., Chang and Orlanski 1993). The downstream atmospheric circulation also results from the synoptic eddy-mean flow interactions, where low-frequency atmospheric circulation is coupled with the transient eddy activity modified over the WBCs (e.g., Haines and Marshall 1987; Nakamura and Wallace 1990). Here, downstream (or remote, or non-local) refer to the region immediately east of the SST forcing and the tail-end of the storm track abutting the west coasts of the continents, as illustrated in Figure 1a.

Many AGCM studies demonstrate a non-local, downstream response in the storm track to WBC SST forcing. Using the observational datasets, Wills et al. (2016) and Joyce et al. (2018) identified significant transient atmospheric circulation responses (storm track and atmospheric blocking) downstream that lag the SSTA in the Gulf Stream extension by several weeks to months. The modeling studies by O'Reilly et al. (2016, 2017) showed that a strengthened storm track over the Gulf Stream leads to the northward shifted atmospheric eddy-driven jet and the increased European blocking frequency far downstream. Along a similar line, Lee et al. (2018) suggested that SST biases near the Gulf Stream trigger extended biases in the simulation of deep convection and downstream circulation via Rossby wave response.

In the North Pacific, O'Reilly and Czaja (2015) found that baroclinic eddies grow faster when the KOE front is in its stable regime (stronger SST gradients). The local shift in baroclinic wave activity leads to the early barotropitization of the baroclinic eddies downstream, resulting in weaker poleward eddy heat flux and increased occurrence of blocking in the eastern Pacific. An AGCM study by Kuwano-Yoshida and Minobe (2017) also suggested the enhanced storm track by the KOE SST fronts leads to a northward shifted storm track in the eastern Pacific. Ma et al. (2015, 2017) showed from AGCM simulations that the transient SSTA associated with the KOE mesoscale eddies leads to a northward shifted storm track and reduced precipitation in parts of western North America (Foussard al. 2019b; Liu et al. 2021; Siqueira et al. 2021).

In the Southern Ocean, Reason (2001) showed that amplified cyclone activity over the warm Agulhas Current yielded an enhanced storm track in the southeast Indian Ocean. Recent aquaplanet AGCM experiments have also demonstrated the critical role of the oceanic fronts in shaping the structure of the baroclinic annular mode variability (e.g., Sampe et al. 2013; Ogawa

et al. 2016; Nakayama et al. 2021), leading modes of variability of the extratropics (e.g., Thompson and Wallace 2000). Evidence exists that the oceanic frontal zones also impact the troposphere-stratosphere interactions (e.g., Hurwitz et al. 2012; Ogawa et al. 2015; Omrani et al. 2014), potentially affecting the entire hemispheric climate patterns.

e. Climate change

Climate change simulations for the 21st Century have emphasized the critical role of ocean circulation leading to natural modes of variability such as ENSO and PDO (Seager et al. 2001), the projected weakening of the Atlantic Meridional Overturning Circulation (AMOC; Weaver et al. 2012), and the delayed warming of the Southern Ocean (Marshall et al. 2014). These changes are relevant to the observed and projected intensification and poleward shift of the Kuroshio and Agulhas, weakening of the Gulf Stream, and changes in the frontal systems of the Antarctic Circumpolar Current (ACC) (e.g., Wu et al. 2012; Yang et al. 2016; Sen Gupta et al. 2021).

The IPCC report (IPCC, 2022) indicates that during the 21st Century, the North Pacific storm track will most likely shift poleward, the North Atlantic storm track is unlikely to have a simple poleward shift, and the Southern Hemisphere storm track will likely shift poleward. Understanding these regional differences in projected changes in midlatitude storm tracks and precipitation and their association with the predicted WBC changes have been the primary goals of high-resolution CGCM studies, especially those that contrast the CGCMs with the eddy-rich ocean (typically 0.1º resolution) to those with the eddy-parameterized ocean (0.5-1º). These studies with increased ocean model resolution to mitigate the known biases in representing the WBC dynamics and separation show distinct responses in SSTs and storm tracks in the WBC regions to anthropogenic climate change.

In these eddy-rich simulations, the KOE front shifted equatorward, contrary to projections by the eddy-parameterized IPCC-class CGCMs, which likely reflects the large natural variability in the North Pacific (Taguchi et al. 2007; Seager and Simpson 2016). In the North Atlantic, the Gulf Stream separation tends to be too far north in lower resolution models, an issue common to other WBCs, but is improved in eddy-rich models. This makes it possible for the separation to move northwards as a response to AMOC weakening in eddy-rich models (Gervais et al. 2018;

Moreno-Chamarro et al. 2021; Grist et al. 2021), leading to a significant projected ocean warming near the US eastern coastline (Figure 7; Karmalkar and Horton 2021). In the Southern Ocean, CMIP5-based climate change simulations indicate delayed warming, often attributed to stratospheric ozone depletion (McLandress et al. 2011; Polvani et al. 2011). However, the recent satellite observations and eddy-rich CGCMs simulations indicate a ubiquitous cooling trend (1961-2005) poleward of the ACC due to the effects of resolved ocean eddies (Bilgen and Kirtman 2020). Analysis of eddy-rich ocean simulations also indicates warmer and stronger Southern Hemisphere WBCs, suggesting that resolved ocean eddies play a critical role in long-term SST changes.

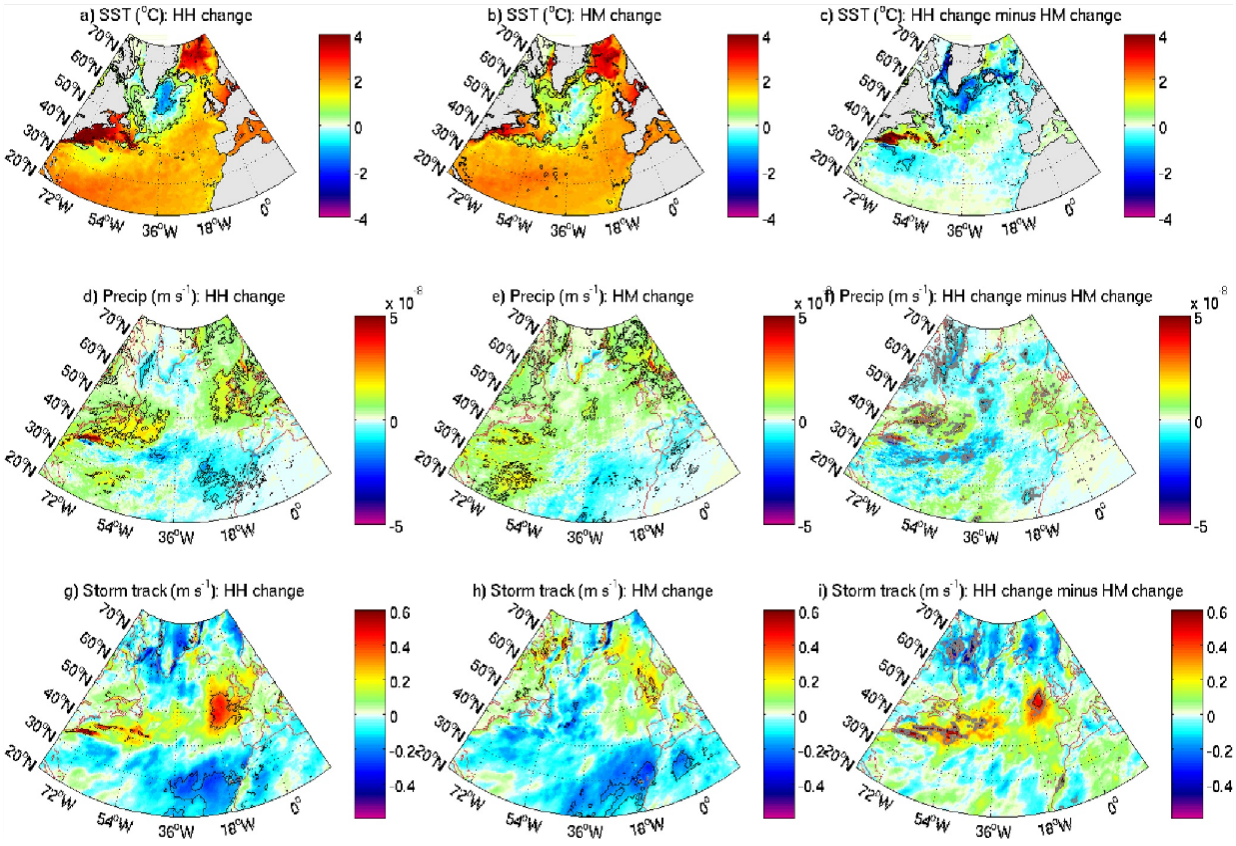

Figure 7: (a-c) 2031–2050 minus 1951–1970 differences simulated by the HadGEM3-GC3.1, with 25 km atmospheric resolution coupled to 1/4° ocean (eddy-permitting, HM) and 1/12° ocean (eddy-rich, HH): SST (°C) (a) HH and (b) HM, precipitation (ms^{-1}) (d) HH and (e) HM; surface storm track (ms^{-1}) (g) HH and (h) HM. Panels (c, f, i) show the difference between the HH future change and the HM change. The black lines denote the 95% significance. Gray lines in (c,f,i) denote the 90% significance. From Grist et al. (2021). The figure needs permission to reproduce.

The reorganization of the oceanic frontal zone and its associated eddy field modulates the atmospheric low-level baroclinicity and the strength and location of the diabatic heating source for the atmosphere. It is clear from this and other studies (Woollings et al. 2012; Winton et al. 2013; Keil et al. 2020) that such features would not occur without ocean circulation changes. However, the exact pattern of large-scale SST change is highly dependent on the ocean model and its resolution (Saba et al. 2016; Menary et al. 2018; Alexander et al. 2020), which also affects the projected WBC responses to climate change (Jackson et al. 2020). Climate projections with eddy-rich oceans have typically been performed with a small number of realizations and for short durations due to high computational costs (e.g., Haarsma et al. 2016). Currently, high-resolution coupled climate modeling projects are underway with much longer integration and multi-ensembles (e.g., Chang et al. 2020; Wengel et al. 2021). These efforts will enable a robust assessment of the forced responses in WBC and ocean circulation from natural variability in response to projected changes in the large-scale climate.

4. Feedback of atmospheric responses onto the ocean

The new insights gained from the studies discussed in Section 3 have also led to improved process understanding and notable revisions of theories of ocean circulation. This section discusses current knowledge of ocean feedback mechanisms, including feedback impacts on ocean biogeochemical cycles, and theories of ocean circulation and model parameterizations to account for eddy-atmosphere interaction. The processes covered in this section correspond mainly to Figures 1e,f.

a. Feedback on ocean circulation

For simplicity, we consider two categories of oceanic mesoscale effects on air-sea fluxes: SST impacts (thermal) described in Section 2b1 and surface current impacts (mechanical) in Section 2b2. The thermal feedback (TFB) results from kinematic and thermodynamic responses in the MABL to mesoscale SSTs, modifying the wind stress and heat fluxes. The current feedback (CFB) represents the frictional processes by which the surface ocean current alters the wind stress, near-surface wind, and turbulent heat fluxes. This subsection focuses on the respective feedback impacts of the air-sea fluxes on ocean circulation.

1) Thermal feedback (TFB) effect

Observed near-surface wind stress responses to mesoscale processes by Chelton et al. (2004) were interpreted based mainly on the TFB effect. Vecchi et al. (2004) and Chelton et al. (2007) hypothesized that the wind stress curl responses to SST fronts exert a vital feedback mechanism driving the evolution of SST fronts via resulting anomalous Ekman pumping. Spall (2007b) considered the impacts of SST-induced Ekman pumping on baroclinic instability in the ocean in the modified linear theory by Eady (1949), showing that the SST-induced Ekman pumping adjusts the growth rate and wavelength of the most unstable waves, especially the low-latitude flows with strong stratification. Hogg et al. (2009) extended SST-induced Ekman pumping to an idealized double-gyre circulation in mid-latitudes, showing that it destabilizes the eastward jet with the enhanced cross-gyre potential vorticity fluxes, stabilizing the double gyre circulation by 30-40%.

Mesoscale SSTAs are damped by induced turbulent heat fluxes (THF), resulting in a negative SST-THF correlation at oceanic mesoscales. Over the KOE, Ma et al. (2016) examined this mesoscale SSTA damping in the context of the eddy potential energy (EPE) budget and the Lorenz energy cycle. Compared to the eddy-filtered coupled model simulation (using a 1000 km-by-1000 km boxcar filter), the eddy-unfiltered simulations showed a significant increase (>70%) in diabatic EPE dissipation, leading to a decrease in eddy kinetic energy (EKE) by 20-40%, most strongly at wavelengths shorter than 100 km (Figure 1d). Other studies find that TFB has a weak impact on EKE (Seo et al. 2016; Seo 2017). It is possible that a large filter cutoff, as used in Ma et al. (2016), overestimates EKE damping and may also smooth large-scale meridional SST gradients, altering the large-scale wind curl and the mean circulation. Bishop et al. (2020) evaluated the EPE damping over the global oceans using eddy-resolving climate model simulations to find that the diabatic EPE damping was systematically stronger over warm-core eddies (Figure 1c,e). Other studies point out that the efficacy of the negative SST-THF correlation in the maintenance of the mesoscale SSTA and their gradients depends on the distribution of the mixed-layer depth, which modulates the effective heat capacity, vertical eddy heat transport, and hence the sensitivity of the SST to the heat flux anomaly (e.g., Tozuka et al. 2017; 2018; Jing et al. 2020).

2) Current feedback (CFB) effect

Although weaker than surface winds, surface currents modify surface stress directly by altering wind speed (Bye 1986). By modulating the stress, the CFB exerts a "bottom-up" effect on the wind, where a positive current anomaly causes a positive wind anomaly via a negative stress anomaly (Renault et al. 2016a; 2019a). The CFB effect has initially focused on impact on wind stress. Using satellite and in situ data, Kelly et al. (2001) showed that CFB reduces the median wind stress from 20% to 50% near the equator, and Chelton et al. (2004) observed a clear imprint of the Gulf Stream flow on the surface stress and the curl.

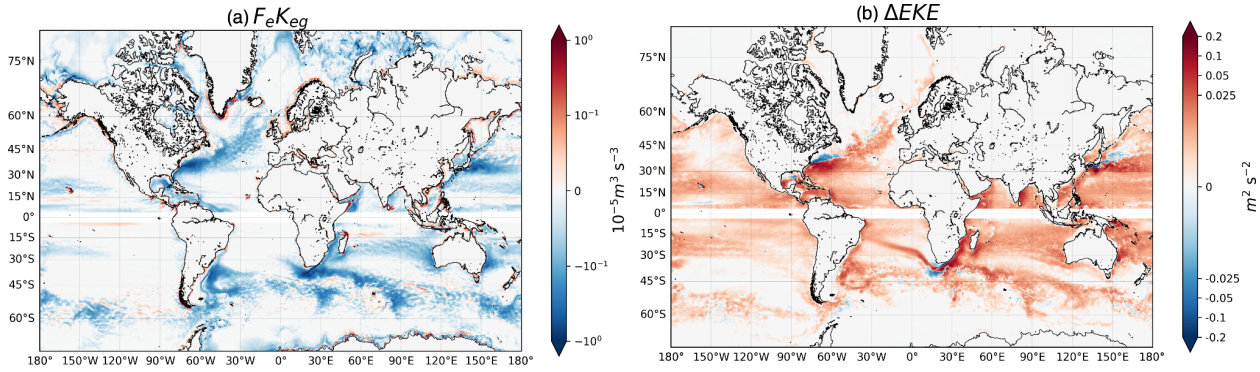

Figure 8: (a) Geostrophic eddy wind work (10^{-5} $m^3 s^{-3}$) estimated from the EC-Earth global coupled simulation (15 km atmosphere coupling 1/12° ocean) with current feedback (CFB). The negative values indicate a momentum transfer from geostrophic mesoscale currents to the atmosphere. This sink of energy is the primary driver of the damping of EKE illustrated in (b), as the difference of EKE ($m^2 s^{-2}$) between the simulations without CFB and with CFB. The positive values indicate the relative increase in EKE in the *absence* of CFB due to the transfer of the momentum to the atmosphere. The geostrophic wind work and EKE are both estimated over 30 years. Details about the coupled model and experiments can be found in Renault et al. (2019c).

Several studies have highlighted the role of CFB as a "top drag" (Dewar and Flierl 1987), acting on the oceanic circulation over a wide range of space-time scales. At the large-scale where the currents tend to flow downwind (Figure 1e), CFB reduces the mean energy input from the atmosphere to the ocean and slows down the mean circulation (Pacanowski et al. 1997). By weakening net energy input to the ocean, CFB triggers a host of changes in eddy-mean flow interactions and the inverse cascade of energy, weakening baroclinic and barotropic instabilities and mesoscale activity (Renault et al. 2017b, 2019a; Figure 8). When the wind and current are in the opposite sense, the CFB serves as a conduit of energy from the ocean to the atmosphere, which can be seen from satellite data as negative mean and eddy wind work (Figure 8a; Scott and Xu 2009; Renault et al. 2016a,b, 2017a). Numerous studies have demonstrated a strong EKE

836 damping effect of ~30% (See references in Jullien et al. 2020; Figure 8b). CFB also induces
837 additional Ekman pumping that weakens an eddy (Gaube et al. 2015) and influences the upper-
838 ocean stratification and SST (Seo et al. 2019; Song et al. 2020).
839
840 Recent studies also have emphasized the CFB impact on near-surface winds (Renault et al.
841 2016a, 2017a, 2019a). Over the shelf oceans where the current speed at tidal frequencies well
842 exceeds the wind speed, tidal currents induce tidal winds, with an amplitude of about one-third
843 of the underlying tidal currents (Renault and Marchesiello 2022). Since the wind curl is more
844 strongly impacted by current gradients (Shi and Bourassa 2019), the consideration of wind-
845 current coupling at tidal frequency might be necessary for the simulation and prediction of
846 surface winds and the MABL momentum EKE balances in the offshore environments.
847
848 There are several open questions. First, little is known about CFB at the submesoscale. For the
849 US West Coast, Renault et al. (2018) highlighted a submesoscale dual effect of CFB: it damps
850 submesoscale eddies but also catalyzes submesoscale current generation. By affecting mixing,
851 stratification, and eddy variability, Second, CFB modulates biogeochemical variability
852 (McGillicuddy et al. 2007), yet the detailed mechanisms behind the biogeochemical impacts are
853 not fully understood, although the impact depends highly on background stratification (e.g.,
854 Kwak et al. 2021). Finally, since CFB and TFB coexist where mesoscale currents are strong
855 (Song et al. 2006; Seo et al. 2007; Takatama and Schneider 2017; Renault et al. 2019b; Shi and
856 Bourassa 2019), CFB likely influences large-scale boundary-layer moisture, clouds,
857 precipitation, and atmospheric circulation via rectified effects. However, this downstream
858 influence is only beginning to be explored (e.g., Seo et al. 2021).
859
860 *b. Wave-current interactions near ocean fronts*
861 While sea state is a salient aspect of air-sea fluxes (Fairall et al. 1996; Cavaleri et al. 2012; Edson
862 et al. 2013), there are other aspects related to surface wave interactions with (sub)mesoscale
863 currents potentially important for small-scale air-sea interaction (Section 6c). For example, it has
864 long been known that sheared currents affect the propagation of surface wave rays (Villas Bôas
865 and Young 2020). In the open ocean, the spatial gradients in mesoscale surface currents
866 dominate the variability of significant wave height, leading to the refraction of waves near steep

vorticity gradients (Ardhuin et al. 2017; Villas Bôas et al. 2020). Similarly, the underpinnings of the Craik-Leibovich theory of Langmuir turbulence specify that rectification of wave-vorticity interactions in the upper ocean leads to Stokes forces, which can cause substantial wave effects on currents (Leibovich et al. 1983; Lane et al. 2007). The LES models that include vortex forces and regional models that include the wave refraction by currents (Romero et al. 2020) illustrate the frontal adjustment and frontogenesis triggered or enhanced by surface wave interactions (McWilliams and Fox-Kemper 2013; Suzuki et al. 2016; Sullivan and McWilliams 2019). Examples are provided in Figure 9 (upper panel), where a submesoscale density front in the downwind and down-Stokes direction interacts with Langmuir turbulence. Strong overturning circulation (downwelling) sharpens the front and strengthens the along-front jet. Classic balances are altered by waves to yield the wavy Ekman balance (McWilliams et al. 2012), the wavy geostrophic balance (McWilliams and Fox-Kemper 2013; Figure 9, lower panel), and the baroclinic and symmetric instabilities affected by waves (Haney et al. 2015).

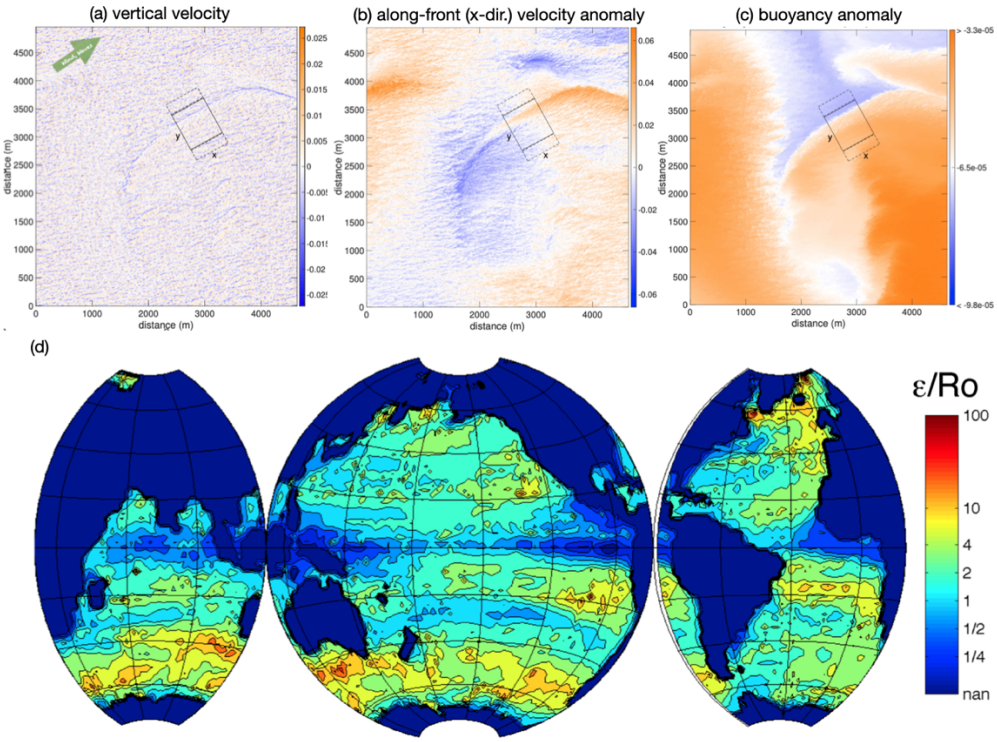

Figure 9: (Upper panel) Examples of a front interacting with Langmuir turbulence (box centered on this feature), which is aligned in the downwind and down-Stokes direction. (a) Vertical velocity (ms^{-1}) at z=-11.25m shows ubiquitous Langmuir cells, but also a long, coherent (downwelling) overturning circulation along the front due to frontogenesis and accelerated by the Stokes shear force. (b) Along-front (x-direction) velocity anomaly (with respect to the horizontal mean, ms^{-1}) at z=-11.25 m shows the frontal flow. (c) Buoyancy anomaly (with respect to the horizontal mean, ms^{-2}) at z=-11.25 shows the front characterized by a

sharp transition in buoyancy (or temperature). Adapted from Suzuki et al. (2016). (d) Estimated ratio of ε (strength of Stokes drift-induced vertical acceleration vs. buoyancy, an indicator of wave contributions added to the traditional hydrostatic balance) to Rossby number (indicating geostrophic balance). This ratio implies the deviation from the hydrostatic balance due to waves compared to the geostrophic balance due to advection. This estimate is based on the de Boyer-Montegut et al. (2004) mixed layer depth climatology (h) and a global simulation of WaveWatch3 and AVISO geostrophic velocity. Figures redrawn from McWilliams and Fox-Kemper (2013).

c. Physics of ocean mesoscale processes and air-sea interaction

Traditionally, mesoscale and submesoscale eddy parameterizations have been deterministic and focused only on effects on the mean and variance of tracers (Gent and McWilliams 1990; Fox-Kemper et al. 2011), while neglecting rectified effects on air-sea coupling. However, in simulations where some eddies are resolved, deterministic closures do not stimulate a resolved eddying response or backscatter (e.g., Bachman et al. 2020). In response, there is a growing desire to implement stochastic parameterizations of the eddy transport into non-eddy-resolving models, for example, via uncertainty in location (Memin 2014), transport (Drivas et al. 2020), closure (Nadiga 2008; Jansen and Held 2014; Zanna et al. 2017; Bachman et al. 2020), or equation of state (Brankart 2013). These efforts should include stochastic parameterizations of the eddy-driven air-sea coupling (Ma et al. 2016; Bishop et al. 2020; Jing et al. 2020). As stratification and rotation parameters vary globally, building scale awareness into parameterizations is also crucial (Hallberg 2013; Dong et al. 2020, 2021). Changing the relative orientation of atmospheric winds and oceanic fronts leads to qualitatively different results (e.g., enhancement *vs.* suppression of submesoscales, Figure 1f), implying that directional subgrid information will be necessary to consider (e.g., D'Asaro et al. 2011; Suzuki et al. 2016; McWilliams 2016). Observed air-sea fluxes are highly variable, indicating a response to high spatio-temporal variability (Yu 2019), scale dependence (Bishop et al. 2017, 2020), and sea state dependence (Kudryavtsev et al. 2014), thus offering the potential for stochastic implementation. While idealized studies have begun to develop a process-level understanding (Sullivan et al. 2020, 2021), no realistic model implementation of stochastic air-sea fluxes seems to have been evaluated carefully.

d. Impacts on primary productivity

Mesoscale air-sea interaction can also influence biogeochemical environments and primary productivity (e.g., McGillicuddy 2016). Satellite observations show that the wind stress

responses to mesoscale SST and currents introduce perturbation Ekman upwelling and downwelling (e.g., Gaube et al. 2015), leading to dramatic mid-ocean mesoscale plankton blooms, such as those observed in the nutrient-replete subtropics (e.g., McGillicuddy et al. 2007). Additionally, eddy-induced modifications of wind stress impact vertical mixing in the upper oceans. Eddy effects on mixed-layer depths are asymmetric between anticyclones and cyclones (e.g., Dufois et al. 2017; Hausmann et al. 2017). However, to what extent this asymmetry stems from the mesoscale modulations of surface wind stress has yet to be determined. Considering the prevalence and persistence of nonlinear mesoscale eddies in the global oceans (Chelton et al. 2011a,b), the relevance of mesoscale eddy impacts on primary productivity via eddy-wind interaction needs robust quantification.

5. State of observational capabilities

Observing mesoscale air-sea interaction processes is challenging since multiple oceanic and atmospheric parameters must be measured with high accuracy and spatio-temporal resolution. The past decade has seen the emergence of many novel in situ and remote sensing platforms that increasingly better capture mesoscale and smaller processes with high accuracy and resolution (e.g., Chapter 9 of Kessler et al. 2019). These novel observational technologies are expected to provide opportunities for multi-platform, coordinated measurements for air-sea interaction studies (e.g., Bony et al. 2017; Wang et al. 2018).

a. In situ observations

Oceanographic moorings can be equipped with meteorological instruments, including direct covariance flux systems and bulk meteorological sensors, to provide directly measured and bulk-estimated air-sea fluxes, respectively. An example system is shown in Figure 10 from the second Salinity Processes in the Upper-ocean Regional Study (SPURS-2) experiment, which computed and telemetered in near-real-time the motion-corrected surface wind stress and sensible and latent heat fluxes from a surface mooring for the first time (Clayson et al. 2019). There is overall a good qualitative agreement between the measured and estimated air-sea fluxes (Bigorre et al. 2013). However, the bulk formula method underestimates the momentum flux and overestimates the buoyancy flux under high wind conditions. These biases are categorically related to

deficiencies in formulations for the drag and heat transfer coefficients. Edson et al. (2013) revised the formulations for drag coefficient in COARE 3.5 to alleviate the low drag coefficient bias and proposed a new formula for heat transfer coefficients. Ayet and Chapron (2022) reviewed potential wave-atmospheric turbulence coupling mechanisms that allow for further refinements. Recently, buoy arrays have been deployed as part of the Ocean Observatories Initiative (OOI, Trowbridge et al. 2019) and operated for years on both coasts. These in situ data and the simultaneous measurements of surface meteorology and wave conditions are crucial to reducing the uncertainty in air-sea flux estimates in modern bulk formulas (Edson et al. 2013; Cronin et al. 2019; Villas-Boas et al. 2019).

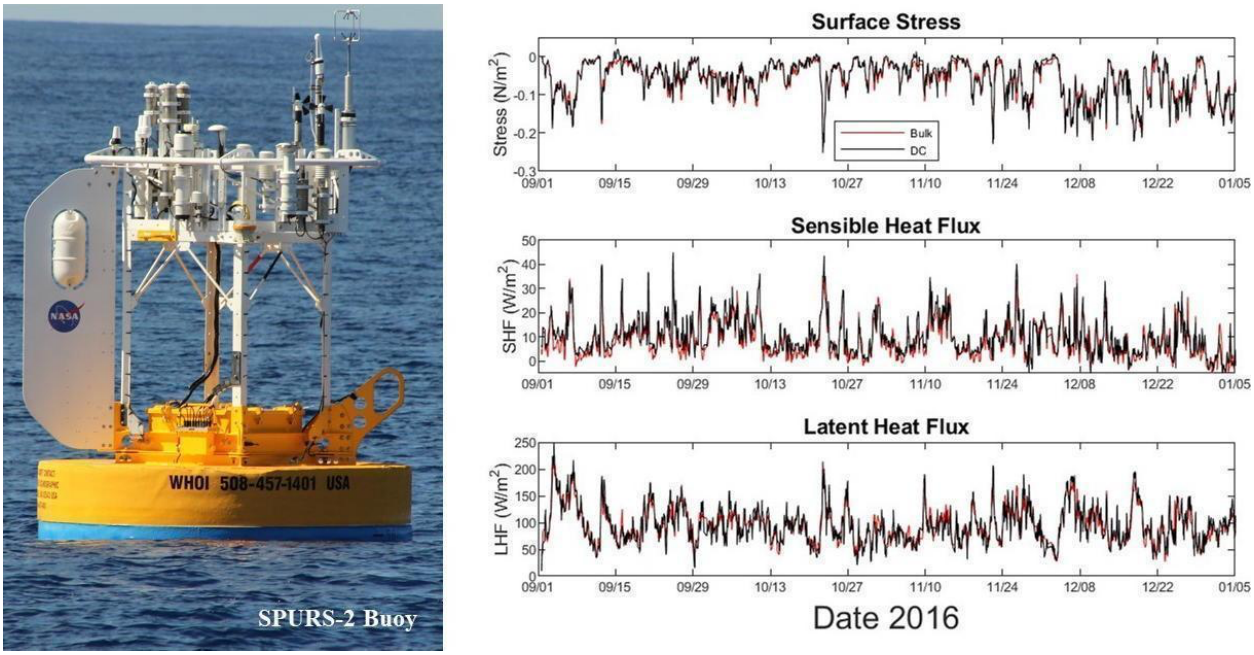

Figure 10: (left) The SPURS-2 central mooring with instrumentation at the upper right includes a sonic anemometer, infrared hygrometer, and sensors to remove buoy motion. The sensor package can directly measure the surface stress, sensible heat, and latent heat fluxes (See Clayson et al. 2019 for more details on instrumentations). (right) Time series of these fluxes showing bulk estimates in red and direct covariance (DC) fluxes in black. A good qualitative agreement is seen between the bulk and DC estimates, with the most significant discrepancies visible in the sensible heat flux (Bigorre et al. 2013). The coincident measurements of direct flux and bulk meteorology from SPURS-2 and prior field campaigns (e.g., CBLAST, DYNAMO, CLIMODE, etc.) are being used for improving the bulk flux algorithm for turbulent heat flux transfer coefficients. Photo by James B. Edson (WHOI).

Autonomous surface vehicles (ASVs) are piloted wave- or wind-propelled surface platforms that can be instrumented with ocean, atmospheric, and biogeochemical sensors. Widely-used ASVs

include Saildrones (Meinig et al. 2019) and Wave Gliders (Thomson and Girton 2017), which have long-endurance (~6 months) and can sample in remote locations and be piloted across fronts. Using numerous instruments can mitigate issues with cross-frontal sampling and thus capture mesoscale and smaller variations in air-sea interaction (Quinn et al. 2021; Stevens et al. 2021).

Drifting platforms can be instrumented with various sensors that capture air-sea interaction. The Global Drifter Program, a global network of surface drifters that typically measure currents, SST, and barometric pressure, has contributed to understanding global mesoscale circulation (Laurindo et al. 2017; Centurioni et al. 2019). Drifting spar buoys (Graber et al. 2000; Edson et al. 2013) have been measuring surface fluxes in situ for decades. In recent years, sophisticated low-profile Lagrangian platforms have been developed, such as SWIFTs (Thomson 2012), to measure surface currents, waves, and near-surface ocean turbulence over various wave conditions. Benefits of drifters include relatively low cost and Lagrangian sampling. However, they tend to converge at fronts; therefore, multiple drifters are necessary to characterize cross-frontal structure (D'Asaro et al. 2018).

Recent advancements in biologging technology may help facilitate autonomous measurements and real-time monitoring of essential ocean variables that may be important for air-sea interaction studies (Harcourt et al. 2019). As the biologging data can track mesoscale eddies and fronts in greater detail (Charrassin et al. 2008; Miyazawa et al. 2019) and can be assimilated into operational models (Yoda et al. 2014; Miyazawa et al. 2015), the application of animal-borne sensors has the potential to advance predictive capabilities of extratropical cyclones that strongly interact with the oceans (Section 3b).

Aircraft measurements are crucial for air-sea interaction studies. The platform's mobility is advantageous because of its ability to obtain in situ measurements of the horizontal and vertical variability in and above the MABL in a short time. With carefully designed flight patterns, it can also derive mesoscale forcing to the boundary layer using the velocity field measured at flight level (Lenschow et al. 1999; Stevens et al. 2003). In the past 20 years, air-deployable sensor packages such as GPS dropsondes, AXBT, AXCTD, and instrumented floats have further

expanded the sampling capability to depict the entire column of the atmosphere and the upper ocean, particularly when low-level flights are not feasible (Doyle et al. 2017). In recent years, airborne measurements have been extended to 10 m above the sea surface using a controlled towed vehicle (Wang et al. 2018). This new capability is significant to air-sea interaction studies, particularly surface flux parameterization.

b. Remote sensing

Emerging remote sensing platforms, including satellite, ground-based, or airborne measurements, present promising means to estimate air-sea fluxes at ocean mesoscale and smaller. Scatterometer and microwave measurements provide collocated global views of ocean vector winds and SST under all wind conditions at daily scales. However, considerable uncertainty exists under extreme conditions due to inconsistent in situ reference wind speeds from dropsondes and moored buoys to calibrate satellite winds (e.g., Polverari et al. 2021). This also implies uncertainties in modeling ocean drag and air-sea interaction. The virtual constellation of scatterometers (Stoffelen et al. 2019) provides good temporal coverage of the extremes, with now 7 scatterometers in space with revisits globally within 30 minutes or a few hours (Gade and Stoffelen 2019). Future satellite observations will need to resolve synoptic variability under strong wind and rain and increase the resolution of the vertical profiles within the MABL to better estimate the relationship between the surface flux and flux profiles.

For momentum fluxes, key variables are surface winds, currents, and waves. In coastal regions, high-frequency radar systems provide surface currents at O(1) km resolution (Kim 2010; Paduan and Washburn 2013; Kirincich et al. 2019), which can be used to infer surface wave conditions and wind stress (e.g., Saviano et al. 2021). The airborne DopplerScatt system simultaneously captures surface wind stress, waves, and currents (Wineteer et al. 2020) and is central to the Sub-Mesoscale Ocean Dynamics Experiment (S-MODE; Farrar et al. 2020). Similar concepts for new satellite observations have been proposed (see Villas Bôas et al. 2019) and are currently in various development stages (e.g., Bourassa et al. 2016; López-Dekker et al. 2019; Gommenginger et al. 2019; Wineteer et al. 2020). Surface waves are crucial for accurate estimates of momentum flux; new satellite missions such as CFOSAT (Chinese-French Oceanography Satellite) simultaneously measuring waves and winds (Ardhuin et al. 2019) are

expected to improve the accuracy of the wind-speed and wave-based formulations in the advanced bulk formula for air-sea flux. Satellite surface measurements of stress-equivalent winds more closely respond to stress than wind (e.g., de Kloe et al. 2017). Given the persistent large-scale and mesoscale errors in NWP reanalyses (Belmonte and Stoffelen 2019; Trindade et al. 2020), these new satellite observations collocated with in situ measurements of surface stress will be valuable for understanding stress-related air-sea coupling and improving ocean modeling and marine forecasting (Bourassa et al. 2019).

In contrast to momentum flux, a critical gap remains in the current satellite remote sensing capability to provide accurate global estimates of turbulent heat and moisture fluxes. Current satellite remote sensing systems rely on bulk parameterizations to estimate net heat and gas fluxes (Cronin et al. 2019). Mesoscale air-sea interaction studies will benefit significantly from a satellite mission that measures co-located, small-scale state variables, including near-surface atmospheric temperature and humidity, SST, and wind speed, that allow accurate estimates of the turbulent heat fluxes (e.g., Gentemann et al. 2020). This will also help validate the numerical models to lower the uncertainty in air-sea heat flux and improve related predictions.

6. Discussion and synthesis

Since the first global-scale surveys of the mesoscale air-sea interactions by Chelton et al. (2004) and Xie (2004), our theoretical understanding and observational and modeling capabilities in the past two decades have advanced significantly, leading to a substantial body of literature related to ocean mesoscale air-sea interaction. Our current scientific understanding indicates that mesoscale eddies perturb the MABL via surface flux anomalies, leading to dynamic and thermodynamic adjustments (Section 2; Figure 1d). The MABL response is communicated to the free troposphere, especially over WBCs (Figure 1b,c), influencing downstream development of weather and short-term climate events (Section 3; Figure 1a,b). The MABL response feeds back to the ocean circulation, modifying WBC dynamics, air-sea gas exchanges, and nutrient distribution (Section 4; Figure 1e,f). This new knowledge has transformed our classical understanding of physical processes, leading to notable revisions of oceanic and atmospheric circulation theories that incorporate the coupled effects of ocean mesoscale processes, wave, and

biogeochemical processes (Section 4). Our observing capability has advanced rapidly to characterize mesoscale air-sea interaction (Section 5). However, numerous challenges and open questions remain. The remainder of the chapter will focus on physical and biological aspects of modeling, observational, and diagnostic approaches that require further research in the coming years.

a. Attribution of near-surface wind convergence

While the WBC SST impact on the MABL dynamics is increasingly better understood, there are some critical remaining questions regarding the essential role of WBC SST forcing on the time-mean atmospheric state. The ongoing debates about the origin of the near-surface wind convergence (NSWC) and the maximum precipitation over WBCs are particularly relevant as they entail important implications pertinent to various aspects of the topics discussed in this article. That is, assessing whether the steady linear boundary layer dynamics account for the time-mean NSWC and vertical motion requires a detailed understanding of the modulation of boundary layer ageostrophic circulation by SST (Section 2; Figure 1d). On the other hand, the demonstrated impacts of storms and atmospheric fronts on the NSWC require a careful examination of extratropical cyclogenesis modulated by the diabatic forcing over the ocean fronts (Section 3; Figure 1b-c). Overall, any approach to quantifying the nature of the relationships between NSWC and SST will need to robustly separate the small magnitude convergence predicted by linear boundary layer theory from the large anomalous convergence induced by storm systems that are several orders of magnitude greater.

b. Robust diagnostic framework

The debate about the role of SST fronts in the NSWC arises partly due to the lack of a robust process-based diagnostics and analytic framework to interpret the observed convergence patterns. The existing analytical model of Schneider and Qiu (2015) discussed in Section 2c offers a complete account of the role of boundary layer dynamics over the SST fronts, providing the two limiting cases of wind response to SST dependent on background wind speed. The model also suggests an extension of the diagnostic framework from the widely used coupling coefficients to lagged regression, impulse response, or corresponding spectral transfer functions. Yet, the model assumes a quasi-steady state and does not account for the stochastic and moist

processes associated with the storm tracks and their synoptic-scale influence on NSWC. A critical path forward is to incorporate the time-dependent and moist processes related to extratropical storms along SST frontal zones and the local SST-induced boundary layer response in a single analytical framework. Given the coexistence of the SST and current feedback effects along the frontal zones, any future development of diagnostic frameworks will also have to consider the mechanical coupling effects simultaneously along with the thermal effects (e.g., Takatama and Schneider 2017; Seo 2017; Renault et al. 2019a).

c. Large-scale impacts in climate models

Numerous studies have demonstrated WBC impacts on downstream atmospheric circulation (Figure 1e). Some studies argue that the sharpness of WBC fronts shifts the storm track and jet stream, influencing the blocking frequency in Europe and Northeastern Pacific (e.g., Kuwano-Yoshida and Minobe 2017; O'Reilly et al. 2015, 2016, 2017; Piazza et al. 2016). Other studies find that meridional shifts of WBC fronts alter the atmospheric transient eddy heat flux downstream (e.g., Frankignoul et al. 2011; Kwon and Joyce 2013; Seo et al. 2017; Joyce et al. 2018). Warm-core eddies near the KOE act as significant oceanic sources of moisture and heat for large-scale circulation, altering downstream precipitation patterns (Ma et al. 2015, 2016; Liu et al. 2021). The importance of the seasonal background state in the atmosphere has also been recognized as it shapes the atmospheric response to SSTA (e.g., Taguchi et al. 2009; Huang et al. 2020).

However, some aspects of the far-field circulation response and its statistical significance remain elusive (Kushnir et al. 2002; Kwon et al. 2010; Czaja et al. 2019). Deriving a robust conclusion on downstream influences is particularly challenging difficult because the studies adopt different methods to define WBC SST impacts, leading to distinct amplitudes/patterns of SST perturbations and atmospheric responses. This uncertainty is in addition to differences in model climatologies. To date, the relative impacts of sharpness of SST gradient, its meridional shift, and activity of warm or cold-core eddies remain unquantified (Parfitt and Seo 2018). The importance of the coordinated modeling and diagnostic approaches regarding this specific point is emphasized in Section 6d.

d. Coordinated climate modeling and improved physical parameterizations

Significant progress can be made in understanding results and uncertainties in climate models of different complexity and resolutions via coordinated modeling experiments with resolutions at or beyond the ocean mesoscale and shared sets of diagnostics. The CMIP6 HighResMIP protocol (Haarsma et al. 2016) and PRIMAVERA project (Bellucci et al. 2021) well represent the community's interests in this direction. Analyses from a subset of these models reveal significant model resolution sensitivity (especially in the oceans) of the simulated air-sea interaction and climate regimes in the extratropics (e.g., Jullien et al. 2020; Moreton et al. 2021). Further advances in model resolution, for example, DYAMOND (Stevens et al. 2019) and the planned HighResMIP2, together with programs such as OASIS (Observing Air-Sea Interaction Strategy, https://airseaobs.org) that aims to bring observations and models closer together, will build on these previous efforts and provide further insights into the fidelity of modeled mesoscale air-sea interactions. Furthermore, in the ocean and coupled models where the ocean eddies are not fully or only partially resolved, their rectified effects on the air-sea heat, momentum, and tracer fluxes are not currently parameterized. Various stochastic representations of eddy transports are being tested and implemented (Section 4c), which can potentially address this issue of low-frequency rectification effects by eddies on large-scale climate via air-sea interaction. (e.g., Siqueira and Kirtman 2016).

e. Air-sea interaction mediated by ocean submesoscale and sea state

The ocean submesoscale processes with length-scales smaller than ~10 km are essential for the ocean energy cycle (Lorenz 1960), global heat balance (Su et al. 2018), and marine biogeochemistry and ecosystems (Omand et al. 2015; Lévy et al. 2018). While the dynamics of the submesoscale ocean instabilities are becoming better understood (e.g., Fox-Kemper et al. 2008; D'Asaro et al. 2011), their direct impact on the MABL and heat and carbon uptake by the oceans (e.g., Johnson et al. 2016; Bachman et al. 2017; du Plessis et al. 2019) remain poorly understood. Thus far, only a few satellite-based studies provide direct observational evidence of relative wind stress response to submesoscale SST fronts (e.g., Beal et al. 1997; Xie et al. 2010; Gaube et al. 2019; Ayet et al. 2021), although prior in situ observational studies have long documented such interactions in localized regions (e.g., Sweet et al. 1981; Friehe et al. 1991; Mahrt et al. 2004). While results from high-resolution numerical simulations (e.g., LES) indicate

submesoscale SST-driven MABL dynamics (Skyllingstad et al. 2007; Lambaert et al. 2013; Wenegrat and Arthur 2018; Lac et al. 2018; Sullivan et al. 2020, 2021), they also recognize the importance of advection and convective organization in characterizing the nonlinear MABL dynamics that co-occur at the submesoscale. As for the oceanic impact, the ocean current feedback dominates the wind stress response at the submesoscale, influencing the kinetic energy cascade (Renault et al. 2018). Spatial variability in sea state and surface roughness is enhanced at the submesoscale, and hence wave-current interactions (e.g., Villas Bôas and Pizzo 2021) and wave-wind interactions (e.g., Deskos et al. 2021) are expected to be critical in determining wind stress, heat flux, and MABL variations (Ayet et al. 2021; Section 4b), yet such processes remain poorly observed, understood, and parameterized. Emerging in situ and satellite observations for near-surface processes (Section 5), combined with dedicated atmospheric and oceanic LES and high-resolution modeling studies, will help improve the physical understanding of air-sea interactions at the submesoscale.

f. Air-sea gas flux exchange and ocean biogeochemistry processes

Estimates of air-sea gas exchange do not fully consider the effects of ocean mesoscale eddies and fronts. One issue is that the gas transfer velocity typically does not consider wind variations introduced by mesoscale air-sea interactions. The transfer velocity is also often based on wind speed (e.g., Wanninkhof 1992). Hence, it only implicitly accounts for the sea state variations. Studies with parameterizations that consider bubble-mediated gas exchanges due to breaking waves (e.g., Frew et al. 2007; Deike and Melville 2018) reveal their significant contribution to regionally-integrated CO_2 flux, especially under midlatitude storm tracks (e.g., Reichl and Deike 2020). To accurately represent the sea state influence modulated by mesoscale processes in the transfer velocity-based flux parameterization (e.g., Fairall et al. 2011; Edson et al. 2011), it is imperative to increase direct measurements of CO_2 flux (e.g., McGillis et al. 2001) along with the coincident observations of wind, waves, solubility, and air-sea partial CO_2 pressure differences.

Further, mesoscale air-sea interaction feeds back to ocean primary productivity (Lévy 2008; McGillicuddy et al. 2016) and tracer concentrations, such as carbon. Since the physical properties of mesoscale eddies and their relationships with biogeochemical variables vary widely

by region (e.g., Chelton et al. 2011; Gaube et al. 2013, 2014; Frenger et al. 2018), future work should aim to identify the specific aspects of this regional variability that are due to mesoscale air-sea interaction and subsequent impacts on upwelling and vertical mixing. Eddy-rich climate model simulations are one avenue to gain quantitative insight into the relevance of the complex coupling of ocean mesoscale features, biogeochemistry, and the atmosphere. Few such simulations exist due to their computational expense (e.g., Harrison et al. 2018), but we expect this to change in the coming years. Dedicated field experiments combined with eddy-resolving coupled physical-biogeochemical models are critical to determining what aspects of mesoscale air-sea interactions need to be considered and represented in non-eddy-resolving models.

g. Final remarks

Prospects for significant advances in mesoscale air-sea interaction in the coming years are incredibly bright. Strong community efforts and enthusiasm exist for building sustained observational networks to characterize detailed physical and biogeochemical processes across the air-sea coupled boundary layers (e.g., OceanObs'19 White Papers; OASIS; US CLIVAR's air-sea interaction research initiatives). New satellite missions with advanced instrument technology and retrieval algorithms will continue to improve our capability to monitor state variables pertinent to air-sea interactions at fine scales and with increased accuracy. These new observations will lead to updated physical parameterizations that are becoming increasingly more scale-aware and that can be potentially built with stochastic schemes that account for rectified effects of eddy transports on air-sea flux and large scales. More field experiments are being coordinated via close integration with process-oriented and data assimilative modeling to help not only develop the sampling plans but also improve the parameterizations and skills in prediction models (e.g., Cronin et al. 2009; Cravatte et al. 2016; Kessler et al. 2019; Sprintall et al. 2020; Shroyer et al. 2021; Shinoda et al. 2021; Newman et al. 2022). The climate modeling community is developing and refining high-resolution Earth system model simulations with advanced physical parametrizations. International partnership and coordination are becoming increasingly solid, enabling the design of multi-model, multi-ensemble, high-resolution coupled modeling protocols and diagnostic frameworks. The identified common biases in mesoscale air-sea interaction in such climate models, in turn, guide the sampling strategy of observing systems and process studies. Ensemble data assimilation systems are rapidly advancing, yielding more

accurate observationally constrained ocean, atmosphere, and biogeochemical state estimates critical for sub-seasonal to decadal predictions (e.g., Penny and Hamill 2017; Verdy and Mazloff 2017). Overall, the successful coordination across observations, modeling, and theories has been critical, and these coordinated efforts will and should continue to enhance Earth system prediction skills across scales from weather forecasts to climate projection scales.

Acknowledgments

The authors of the paper are the scientists participating in the US CLIVAR Working Group on *Mesoscale and frontal-scale ocean-atmosphere interactions and influence on large-scale climate*. The authors thank Mike Patterson, Jennie Zhu, and Sam Coakley at US CLIVAR for sponsoring and supporting the Working Group activities. The authors thank Dr. Kuwano-Yoshida and two anonymous reviewers for their constructive comments. We also thank Natalie Renier at the WHOI Creative Studio for her assistance with scientific illustrations. Seo acknowledges support from NSF (OCE-2022846, OCE-2148120), NOAA (NA19OAR4310376), NASA (80NSSC21K1524), and WHOI (Francis E. Fowler IV Center for Ocean and Climate).

Data Availability Statement

Datasets used in the figures are based on ERA5 (Hersbach et al. 2020), NOAA OI SST (Reynolds et al. 2007), climate model simulations from the HighResMIP (Haarsma et al. 2016), or already published papers as cited in the figure captions.

References

Alexander, M. A., and J. D. Scott, 1997: Surface flux variability over the North Pacific and North Atlantic Oceans. *J. Climate*, **10**, 2963-2978.

Alexander, M. A., S. Shin, J. D. Scott, E. Curchitser, and C. Stock, 2020: The Response of the Northwest Atlantic Ocean to Climate Change. *J. Climate*, **33**, 405-428.

Ardhuin, F., S. T. Gille, D. Menemenlis, C. B. Rocha, N. Rascle, B. Chapron, J. Gula, and J. Molemaker, 2017: Small-scale open ocean currents have large effects on wind wave heights. *J. Geophys. Res. Oceans,* **122**, 4500–4517.

Ardhuin, F., and Coauthors, 2019: Observing Sea States. *Front. Mar. Sci*. **6**, 124.

Ayet, A., B. Chapron, 2022: The Dynamical Coupling of Wind-Waves and Atmospheric Turbulence: A Review of Theoretical and Phenomenological Models. *Boundary-Layer Meteorol*., **183**, 1–33.

Ayet, A., N. Rascle, B. Chapron, F. Couvreux, and L. Terray, 2021: Uncovering air-sea interaction in oceanic submesoscale frontal regions using high-resolution satellite observations. *US CLIVAR Variations*, **19**, 10-17.

Bachman, S. D., J. R. Taylor, K. A. Adams, and P. J. Hosegood, 2017: Mesoscale and Submesoscale Effects on Mixed Layer Depth in the Southern Ocean. *J. Phys. Oceanogr*, **47**, 2173-2188.

Bachman, S. D., B. Fox-Kemper, and F. O. Bryan, 2020: A diagnosis of anisotropic eddy diffusion from a high-resolution global ocean model. *J. Adv. Model. Earth Syst.*, **12**, e2019MS001904.

Battisti, D., E. Sarachik, and A. Hirst, 1999: A consistent model for the large-scale steady surface atmospheric circulation in the tropics. *J. Climate*, **12**, 2956–2964.

Beal, R. C., V. N. Kudryavtsev, D. R. Thompson, S. A. Grodsky, D. G. Tilley, V. A. Dulov, and H. C. Graber, 1997: The influence of the marine atmospheric boundary layer on ERS 1 synthetic aperture radar imagery of the Gulf Stream. *J. Geophys. Res.*, **102**, 5799– 5814.

Bellucci, A., Athanasiadis, P., Scoccimarro, E., Ruggieri, P., Gualdi, S., Fedele, R., Haarsma, R. J., Garcia-Serrano, J., Castrillo, M., Putrasahan, D., Sanchez-Gomez E., Moine, M.-P., Roberts, C. D.,Roberts, M. J., Seddon, J., and Vidale, P. L., 2021: Air-Sea interaction over the Gulf Stream in an ensemble of HighResMIP present climate simulations. *Clim Dyn*., **56**, 2093–2111.

1286 Belmonte Rivas, M., and A. Stoffelen, 2019: Characterizing ERA-interim and ERA5 surface
1287 wind biases using ASCAT. *Ocean Sci. Discuss.,* **15**, 831–852.
1288 Bigorre, S, R. A. Weller, J. Lord, J. B. Edson and J. D. Ware, 2013: A surface mooring for air-
1289 sea interaction research in the Gulf Stream. Part 2: Analysis of the observations and their
1290 accuracies. *J. Atmos. Oceanic Tech*., **30**, 450–469.
1291 Bilgen, S. I., and B. P. Kirtman, 2020: Impact of ocean model resolution on understanding the
1292 delayed warming of the Southern Ocean. *Environ. Res. Lett*., **15**, 114012.
1293 Bishop, S. P., R. J. Small, F. O. Bryan, and R. A. Tomas, 2017: Scale dependence of mid-latitude
1294 air-sea interaction. *J. Climate*, **30**, 8207–8221.
1295 Bishop, S. P., R. J. Small, and F. O. Bryan, 2020: The global sink of available potential energy
1296 by mesoscale air-sea interaction. *J. Adv. Model. Earth Syst.*, **12**, e2020MS002118.
1297 Bladé, I., 1997: The Influence of Midlatitude Ocean-Atmosphere Coupling on the Low-
1298 Frequency Variability of a GCM. Part I: No Tropical SST Forcing. *J. Climate*, **10**, 2087-
1299 2106.
1300 Bony, S., Stevens, B., Ament, F. et al., 2017: EUREC4A: A Field Campaign to Elucidate the
1301 Couplings Between Clouds, Convection and Circulation. *Surv. Geophys.*, **38**, 1529–1568.
1302 Bourassa, M. A., and Coauthors, 2013: High-latitude ocean and sea ice surface fluxes:
1303 requirements and challenges for climate research. *Bull. Amer. Meteo. Soc.,* **94**, 403–423.
1304 Bourassa, M. A., E. Rodríguez, and D. B. Chelton, 2016: Winds and Currents Mission: Ability to
1305 observe mesoscale AIR/SEA coupling. *Geosci. and Remote Sens. Symposium (IGARSS)*,
1306 doi: 10.1109/IGARSS.2016.7730928.
1307 Bourassa, M. A., and Coauthors 2019: Remotely Sensed Winds and Wind Stresses for Marine
1308 Forecasting and Ocean Modeling. *Front. Mar. Sci.,* **6**, 443.
1309 Booth, J. F., L. Thompson, J. Patoux, K. A. Kelly, and S. Dickinson, 2010: The signature of
1310 midlatitude tropospheric storm tracks in the surface winds. *J. Climate*, **23**, 1160–1174.
1311 Booth, J. F., L. Thompson, J. Patoux, and K. A. Kelly, 2012: Sensitivity of midlatitude
1312 storm intensification to perturbations in the sea surface temperature near the Gulf Stream.
1313 *Mon. Wea. Rev*., **140**, 1241–1256.
1314 Booth, J. F., Y. O. Kwon, S. Ko, R. J. Small, and R. Msadek, 2017: Spatial patterns and intensity
1315 of the surface storm tracks in CMIP5 models. *J. Climate*, **30**, 4965–4981.

1316 Brachet, S., F. Codron, Y. Feliks, M. Ghil, H. Le Treut, and E. Simonnet, 2012:
1317 Atmospheric Circulations Induced by a Midlatitude SST Front: A GCM Study. *J.*
1318 *Climate*, **25**, 1847–1853.
1319 Brankart, J.-M., 2013: Impact of uncertainties in the horizontal density gradient upon low
1320 resolution global ocean modelling. *Ocean Modell*., **66**, 64-76.
1321 Bryan, F. O., R. Tomas, J. M. Dennis, D. B. Chelton, N. G. Loeb, and J. L. McClean, 2010:
1322 Frontal Scale Air-Sea Interaction in High-Resolution Coupled Climate Models. *J.*
1323 *Climate*, **23**, 6277-6291.
1324 Bye, J. A. T., 1986: Momentum exchange at the sea surface by wind stress and understress.
1325 *Quart. J. Roy. Met. Soc.,* **112**, 501–510.
1326 Byrne, D, L Papritz, I Frenger, M Münnich, and N Gruber. 2015 Atmospheric Response to
1327 Mesoscale Sea Surface Temperature Anomalies: Assessment of Mechanisms and
1328 Coupling Strength in a High-Resolution Coupled Model over the South Atlantic. *J.*
1329 *Atmos. Sci.,* 72, 1872-1890.
1330 Cavaleri, L., B. Fox-Kemper, and M. Hemer, 2012: Wind waves in the coupled climate
1331 system. *Bull. Amer. Meteorol. Soc.*, **93**, 1651–1661.
1332 Centurioni, L. R. and Coauthors, 2019: Global in situ Observations of Essential Climate and
1333 Ocean Variables at the Air-Sea Interface. *Front. Mar. Sci*., **6**, 419.
1334 Chang, E. K. M., 1993: Downstream development of baroclinic waves as inferred from
1335 regression analysis. *J. Atmos. Sci*., **50**, 2038–2053.
1336 Chang, E. K. M., and I. Olanski, 1993: On the dynamics of a storm track. *J. Atmos. Sci*., **50**, 999–
1337 1015.
1338 Chang, E. K. M., S. Lee, and K. L. Swanson, 2002. Storm Track Dynamics. *J. Climate,* **15**,
1339 2163-2183.Chang, P., and Coauthors, 2020: An unprecedented set of high-resolution
1340 Earth system simulations for understanding multiscale interactions in climate variability
1341 and change. *J. Adv. Model. Earth Sys*. **12**, e2020MS002298.
1342 Charney, J. G., 1947: The dynamics of long waves in a baroclinic westerly current. *J.*
1343 *Meteor.*, **4**, 135–162.
1344 Charrassin, J. B., and Coauthors, 2008: Southern Ocean frontal structure and sea-ice formation
1345 rates revealed by elephant seals. *Proc. Natl. Acad. Sci*., **105**, 11634–11639.

1346 Chelton, D. B., and Coauthors, 2001: Observations of coupling between surface wind stress and
1347 sea surface temperature in the eastern tropical Pacific. *J. Climate,* **14**, 1479–1498.
1348 Chelton, D. B., M. G. Schlax, M. H. Freilich, and R. F. Milliff, 2004: Satellite measurements
1349 reveal persistent small-scale features in ocean winds. *Science*, **303**, 978–983.
1350 Chelton, D. B., 2005: The Impact of SST Specification on ECMWF Surface Wind Stress Fields
1351 in the Eastern Tropical Pacific. *J. Climate*, **18**, 530-550.
1352 Chelton, D. B., M. G. Schlax and R. M. Samelson, 2007: Summertime Coupling between Sea
1353 Surface Temperature and Wind Stress in the California Current System. *J. Phys.*
1354 *Oceanogr.*, **37**, 495-517.
1355 Chelton, D. B., and S.-P. Xie, 2010: Coupled ocean-atmosphere interaction at oceanic
1356 mesoscales. *Oceanogr.*, **23**, 52-69.
1357 Chelton, D. B., P. Gaube, M. G. Schlax, J. J. Early, and R. M. Samelson, 2011a: The Influence
1358 of Nonlinear Mesoscale Eddies on Near-Surface Oceanic Chlorophyll. *Science*, **334**,
1359 328–332.
1360 Chelton, D. B., M. G. Schlax, and R. M. Samelson, 2011b: Global observations of nonlinear
1361 mesoscale eddies. *Prog. Oceanogr.*, **91**, 167-216.
1362 Clayson, C. A., J. B. Edson, A. Paget, R. Graham, and B. Greenwood, 2019: The effects of
1363 rainfall on the atmosphere and the ocean during SPURS-2. *Oceanogr.*, **32**, 86–97.
1364 Cravatte, S., W. S. Kessler, N. Smith, S. E. Wijffels, and Contributing Authors, 2016: First
1365 Report of TPOS 2020. GOOS-215, 200 pp. [Available online at http://tpos2020.org/first-
1366 report/.]
1367 Cronin, M. F., S.-P. Xie, and H. Hashizume, 2003: Barometric pressure variations associated
1368 with eastern Pacific tropical instability waves. *J. Climate*, **16**, 3050- 3057.
1369 Cronin, M. F., S. Legg, and P. Zuidema, 2009: Best practices for process studies. *Bull. Amer.*
1370 *Meteor. Soc.*, **90**, 917–918.
1371 Cronin, M. F., and Coauthors, 2019: Air-Sea Fluxes with a Focus on Heat and Momentum.
1372 *Front. Mar. Sci.*, **6**, 430.
1373 Czaja, A., and N. Blunt, 2011: A new mechanism for ocean-atmosphere coupling in
1374 midlatitudes. *Quart. J. Roy. Met. Soc.,* **137**, 1095–1101.

Czaja, A., C. Frankignoul, S. Minobe, and B. Vannière, 2019: Simulating the Midlatitude Atmospheric Circulation: What Might We Gain From High-Resolution Modeling of Air-Sea Interactions? *Curr. Clim. Change Rep.*, **5**, 390–406.

D'Asaro, E., C. Lee, L. Rainville, R. Harcourt, and L. Thomas, 2011: Enhanced Turbulence and Energy Dissipation at Ocean Fronts. *Science*, **332**, 318-322.

D'Asaro, E. A., 2014: Turbulence in the Upper-Ocean Mixed Layer, *Annu. Rev. Mar. Sci*., **6**, 101–15.

D'Asaro, E., and Coauthors, 2018: Ocean convergence and dispersion of flotsam. *Proc. Natl. Acad. Sci.,* **115**, 1162–1167.

Davis, C. A., and K. A. Emanuel, 1988: Observational Evidence for the Influence of Surface Heat Fluxes on Rapid Maritime Cyclogenesis. *Mon. Wea. Rev*., **116**, 2649-2659.

de Boyer Montégut, C., G. Madec, A. S. Fischer, A. Lazar, and D. Iudicone, 2004: Mixed layer depth over the global ocean: An examination of profile data and a profile-based climatology. *J. Geophys. Res*., **109**, C12003.

de Kloe, J., A. Stoffelen, and A. Verhoef, 2017: Improved use of scatterometer measurements by using stress-equivalent reference winds. *IEEE J. Sel. Top. Appl. Earth Observ. Remote Sens*., **10**, 2340–2347.

de Szoeke, S. P., and C. S. Bretherton, 2004: Quasi-Lagrangian large eddy simulations of cross-equatorial flow in the east Pacific atmospheric boundary layer. *J. Atmos. Sci*., **61**, 1837-1858.

de Szoeke, S. P., and E. D. Maloney, 2020: Atmospheric Mixed Layer Convergence from Observed MJO Sea Surface Temperature Anomalies. *J. Climate*, **33**, 547-558.

de Szoeke, S. P., J. B. Edson, J. R. Marion, C. W. Fairall, and L. Bariteau, 2015: The MJO and Air–Sea Interaction in TOGA COARE and DYNAMO. *J. Climate*, 28, 597–622.

de Szoeke, S. P., E. D. Skyllingstad, P. Zuidema, and A. S. Chandra, 2017: Cold pools and their influence on the tropical marine boundary layer, *J. Atmos. Sci*., **74**, 1149-1168.

Deike, L., and W. K. Melville, 2018: Gas transfer by breaking waves. *Geophys. Res. Lett.*, **45**, 10,482–10,492.

Deser, C., J. J. Bates, and S. Wahl, 1993: The influence of sea surface temperature gradients on stratiform cloudiness along the equatorial front in the Pacific Ocean. *J. Climate*, **6**, 1172–1180.

1406 Deser, C., R. A. Tomas, and S. Peng, 2007: The Transient Atmospheric Circulation Response to
1407 North Atlantic SST and Sea Ice Anomalies. *J. Climate*, **20**, 4751-4767.
1408 Deskos, G., J. C. Y. Lee, C. Draxl, and M. A. Sprague, 2021: Review of wind-wave coupling
1409 models for large-eddy simulation of the marine atmospheric boundary layer. *J. Atmos.*
1410 *Sci*., **78**, 3025-3045
1411 Dewar, W., and G. Flierl, 1987: Some effects of the wind on rings. *J. Phys. Oceanogr*., **17**,
1412 1653–1667.
1413 Domingues R, and Coauthors, 2019: Ocean Observations in Support of Studies and Forecasts of
1414 Tropical and Extratropical Cyclones. *Front. Mar. Sci*., **6**, 446.
1415 Dong, J., B. Fox-Kemper, H. Zhang, and C. Dong, 2020: The scale of submesoscale baroclinic
1416 instability globally. *J. Phys. Oceanogr.*, **50**, 2649–2667.
1417 Dong, J., B. Fox-Kemper, H. Zhang, and C. Dong, 2021: The Scale and Activity of Symmetric
1418 Instability Estimated from a Global Submesoscale-Permitting Ocean Model. *J. Phys.*
1419 *Oceanogr*., **51**, 1655-1670.
1420 Doyle, J. D., and Coauthors, 2017: A view of tropical cyclones from above: The Tropical
1421 Cyclone Intensity Experiment. *Bull. Amer. Meteor. Soc*., **98**, 2113–2134.
1422 Drivas, T. D., D. D. Holm, and J. M. Leahy, 2020: Lagrangian Averaged Stochastic Advection
1423 by Lie Transport for Fluids. *J. Stat. Phys.,* **179**, 1304–1342.
1424 du Plessis, M., S. Swart, I. J. Ansorge, A. Mahadevan, and A. F. Thompson, 2019: Southern
1425 Ocean Seasonal Restratification Delayed by Submesoscale Wind–Front Interactions. *J.*
1426 *Phys. Oceanog*r., **49**, 1035-1053.
1427 Dufois, F., N. J. Hardman-Mountford, M. Fernandes, B. Wojtasiewicz, D. Shenoy, D. Slawinski,
1428 M. Gauns, J. Greenwood, and R. Toresen, 2017: Observational insights into chlorophyll
1429 distributions of subtropical South Indian Ocean eddies. *Geophys. Res. Lett.*, **44**, 3255–
1430 3264.
1431 Eady, E., 1949: Long waves and cyclone waves. *Tellus*, **1**, 33–52.
1432 Edson, J. B., and C. W. Fairall, 1998: Similarity relationships in the marine atmospheric surface
1433 layer for terms in the TKE and scalar variance budgets. *J. Atmos. Sci.,* **55**, 2311– 2328.
1434 Edson, J., and Coauthors, 2007: The coupled boundary layers and air-sea transfer experiment in
1435 low winds. *Bull. Amer. Meteor. Soc*., **88**, 341-356.

1436 Edson, J. B., C. W. Fairall, L. Bariteau, C. J. Zappa, A. Cifuentes-Lorenzen, W. M. McGillis, S.
1437 Pezoa, J. E. Hare, and D. Helmig, 2011: Direct-covariance measurement of CO2 gas
1438 transfer velocity during the 2008 Southern Ocean Gas Exchange Experiment. *J. Geophys.*
1439 *Res*., **116**, C00F10.
1440 Edson, J. B., V. Jampana, R. Weller, S. Bigorre, A. Plueddemann, C. Fairall, S. Miller, L.
1441 Mahrt, D. Vickers, and H. Hersbach, 2013: On the exchange of momentum over the open
1442 ocean. *J. Phys. Oceanogr*., **43**, 1589–1610.
1443 Fairall C. W., E. F. Bradley, D. P. Rogers, J. D. Edson, and G. S. Young, 1996: Bulk
1444 parameterization of air-sea fluxes for Tropical Ocean Global Atmosphere Coupled-Ocean
1445 Atmosphere Response Experiment. *J. Geophys. Res.*, **15**, 3747-3764.
1446 Fairall, C.W., E.F. Bradley, J.E. Hare, A.A. Grachev, and J.B. Edson, 2003: Bulk
1447 parameterization of air-sea fluxes: Updates and verification for the COARE algorithm. *J.*
1448 *Climate*, **16**, 571-591.
1449 Fairall, C. W., M. Yang, L. Bariteau, J. B. Edson, D. Helmig, W. McGillis, S. Pezoa, J. E. Hare,
1450 B. Huebert, and B. Blomquist, 2011: Implementation of the COARE algorithm with O3,
1451 CO2 and DMS. *J. Geophys. Res.*, **116**, C00F09.
1452 Farrar, J. T., and Coauthors, 2020: S-MODE: The Sub-Mesoscale Ocean Dynamics Experiment.
1453 *IGARSS 2020-2020 IEEE International Geoscience and Remote Sensing Symposium*.
1454 3533-3536. 10.1109/IGARSS39084.2020.9323112.
1455 Feliks, Y., M. Ghil, and E. Simonnet, 2004: Low-frequency variability in the midlatitude
1456 atmosphere induced by an oceanic thermal front. *J. Atmos. Sci*., **61**, 961–981.
1457 Ferreira, D., and C. Frankignoul, 2005: The transient atmospheric response to midlatitude SST
1458 anomalies. *J. Climate*, **18**, 1049-1067.
1459 Ferreira, D., and C. Frankignoul, 2008: Transient atmospheric response to interactive SST
1460 anomalies. *J. Climate*, **21**, 584-592.
1461 Fox-Kemper, B., R. Ferrari, and R. Hallberg, 2008: Parameterization of mixed layer eddies. I:
1462 Theory and diagnosis. *J. Phys. Oceanogr.*, **38**, 1145-1165.
1463 Fox-Kemper, B., G. Danabasoglu, R. Ferrari, S. M. Griffies, R. W. Hallberg, M. M. Holland, M.
1464 E. Maltrud, S. Peacock, and B. L. Samuels, 2011: Parameterization of mixed layer
1465 eddies. III: Implementation and impact in global ocean climate simulations. *Ocean*
1466 *Modell*., **39**, 61-78.

1467 Fox-Kemper, B., S. Marsland, E. Chassignet, E. Curchitser, S. Griffies, I. Montes, H. Seo, A. M.
1468 Treguier, and W. Weijer, 2019: Sources and sinks of ocean mesoscale eddy energy. 5,
1469 page 21. A Joint US CLIVAR and CLIVAR Workshop Report. Available from
1470 http://dx.doi.org/10.5065/CH5R-5034.
1471 Fox-Kemper, B., L. Johnson, and F. Qiao, 2022: Ocean Mixing. Chapter 4. Ocean Near-Surface
1472 Layers, 65-94, Elsevier. https://doi.org/10.1016/B978-0-12-821512-8.00011-6
1473 Foussard, A., G. Lapeyre, and R. Plougonven, 2019a: Response of surface wind divergence to
1474 mesoscale SST anomalies under different wind conditions. *J. Atmos. Sci.*, **76**, 2065-2082.
1475 Foussard, A., G. Lapeyre, and R. Plougonven, 2019b: Storm Track Response to Oceanic Eddies
1476 in Idealized Atmospheric Simulations. *J. Climate*, **32**, 445-463.
1477 Frankignoul, C., 1985: Sea surface temperature anomalies, planetary waves, and air-sea feedback
1478 in midlatitudes. *Rev. Geophys.*, **23**, 357–390.
1479 Frankignoul, C., and K. Hasselmann, 1977; Stochastic climate models, Part II Application to sea-
1480 surface temperature anomalies and thermocline variability. *Tellus*, **29**, 289-305.
1481 Frankignoul, C., N. Sennechael, Y.-O. Kwon, and M. A. Alexander, 2011: Influence of the
1482 meridional shifts of the Kuroshio and the Oyashio Extensions on the atmospheric
1483 circulation. *J. Climate*, **24**, 762–777.
1484 Frenger, I., N. Gruber, R. Knutti, and M. Münnich, 2013: Imprint of Southern Ocean eddies on
1485 winds, clouds and rainfall. *Nature Geosci*., **6**, 608–612.
1486 Frenger, I., and Coauthors, 2018: Imprint of Southern Ocean mesoscale eddies on
1487 chlorophyll. *Beigeosciences*, **15**, 4781-479.
1488 Frew, N. M., D. M. Glover, E. J. Bock, and S. J. McCue, 2007: A new approach to estimation of
1489 global air-sea gas transfer velocity fields using dual-frequency altimeter backscatter. *J.*
1490 *Geophys. Res*., **112**, C11003.
1491 Friehe, C. A., W. J. Shaw, D. P. Rogers, K. L. Davidson, W. G. Large, S. A. Stage, G. H.
1492 Crescenti, S. J. S. Khalsa, G. K. Greenhut, and F. Li, 1991: Air-sea fluxes and surface
1493 layer turbulence around a sea surface temperature front, *J. Geophys. Res*., **96**, 8593–8609.
1494 Gade, M., and A. Stoffelen, 2019: An Introduction to Microwave Remote Sensing of the Asian
1495 Seas. In: Barale V., Gade M. (eds) Remote Sensing of the Asian Seas. Springer,
1496 Cham. https://doi.org/10.1007/978-3-319-94067-0_4.

Gaube, P., D. B. Chelton, P. G. Strutton, and M. J. Behrenfeld, 2013: Satellite observations of chlorophyll, phytoplankton biomass, and Ekman pumping in nonlinear mesoscale eddies. *J. Geophys. Res. Oceans*, **118**, 6349–6370.

Gaube, P., D. J. McGillicuddy, D. B. Chelton, M. J. Behrenfeld, and P. G. Strutton, 2014: Regional variations in the influence of mesoscale eddies on near-surface chlorophyll. *J. Geophys. Res. Oceans*, **119**, 8195-8220.

Gaube, P. D. B. Chelton, R. M. Samelson, M. G. Schlax, and L. W. O'Neill, 2015: Satellite Observations of Mesoscale Eddy-Induced Ekman Pumping. *J. Phys. Oceanogr.*, **45**, 104–132.

Gaube, P., C. C. Chickadel, R. Branch, and A. Jessup, 2019: Satellite observations of SST-induced wind speed perturbation at the oceanic submesoscale. *Geophys. Res. Lett.*, **46**, 2690–2695.

Gent, P. R., and J. C. McWilliams, 1990: Isopycnal Mixing in Ocean Circulation Models. *J. Phys. Oceanogr*, **20**, 150-155.

Gentemann, C., C. A. Clayson, S. Brown, T. Lee, R. Parfitt, J. T. Farrar, M. Bourassa, P. J. Minnett, H. Seo, S. T. Gille, and V. Zlotnicki, 2020: FluxSat: Measuring the ocean-atmosphere turbulent exchange of heat and moisture from space. *Remote Sens*., **12**, 1796.

Gervais, M., J. Shaman, and Y. Kushnir, 2018: Mechanisms Governing the Development of the North Atlantic Warming Hole in the CESM-LE Future Climate Simulations. *J. Climate*, **31**, 5927-5946.

Graber, H. C., E. A. Terray, M. A. Donelan, W. M. Drennan, J. C. Van Leer, and D. B. Peters, 2000: ASIS—A New Air–Sea Interaction Spar Buoy: Design and Performance at Sea. *J. Atmos. Ocean Tech*., **17**, 708-720.

Gommenginger, C., and Coauthors, 2019: SEASTAR: A Mission to Study Ocean Submesoscale Dynamics and Small-Scale Atmosphere-Ocean Processes in Coastal, Shelf and Polar Seas. *Front. Mar. Sci*., **6**, 457.

Grist, J. P., S. A. Josey, B. Sinha, J. L. Catto, M. J. Roberts, and A. C. Coward, 2021: Future evolution of an eddy rich ocean associated with enhanced east Atlantic storminess in a coupled model projection. *Geophys. Res. Lett.*, **48**, e2021GL092719.

Haarsma, R. J., M. Roberts and Coauthors, 2016: High Resolution Model Intercomparison Project (HighResMIP). *Geosci Model Dev*., **9**, 4185–4208.

1528 Haines, K., and J. Marshall, 1987: Eddy-forced coherent structures as a prototype of atmospheric
1529 blocking, *Q. J. R. Meteorol. Soc*., **113**, 681–709.
1530 Hallberg, R., 2013: Using a resolution function to regulate parameterizations of oceanic
1531 mesoscale eddy effects. *Ocean Modell*., **72**, 92-103.
1532 Hand, R., and Coauthors, 2014: Simulated response to inter-annual SST variations in the Gulf
1533 Stream region. *Clim Dyn* **42,** 715–731.
1534 Haney, S., B. Fox-Kemper, K. Julien, and A. Webb, 2015: Symmetric and geostrophic
1535 instabilities in the wave-forced ocean mixed layer. *J. Phys. Oceanogr.,* **45**, 3033–3056.
1536 Harcourt R, and Coauthors, 2019: Animal-Borne Telemetry: An Integral Component of the
1537 Ocean Observing Toolkit. *Front. Mar. Sci*., **6**, 326.
1538 Harrison, C. S., M. C. Long, N. S. Lovenduski, and J. K. Moore, 2018: Mesoscale effects on
1539 carbon export: a global perspective. *Glob. Biogeochem. Cycles*, **32**, 680–703.
1540 Hashizume, H., S.-P. Xie, M. Fujiwara, M. Shiotani, T. Watanabe, Y. Tanimoto, W. T. Liu, and
1541 K. Takeuchi, 2002: Direct observations of atmospheric boundary layer response to SST
1542 variations associated with tropical instability waves over the eastern equatorial Pacific. *J.*
1543 *Climate*, **15**, 3379–3393.
1544 Hausmann, U., D. J. McGillicuddy, and J. Marshall, 2017: Observed mesoscale eddy signatures
1545 in Southern Ocean surface mixed-layer depth. *J. Geophys. Res. Oceans*, **122**, 617–635,
1546 Hawcroft, M. K., L. C. Shaffrey, K. I. Hodges, and H. F. Dacre, 2012: How much Northern
1547 Hemisphere precipitation is associated with extratropical cyclones? *Geophys. Res.*
1548 *Lett.*, **39**, L24809.
1549 Hayasaki, M., R. Kawamura, M. Mori, and M. Watanabe, 2013: Response of extratropical
1550 cyclone activity to the Kuroshio large meander in northern winter. *Geophys. Res.*
1551 *Lett*., **40**, 2851–2855.
1552 Hayes, S. P., M. J. McPhaden, and J. M. Wallace, 1989: The Influence of Sea Surface
1553 Temperature on Surface Wind in the Eastern Equatorial Pacific: Weekly to Monthly
1554 Variability. *J. Climate*, **2**, 1500-1506.
1555 Hersbach, H., and Coauthors, 2020: The ERA5 global reanalysis. *Quart. J. Roy. Met. Soc.,* **146**,
1556 1999-2049.
1557 Hewitt, H. T., M. Roberts, P. Mathiot, et al. 2020: Resolving and Parameterising the Ocean
1558 Mesoscale in Earth System Models. *Curr. Clim. Change Rep.,* **6**, 137–152.

Hirata, H., R. Kawamura, M. Nonaka, and K. Tsuboki, 2019: Significant impact of heat supply from the Gulf Stream on a "superbomb" cyclone in January 2018. *Geophys. Res. Lett*, **46**, 7718–7725.

Hirata, H., and M. Nonaka, 2021: Impacts of strong warm ocean currents on development of extratropical cyclones through the warm and cold conveyor belts: A review. Elsevier, 9780128181577, 267-293 pp., doi:http://www.sciencedirect.com/science/article/pii/B9780128181560000149.

Hogg, A., W. K. Dewar, P. Berloff, S. Kravtsov, and D. K. Hutchinson, 2009: The effects of mesoscale ocean-atmosphere coupling on the large-scale ocean circulation. *J. Climate*, **22**, 4066-4082.

Holton, J. R., 1965a: The influence of viscous boundary layers on transient motions in a stratified rotating fluid. Part I. *J. Atmos. Sci*., **22**, 402–411.

Holton, J. R., 1965b: The influence of viscous boundary layers on transient motions in a stratified rotating fluid. Part II. *J. Atmos. Sci*., **22**, 535– 540.

Hoskins, B. J., and D. J. Karoly, 1981: The steady linear response of a spherical atmosphere to thermal and orographic forcing, *J. Atmos. Sci*., **38**, 1179-1196.

Hoskins, B. J., and K. I. Hodges, 2002: New Perspectives on the Northern Hemisphere Winter Storm Tracks. *J. Atmos. Sci.*, **59**, 1041–1061.

Hoskins, B. J., and P. J. Valdes, 1990: On the existence of storm tracks. *J. Atmos. Sci*., 47, 1854–1864.

Hotta, D., and H. Nakamura, 2011: On the significance of sensible heat supply from the ocean in the maintenance of mean baroclinicity along storm tracks. *J. Climate*, **24**, 3377–3401.

Huang, J., Y. Zhang, X. Q. Yang, X. Ren, and H. Hu, 2020: Impacts of north pacific subtropical and subarctic oceanic frontal zones on the wintertime atmospheric large-scale circulations. *J. Climate*, **33**(5), 1897–1914.

Hurwitz, M. M., P. A. Newman, and C. I. Garfinkel, 2012: On the influence of North Pacific sea surface temperature on the Arctic winter climate, *J. Geophys. Res*., **117**, D19110.

Infanti, J. M., and B. P. Kirtman, 2019: A comparison of CCSM4 high-resolution and low-resolution predictions for south Florida and southeast United States drought. *Clim. Dynm*., 52, 6877-6892.

IPCC, 2021: Climate Change 2021. The Physical Science Basis. Contribution of Working Group I to the Sixth Assessment Report of the Intergovernmental Panel on Climate Change [Masson-Delmotte, V., P. Zhai, A. Pirani, S.L. Connors, C. Péan, S. Berger, N. Caud, Y. Chen, L. Goldfarb, M.I. Gomis, M. Huang, K. Leitzell, E. Lonnoy, J.B.R. Matthews, T.K. Maycock, T. Waterfield, O. Yelekçi, R. Yu, and B. Zhou (eds.)]. Cambridge University Press. In Press. doi:10.1017/9781009157896.

Jackson, L. C., and Coauthors, 2020: Impact of ocean resolution and mean state on the rate of AMOC weakening. *Clim. Dyn.,* **55,** 1711–1732.

Jansen, M. F., and I. M. Held, 2014: Parameterizing subgrid-scale eddy effects using energetically consistent backscatter. *Ocean Modell.*, **80**, 36-48.

Jing, Z., and Coauthors, 2020: Maintenance of mid-latitude oceanic fronts by mesoscale eddies. *Sci. Adv.*, **6**, eaba7880

Johnson, L., C. M. Lee, and E. A. D'Asaro, 2016: Global Estimates of Lateral Springtime Restratification. *J. Phys. Oceanogr.*, **46**, 1555-1573.

Jones, D. G., and Coauthors, 2015: Developments since 2005 in understanding potential environmental impacts of CO2 leakage from geological storage. *Int. J. Greenh. G. Con.,* **40**, 350–377.

Joyce, T. M., Y.-O. Kwon, H. Seo, and C. C. Ummenhofer, 2019: Meridional Gulf Stream shifts can influence wintertime variability in the North Atlantic Storm Track and Greenland Blocking. *Geophys. Res. Lett.*, **46**, 46,1702-1708.

Jullien, S., S. Masson, V. Oerder, G. Samson, F. Colas, and L. Renault, 2020: Impact of ocean-atmosphere current feedback on the ocean mesoscale activity: regional variations, and sensitivity to model resolution. *J. Climate*, **33**, 2585-2602.

Jury, M. R., and S. Courtney, 1991: A transition in weather over the Agulhas Current. *S. Afr. J. Mar. Sci.,* **10**, 159–171.

Karmalkar, A.V., and R. M. Horton, 2021: Drivers of exceptional coastal warming in the northeastern United States. *Nat. Clim. Chang.,* **11,** 854–860.

Kaspi, Y., and T. Schneider, 2013: The role of stationary eddies in shaping midlatitude storm tracks. *J. Atmos. Sci.,* **70**, 2596–2613.

Keil, P., and Coauthors, 2020: Multiple drivers of the North Atlantic warming hole. *Nat. Clim. Chang.*, **10**, 667–671.

1620 Kelly, K. A., S. Dickinson, M. J. McPhaden, and G. C. Johnson, 2001: Ocean Currents Evident
1621 in Satellite Wind Data. *Geophys. Res. Lett.*, **28**, 2469-2472.
1622 Kelly, K. A., R. J. Small, R. M. Samelson, B. Qiu, T. M. Joyce, Y. Kwon, and M. F. Cronin,
1623 2010: Western Boundary Currents and Frontal Air–Sea Interaction: Gulf Stream and
1624 Kuroshio Extension. *J. Climate*, **23**, 5644-5667.
1625 Kessler, W.S., S. E. Wijffels, S. Cravatte, N. Smith, and Contributing Authors, 2019: Second
1626 Report of TPOS 2020. GOOS-234, 265 pp. http://tpos2020.org/second-report/.
1627 Kilpatrick, T., N. Schneider, and B. Qiu, 2014: Boundary layer convergence induced by strong
1628 winds across a midlatitude SST front. *J. Climate*, **27**, 1698–1718.
1629 Kilpatrick, T., N. Schneider, and B. Qiu, 2016: Atmospheric response to a midlatitude SST front:
1630 Alongfront winds. *J. Atmos. Sci*., **73**, 3489–3509.
1631 Kim, S.-Y., 2010: Observations of submesoscale eddies using high-frequency radar-derived
1632 kinematic and dynamic quantities. *Cont. Shelf. Res*., **30**, 1639-1655.
1633 Kirincich, A., B. Emery, L. Washburn, and P. Flament, 2019: Improving Surface Current
1634 Resolution Using Direction Finding Algorithms for Multiantenna High-Frequency
1635 Radars, *J. Atmos. and Oceanic Technol*., **36**, 1997-2014.
1636 Kirtman, B. P., and Coauthors, 2012: Impact of ocean model resolution on CCSM climate
1637 simulations. *Clim. Dyn*., **39**, 1303– 1328.
1638 Kudryavtsev, V., B. Chapron, and V. Makin, 2014: Impact of wind waves on the air-sea fluxes:
1639 A coupled model. *J. Geophys. Res. Oceans,* **119**, 1217-1236.
1640 Kushnir, Y., W. A. Robinson, I. Blade, N. M. J. Hall, S. Peng, and R. Sutton, 2002: Atmospheric
1641 GCM response to extratropical SST anomalies: Synthesis and evaluation. *J. Climate*, **15**,
1642 2233-2256.
1643 Kuwano-Yoshida, A., and S. Minobe, 2017. Storm track response to SST fronts in the
1644 Northwestern Pacific region in an AGCM. *J. Climate*, **30**, 1081-1102.
1645 Kwak, K. H. Song, J. Marshall, H. Seo, and D. McGillicuddy, Jr., 2021: Suppressed pCO_2 in the
1646 Southern Ocean due to the interaction between current and wind. *J. Geophys. Res.*
1647 *Oceans*, **126**, e2021JC017884.
1648 Kwon, Y.-O., M. A. Alexander, N. A. Bond, C. Frankignoul, H. Nakamura, B. Qiu, and L. A.
1649 Thompson, 2010. Role of the Gulf Stream and Kuroshio-Oyashio Systems in Large-Scale
1650 Atmosphere-Ocean Interaction: A Review. *J. Climate*, **23**, 3249-3281.

1651 Kwon, Y.-O., and T. M. Joyce, 2013: Northern Hemisphere Winter Atmospheric Transient Eddy
1652 Heat Fluxes and the Gulf Stream and Kuroshio-Oyashio Extension Variability. *J.*
1653 *Climate*, **26**, 9839-9859.
1654 Lambaerts, J., G. Lapeyre, R. Plougonven, and P. Klein, 2013: Atmospheric response to sea
1655 surface temperature mesoscale structures. *J. Geophys. Res. Atmos*., **118**, 9611–9621.
1656 Lac, C., and Coauthors, 2018: Overview of the Meso-NH model version 5.4 and its applications.
1657 *Geosci. Model Dev*., **11**, 1929-1969.
1658 Lane, E. M., J. M. Restrepo, and J. C. McWilliams, 2007: Wave–current interaction: A
1659 comparison of radiation-stress and vortex-force representations. *J. Phys. Oceanogr*,
1660 **37**, 1122–1141.
1661 Laurindo, L. C., A. Mariano, and R. Lumpkin, 2017: An improved surface velocity climatology
1662 for the global ocean from drifter observations. *Deep Sea Res. I,* **124**, 73–92.
1663 Laurindo, L. C., L. Siqueira, A. J. Mariano, and B. Kirtman, 2019: Cross-spectral analysis of the
1664 SST/10-m wind speed coupling resolved by satellite products and climate model
1665 simulations. *Clim. Dyn*., **52**, 5071–5098.
1666 Lee, R. W., T. J. Woollings, B. J. Hoskins, K. D. Williams, C. H. O'Reilly, and G. Masato, 2018:
1667 Impact of Gulf Stream SST biases on the global atmospheric circulation. *Clim Dyn.*, **51**,
1668 3369–3387.
1669 Leibovich, S., 1983: The Form and Dynamics of Langmuir Circulations. *Annu. Rev. Fluid*
1670 *Mech.*, **15**, 391-427.
1671 Lenschow, D. H., P. B. Krummel, and S. T. Siems, 1999: Measuring Entrainment, Divergence,
1672 and Vorticity on the Mesoscale from Aircraft. *J. Atmos. Ocean Tech*., **16**, 1384-1400.
1673 Lévy, M., 2008: The modulation of biological production by oceanic mesoscale turbulence. In
1674 *Transport and Mixing in Geophysical Flows*, ed. J Weiss, A Provenzale, pp. 219–61.
1675 Berlin: Springer
1676 Lévy, M., P. J. S. Franks, and K. S. Smith, 2018: The role of submesoscale currents in
1677 structuring marine ecosystems. *Nat. Commun*., **9**, 4758.
1678 Li, Y., and R. E. Carbone, 2012: Excitation of rainfall over the tropical western Pacific. *J. Atmos.*
1679 *Sci*., **69**, 2983–2994.
1680 Lindzen, R. S., and B. Farrell, 1980: A Simple Approximate Result for the Maximum Growth
1681 Rate of Baroclinic Instabilities. *J. Atmos. Sci*., **37**, 1648-1654.

1682 Lindzen, R. S., and S. Nigam, 1987: On the role of sea surface temperature gradients in forcing
1683 low-level winds and convergence in the tropics. *J. Atmos. Sci*., **44**, 2418–2436.
1684 Liu, W., A. V. Fedorov, S.-P. Xie, and S. Hu, 2020: Climate impacts of a weakened Atlantic
1685 meridional overturning circulation in a warming climate. *Science Advances*, **6**, eaaz4876.
1686 Liu, X., X. Ma, P. Chang, Y. Jia, D. Fu, G. Xu, L. Wu, R. Saravanan, and C. M. Patricola,
1687 2021: Ocean fronts and eddies force atmospheric rivers and heavy precipitation
1688 in western North America. *Nat. Commun*., **12**, 1268.
1689 López-Dekker, P., H. Rott, P. Prats-Iraola, B. Chapron, K. Scipal, and E. D. Witte, 2019:
1690 Harmony: an Earth Explorer 10 Mission Candidate to Observe Land, Ice, and Ocean
1691 Surface Dynamics, in: IGARSS 2019 - 2019 IEEE International Geoscience and Remote
1692 Sensing Symposium, pp. 8381–8384, https://doi.org/10.1109/IGARSS.2019.8897983.
1693 Lorenz, E., 1960: Generation of available potential energy and the intensity of the general
1694 circulation. In R. L. Pfeffer (Ed.), Dynamics of climate (pp. 86–92). Oxford: Pergamon
1695 Press.
1696 Luo, J.-J., S. Masson, E. Roeckner, G. Madec, and T. Yamagata, 2005: Reducing Climatology
1697 Bias in an Ocean-Atmosphere CGCM with Improved Coupling Physics. *J. Climate*, **18**,
1698 2344-2360
1699 Ma, X., P. Chang, R. Saravanan, R. M. J.-S. Hseih, D. Wu, X. Lin, L. Wu, and Z. Jing, 2015:
1700 Distant influence of Kuroshio eddies on North Pacific weather patterns. *Sci. Rep*., **5**,
1701 17785.
1702 Ma, X., and Coauthors, 2016: Western boundary currents regulated by interaction between ocean
1703 eddies and the atmosphere. *Nature*, **535**, 533–537.
1704 Ma, X., P. Chang, R. Saravanan, R. Montuoro, H. Nakamura, D. Wu, X. Lin, and L. Wu, 2017:
1705 Importance of resolving Kuroshio Front and eddy influence in simulating the North
1706 Pacific storm track. *J. Climate*, **30**, 1861-1880.
1707 Mahrt, L., D. Vickers, and E. Moore, 2004: Flow Adjustments Across Sea-Surface Temperature
1708 Changes. *Boundary-Layer Meteorology* **111,** 553–564.
1709 Marshall, J., and Coauthors, 2009: The Climode Field Campaign: Observing the Cycle of
1710 Convection and Restratification over the Gulf Stream. *Bull. Amer. Meteor. Soc.*, **90**,
1711 1337–1350.

1712 Marshall, J., J. Scott, K. Armour, J.-M. Campin, M. Kelley, and A. Romanou, 2014: The ocean's
1713 role in the transient response of climate to abrupt greenhouse gas forcing. *Clim. Dyn*.,
1714 **44,** 2287–2299.
1715 Martin, A., and K. Richards, 2001: Mechanisms for vertical nutrient transport within a North
1716 Atlantic mesoscale eddy. *Deep Sea Res.–II*, **48**, 757–773.
1717 Masunaga, R., H. Nakamura, B. Taguchi and T. Miyasaka, 2020a: Processes Shaping the
1718 Frontal-Scale Time-Mean Surface Wind Convergence Patterns around the Kuroshio
1719 Extension in Winter. *J. Climate,* **33**, 3-25.
1720 Masunaga, R., H. Nakamura, B. Taguchi, and T. Miyasaka, 2020b: Processes Shaping
1721 the Frontal-Scale Time-Mean Surface Wind Convergence Patterns around the
1722 Gulf Stream and Agulhas Return Current in Winter. *J. Climate*, **33**, 9083–9101.
1723 Masunaga, R. and N. Schneider, 2022: Surface wind responses to mesoscale sea surface
1724 temperature over western boundary current regions assessed by spectral transfer
1725 functions. *J. Atmos. Sci*., https://doi.org/10.1175/JAS-D-21-0125.1.
1726 McGillicuddy, D. J., and Coauthors, 2007: Eddy/Wind Interactions Stimulate Extraordinary
1727 Mid-Ocean Plankton Blooms. *Science*, **316**, 1201.
1728 McGillicuddy, D. J., 2016: Mechanisms of physical-biological-biogeochemical interaction at the
1729 oceanic mesoscale. *Ann. Rev. Mar. Sci.*, **8**, 125-159.
1730 McGillis, W. R., J. B. Edson, J. E. Hare, and C. W. Fairall, 2001: Direct covariance air-sea CO2
1731 fluxes. *J. Geophys. Res.,* **106**, 16729-16745.
1732 McLandress, C., T. Shepherd, J. Scinocca, D. Plummer, M. Sigmond, A. Jonsson, and M.
1733 Reader, 2011: Separating the dynamical effects of climate change and ozone depletion.
1734 Part II: Southern hemisphere troposphere. *J. Climate*, **24**, 1850–1868.
1735 McWilliams, J. C., E. Huckle, J. Liang, and P. P. Sullivan, 2012: The Wavy Ekman Layer:
1736 Langmuir Circulations, Breaking Waves, and Reynolds Stress. *J. Phys. Oceanogr*., **42**,
1737 1793-1816.
1738 McWilliams, J. C., and B. Fox-Kemper, 2013: Oceanic wave-balanced surface fronts and
1739 filaments. *J. Fluid Mech*., **730**, 464-490.
1740 McWilliams, J. C., 2016: Submesoscale currents in the ocean. *Proc. R. Soc. A*, **472**, 20160117.

Meinig, C., and Coauthors, 2019: Public-Private Partnerships to Advance Regional Ocean-Observing Capabilities: A Saildrone and NOAA-PMEL Case Study and Future Considerations to Expand to Global Scale Observing. *Front. Mar. Sci.*, **6**, 448.

Mémin, E. 2014: Fluid flow dynamics under location uncertainty. *Geophysical & Astrophysical Fluid Dynamics*, **108**, 119-146.

Menary, M. B., and Coauthors, 2018: Preindustrial control simulations with HadGEM3-GC3.1 for CMIP6. *J. Adv. Model. Earth Syst.*, **10**, 3049– 3075.

Messager, C., and S. Swart, 2016: Significant atmospheric boundary layer change observed above an Agulhas Current warm core eddy. *Adv. Meteor*., 2016, 3659657.

Mey, R. D., N. D. Walker, and M. R. Jury, 1990: Surface heat fluxes and marine boundary layer modification in the Agulhas Retroflection Region. *J. Geophys. Res.,* **95,** 15 997–16 015.

Minobe, S., A. Kuwano-Yoshida, N. Komori, S.-P. Xie, and R. J. Small, 2008: Influence of the Gulf Stream on the troposphere. *Nature*, **452**, 206–209.

Minobe, S., M. Miyashita, A. Kuwano-Yoshida, H. Tokinaga, and S.-P. Xie, 2010: Atmospheric response to the Gulf Stream: Seasonal variations. *J. Climate*, **23**, 3699–3719.

Miyamoto, A., H. Nakamura, T. Miyasaka, and Y. Kosaka, 2022: Wintertime Weakening of Low-Cloud Impacts on the Subtropical High in the South Indian Ocean, *J. Climate*, **35**, 323-334.

Miyamoto, A., H. Nakamura, and T. Miyasaka, 2018: Influence of the subtropical high and storm track on low-cloud fraction and its seasonality over the South Indian Ocean. *J. Climate*, **31**, 4017–4039.

Miyazawa, Y. and Coauthors, 2019: Temperature profiling measurements by sea turtles improve ocean state estimation in the Kuroshio-Oyashio Confluence region. *Ocean Dynamics*, **69**, 267–282.

Moreno-Chamarro, E., L.-P. Caron, P. Ortega, S. Loosveldt Tomas, and M. J. Roberts, 2021: Can we trust CMIP5/6 future projections of European winter precipitation? *Environ. Res. Lett*., **16**, 054063.

Moreton, S., D. Ferreira, M. Roberts, and H. Hewitt, 2021: Air-Sea Turbulent Heat Flux Feedback over Mesoscale Eddies. *Geophys. Res. Lett*., **48**, e2021GL095407.

Nadiga, B. T., 2008: Orientation of eddy fluxes in geostrophic turbulence. *Phil. Trans. R. Soc. A.,* **366,** 2489-2508.

1772 Nakamura, H., and J. M. Wallace, 1990: Observed changes in baroclinic wave activity during the
1773 life cycles of low-frequency circulation anomalies. *J. Atmos. Sci*., **47**, 1100–1116.
1774 Nakamura H., T. Sampe, Y. Tanimoto, and A. Shimpo, 2004: Observed associations among
1775 storm tracks, jet streams and midlatitude oceanic fronts. "Earth's climate: the ocean-
1776 atmosphere interaction". *AGU Geophys Monogr.,* **147**, 329–346.
1777 Nakamura, H., T. Sampe, A. Goto, W. Ohfuchi, and S.-P. Xie, 2008: On the importance of
1778 midlatitude oceanic frontal zones for the mean state and dominant variability in the
1779 tropospheric circulation. *Geophys. Res. Lett.*, **35**, L15709.
1780 Nakamura, H., and A. Shimpo, 2004: Seasonal Variations in the Southern Hemisphere Storm
1781 Tracks and Jet Streams as Revealed in a Reanalysis Dataset. *J. Climate*, **17**, 1828–1844.
1782 Nakamura, H., A. Nishina, and S. Minobe, 2012: Response of storm tracks to bimodal Kuroshio
1783 path states south of Japan. *J. Climate*, **25**, 7772–7779.
1784 Nakamura, H., and Coauthors, 2015: "Hot Spots" in the climate system—new developments in
1785 the extratropical ocean-atmosphere interaction research: a short review and an
1786 introduction. *J. Oceanogr.,* **71**, 463–467.
1787 Nakayama, M., H. Nakamura, and F. Ogawa, 2021: Impacts of a Midlatitude Oceanic Frontal
1788 Zone for the Baroclinic Annular Mode in the Southern Hemisphere. *J. Climate*, **34**, 7389-
1789 7408.
1790 Newman, L., Hancock, M. A., Hofmann, E., Williams, M. J. M., Henley, S. F., et. al., (2022).
1791 The Southern Ocean Observing System 2021-2025 Science and Implementation Plan.
1792 https://doi.org/10.5281/zenodo.6324359.
1793 Nkwinkwa Njouodo, A. S., S. Koseki, N. Keenlyside, and M. Rouault, 2018: Atmospheric
1794 signature of the Agulhas Current. *Geophys. Res. Lett.,* **45**, 5185–5193.
1795 Nonaka, M., H. Nakamura, B. Taguchi, N. Komori, A. Yoshida-
1796 Kuwano, and K. Takaya, 2009: Air-sea heat exchanges characteristic to a prominent
1797 midlatitude oceanic front in the South Indian Ocean as simulated in a high-resolution
1798 coupled GCM. *J. Climate*, **22**, 6515–6535.
1799 Ogawa, F., N.-E. Omrani, K. Nishii, H. Nakamura, and N. Keenlyside, 2015: Ozone-induced
1800 climate change propped up by the Southern Hemisphere oceanic front, *Geophys. Res.*
1801 *Lett.*, **42**, 10,056–10,063.

1802 Ogawa, F., H. Nakamura, K. Nishii, T. Miyasaka, and A. Kuwano-Yoshida, 2016: Importance of
1803 Midlatitude Oceanic Frontal Zones for the Annular Mode Variability: Interbasin
1804 Differences in the Southern Annular Mode Signature, *J. Climate*, **29**, 6179-6199.
1805 Omand, M. M., E. A. D'Asaro, C. M. Lee, M.-J. Perry, N. Briggs, I. Cetinić, and A. Mahadevan,
1806 2015: Eddy-driven subduction exports particulate organic carbon from the spring bloom.
1807 *Science*, **348**, 222-225.
1808 Omrani, NE., Ogawa, F., Nakamura, H. et al., 2019: Key Role of the Ocean Western Boundary
1809 currents in shaping the Northern Hemisphere climate. *Sci. Rep*., **9**, 3014.
1810 Olivier, L., and Coauthors, 2021: Impact of North Brazil Current rings on air-sea CO2 flux
1811 variability in winter 2020. *Biogeosciences*, https://doi.org/10.5194/bg-2021-269.
1812 O'Neill, L. W., D. B. Chelton, and S. K. Esbensen, 2003: Observations of SST-induced
1813 perturbations of the wind stress field over the Southern Ocean on seasonal timescales. *J.*
1814 *Climate*, **16**, 2340– 2354.
1815 O'Neill, L. W., D. B. Chelton, and S. K. Esbensen, 2010: The effects of SST-induced wind speed
1816 and direction gradients on mid-latitude surface vorticity and divergence. *J. Climate*, **23**,
1817 255-281.
1818 O'Neill, L. W., D. B. Chelton, and S. K. Esbensen, 2012: Covariability of surface wind and
1819 stress responses to sea surface temperature fronts. *J. Climate*, **25**, 5916–5942.
1820 O'Neill, L. W., 2012: Wind Speed and Stability Effects on Coupling between Surface
1821 Wind Stress and SST Observed from Buoys and Satellites. *J. Climate, **25***, 1544-1569.
1822 O'Neill, L. W., T. Haack, and T. Durland, 2015: Estimation of time-averaged surface divergence
1823 and vorticity from satellite ocean vector winds. *J. Climate*, **28**, 7596–7620.
1824 O'Neill, L. W., T. Haack, D. B. Chelton, and E. D. Skyllingstad, 2017: The Gulf Stream
1825 Convergence Zone in the time-mean winds. *J. Atmos. Sci*., **74**, 2383-2412.
1826 O'Reilly, C. H., and A. Czaja, 2015: The response of the Pacific storm track and atmospheric
1827 circulation to Kuroshio Extension variability. *Quart. J. Roy. Met. Soc*., **141**, 52–66.
1828 O'Reilly, C. H., S. Minobe, and A. Kuwano-Yoshida, 2016: The influence of the Gulf Stream on
1829 wintertime European blocking. *Clim. Dyn.*, **47**, 1545–1567.
1830 O'Reilly, C. H., S. Minobe, A. Kuwano-Yoshida, and T. Woollings, 2017: The Gulf Stream
1831 influence on wintertime North Atlantic jet variability. *Quart. J. Roy. Meteor. Soc*., **143**,
1832 173–183.

1833 Pacanowski, R. C., 1987: Effect of Equatorial Currents on Surface Stress. *J. Phys.*
1834 *Oceanogr.*, **17**, 833-838.
1835 Paduan, J. D., and L. Washburn, 2013: High-Frequency Radar Observations of Ocean Surface
1836 Currents. *Ann. Rev. Mar. Sci.,* **5**, 115-136.
1837 Palmer, T. N., and Z. Sun, 1985: A modeling and observational study of the relationship between
1838 sea-surface temperature in the northwest Atlantic and the atmospheric general circulation,
1839 *Quart. J. Roy. Meteor. Soc*., **111**, 947-975.
1840 Parfitt, R., A. Czaja, S. Minobe, and A. Kuwano-Yoshida, 2016: The atmospheric frontal
1841 response to SST perturbations in the Gulf Stream region. *Geophys. Res. Lett*., **43**, 2299–
1842 2306.
1843 Parfitt, R., and A. Czaja, 2016: On the contribution of synoptic transients to the mean
1844 atmospheric state in the Gulf Stream region. *Quart. J. Roy. Met. Soc.,* **142**, 1554–1561.
1845 Parfitt, R., and H. Seo, 2018: A New Framework for Near-Surface Wind Convergence over the
1846 Kuroshio Extension and Gulf Stream in Wintertime: The Role of Atmospheric
1847 Fronts. *Geophys*. *Res. Lett*., **45**, 9909–9918.
1848 Peng, S., A. Robinson, and M. P. Hoerling, 1997: The modeled atmospheric response to
1849 midlatitude SST anomalies and its dependence on background circulation states. *J.*
1850 *Climate*, **10**, 971–987.
1851 Penny, S. G., and T. Hamill, 2017: Coupled data assimilation for integrated Earth system
1852 analysis and prediction. *Bull. Amer. Meteor. Soc*, **97**, ES169–ES172.
1853 Perlin, N., S. P. de Szoeke, D. B. Chelton, R. M. Samelson, E. D. Skyllingstad, and L. W.
1854 O'Neill, 2014: Modeling the Atmospheric Boundary Layer Wind Response to Mesoscale
1855 Sea Surface Temperature Perturbations. *Mon. Wea. Rev.*, **142**, 4284–4307.
1856 Pezzi, L. P., R. B. Souza, M. S. Dourado, C. A. E. Garcia, M. M. Mata, and M. A. F. Silva-Dias,
1857 2005: Ocean-atmosphere in situ observations at the Brazil-Malvinas Confluence region.
1858 *Geophys. Res. Lett*., **32**, L22603.
1859 Pezzi, L. P., and Coauthors, 2021*:* Oceanic eddy-induced modifications to air-sea heat and
1860 CO_2 fluxes in the Brazil-Malvinas Confluence. *Sci. Rep.,* **11**, 10648.
1861 Piazza, M., L. Terray, J. Boé, E. Maisonnave, and E. Sanchez- Gomez, 2016: Influence of small-
1862 scale North Atlantic sea surface temperature patterns on the marine boundary layer and

free troposphere: A study using the atmospheric ARPEGE model. *Climate Dyn*., **46**, 1699–1717.

Plagge, A. M., D. Vandemark, and B. Chapron, 2012: Examining the Impact of Surface Currents on Satellite Scatterometer and Altimeter Ocean Winds. *J. Atmos. Oceanic Tech*., **29**, 1776-1793.

Polvani, L. M., D. W. Waugh, G. J. P. Correa, and S. Son, 2011: Stratospheric ozone depletion: The main driver of 20th century atmospheric circulation changes in the southern hemisphere*, J. Climate*, **24**, 795–812.

Polverari, F., M. Portabella, W. Lin, J. W. Sapp, A. Stoffelen, Z. Jelenak, and P. S. Chang, 2021: On High and Extreme Wind Calibration Using ASCAT. *IEEE Trans. Geosci. Remote Sens.*, 0.1109/TGRS.2021.3079898

Quinn, P. K., and Coauthors, 2021: Measurements from the RV Ronald H. Brown and related platforms as part of the Atlantic Tradewind Ocean-Atmosphere Mesoscale Interaction Campaign (ATOMIC). *Earth Syst. Sci. Data*, **13**, 1759–1790.

Reason, C. J. C., 2001: Evidence for the influence of the Agulhas Current on regional atmospheric circulation patterns*. J. Climate*, **14**, 2769–2778.

Reichl, B. G., and Deike, L., 2020: Contribution of sea-state dependent bubbles to air-sea carbon dioxide fluxes. *Geophys. Res. Lett.*, **47**, e2020GL087267.

Reeder, M. J., T. Spengler, and C. Spensberger, 2021: The Effect of Sea Surface Temperature Fronts on Atmospheric Frontogenesis. *J. Atmos. Sci*., **78**, 1753-1771.

Renault, L., J. C. McWilliams, A. F. Shchepetkin, F. Lemarié, D. Chelton, S. Illig, and A. Hall, 2016a: Modulation of wind work by oceanic current interaction with the atmosphere*. J. Phys. Oceanogr.*, **46**, 1685–1704.

Renault, L., M. J. Molemaker, J. Gula, S. Masson, and J. C. McWilliams, 2016b: Control and stabilization of the Gulf Stream by oceanic current interaction with the atmosphere. *J. Phys. Oceanogr*., **46**, 3439–3453.

Renault, L., J. C. McWilliams, and P. Penven, 2017a: Modulation of the Agulhas Current retroflection and leakage by oceanic current interaction with the atmosphere in coupled simulations. *J. Phys. Oceanogr*, **47**, 2077–2100.

Renault, L., J. C. McWilliams, and S. Masson, 2017b: Satellite observations of imprint of oceanic current on wind stress by air-sea coupling. *Sci. Rep.*, **7**, 17747.

Renault, L., J. C. McWilliams, and J. Gula, 2018: Dampening of submesoscale currents by air-sea stress coupling in the Californian upwelling system. *Sci. Rep.*, **8**, 13388.

Renault, L., S. Masson, V. Oerder, S. Jullien, and F. Colas, 2019a: Disentangling the mesoscale ocean-atmosphere interactions. *J. Geophys. Res. Oceans*, **124**, 2164–2178.

Renault, L., P. Marchesiello, S. Masson, and J. C. McWilliams, 2019b: Remarkable control of western boundary currents by eddy killing, a mechanical air-sea coupling process. *Geophys. Res. Lett.*, **46**, 2743–2751.

Renault, L., F Lemarié, and T. Arsouze, 2019c: On the implementation and consequences of the oceanic currents feedback in ocean–atmosphere coupled models. *Ocean Modelling*, **141**, 101423.

Renault, L., S. Masson, T. Arsouze, G. Madec, and J. C. McWilliams, 2020: Recipes for how to force oceanic model dynamics. *J. Adv. Modeling Earth Syst.*, **12**, e2019MS001715.

Renault, L., and P. Marchesiello, 2022: Ocean tides can drag the atmosphere and cause tidal winds over broad continental shelves. *Commun Earth Environ.,* **3**, 70. Reynolds, R. W., T. M. Smith, C. Liu, D. B. Chelton, K. S. Casey, and M. G. Schlax, 2007: Daily high-resolution-blended analyses for sea surface temperature. *J. Climate*, **20**, 5473-549.

Reynolds, R. W., T. M. Smith, C. Liu, D. B. Chelton, K. S. Casey, and M. G. Schlax, 2007: Daily high-resolution-blended analyses for sea surface temperature. *J. Climate*, **20**, 5473–5496.

Roberts, M. J., Hewitt, H. T., Hyder, P., Ferreira, D., Josey, S. A., Mizielinski, M., and Shelly, A., 2016: Impact of ocean resolution on coupled air-sea fluxes and large-scale climate, *Geophys. Res. Lett.*, **43**, 10,430– 10,438.

Robinson, W., P. Chang, E. Chassignet, and S. Speich, 2020: *Ocean Mesoscale Eddy Interactions with the Atmosphere* (No. 2020-05). (J. Zhu and M. Patterson, Eds.). Washington, DC: U.S. CLIVAR Project Office. doi:10.5065/ebjm-5q77.

Robinson, W., S. Speich, and E. Chassignet, 2018: Exploring the interplay between ocean eddies and the atmosphere, *Eos,* **99**, https://doi.org/10.1029/2018EO100609.

Romero, L., D. Hypolite, and J. C. McWilliams, 2020: Submesoscale current effects on surface waves. *Ocean Modell*., **153**, 101662.

1923 Rousseau, V., E. Sanchez-Gomez, R. Msadek, and M. Moine, 2021: Mechanisms shaping wind
1924 convergence under extreme synoptic situations over the Gulf Stream region. *J. Climate*,
1925 **34**, 9481-9500.
1926 Saba, V. S., and Coauthors, 2016: Enhanced warming of the Northwest Atlantic Ocean under
1927 climate change. *J. Geophys. Res. Oceans*, **121**, 118-132.
1928 Samelson R., E. Skyllingstad, D. Chelton, S. Esbensen, L. O'Neill, and N. Thum, 2006: On the
1929 coupling of wind stress and sea surface temperature. *J. Climate*, **19**, 1557-1566.
1930 Samelson, R. M., L. W. O'Neill, D. B. Chelton, E. D. Skyllingstad, P. L. Barbour, and S. M.
1931 Durski, 2020: Surface Stress and Atmospheric Boundary Layer Response to Mesoscale
1932 SST Structure in Coupled Simulations of the Northern California Current System. *Mon.*
1933 *Wea. Rev.,* **148**, 259-287.
1934 Sampe, T., and S.-P. Xie, 2007: Mapping high sea winds from space: A global climatology. *Bull.*
1935 *Amer. Meteor. Soc.*, **88**, 1965-1978.
1936 Sampe, T., H. Nakamura, and A. Goto, 2013: Potential influence of a midlatitude oceanic frontal
1937 zone on the annular variability in the extratropical atmosphere as revealed by aqua-planet
1938 experiments. *J. Meteor. Soc. Japan*, **91**, 243–267
1939 Saviano, S., and Coauthors, 2021: Wind Direction Data from a Coastal HF Radar System in the
1940 Gulf of Naples (Central Mediterranean Sea, *Remote Sens*., **13**, 1333.
1941 Schneider, N., and B. Qiu, 2015: The atmospheric response to weak sea surface temperature
1942 fronts*. J. Atmos. Sci.,* **72**, 3356–3377.
1943 Schneider, N., 2020: Scale and Rossby Number Dependence of Observed Wind Responses to
1944 Ocean-Mesoscale Sea Surface Temperatures. *J. Climate*, **77**, 3171-3192.
1945 Scott, R. B., and Y. Xu, 2009: An update on the wind power input to the surface geostrophic
1946 flow of the World Ocean. *Deep-Sea Res.*, **56**, 295–304.
1947 Seager, R., Y. Kushnir, N. H. Naik, M. A. Cane, and J. Miller, 2001: Wind-Driven Shifts in the
1948 Latitude of the Kuroshio–Oyashio Extension and Generation of SST Anomalies
1949 on Decadal Timescales. *J. Climate*, **14**, 4249-4265.
1950 Seager, R., and I. R. Simpson, 2016: Western boundary currents and climate change. *J. Geophys.*
1951 *Res. Oceans*, **121**, 7212–7214. Sen Gupta, A., A. Stellema, G. M. Pontes, G.M. et al.,
1952 2021: Future changes to the upper ocean Western Boundary Currents across
1953 two generations of climate models. *Sci. Rep.,* **11***,* 9538*.*

1954 Seo, H., M. Jochum, R. Murtugudde, A. J. Miller, and J. O. Roads, 2007: Feedback of Tropical
1955 Instability Wave - induced Atmospheric Variability onto the Ocean. *J. Climate*, **20**, 5842-
1956 5855.
1957 Seo, H., Y.-O. Kwon, and J.-J. Park, 2014: On the effect of the East/Japan Sea SST variability on
1958 the North Pacific atmospheric circulation in a regional climate model. *J. Geophys. Res.*
1959 *Atmos*., **119**, 418–444.
1960 Seo, H., A. J. Miller, and J. R. Norris, 2016: Eddy-wind interaction in the California Current
1961 System: dynamics and impacts. *J. Phys. Oceanogr*., **46**, 439-459.
1962 Seo, H., 2017: Distinct influence of air-sea interactions mediated by mesoscale sea surface
1963 temperature and surface current in the Arabian Sea. *J. Climate,* **30**, 8061-8079.
1964 Seo, H., Y.-O. Kwon, T. M. Joyce, and C. C. Ummenhofer, 2017: On the predominant nonlinear
1965 response of the extratropical atmosphere to meridional shift of the Gulf Stream. *J.*
1966 *Climate,* **30**, 9679-9702.
1967 Seo, H., A. C. Subramanian, H. Song, and J. S. Chowdary, 2019: Coupled effects of ocean
1968 current on wind stress in the Bay of Bengal: Eddy energetics and upper ocean
1969 stratification. *Deep-Sea Res. II,* **168**, 104617.
1970 Seo, H., H. Song, L. W. O'Neill, M. R. Mazloff, and B. D. Cornuelle, 2021: Impacts of ocean
1971 currents on the South Indian Ocean extratropical storm track through the relative wind
1972 effect. *J. Climate,* **34**, 9093-9113.
1973 Sheldon, L., A. Czaja, B. Vannière, C. Morcrette, B. Sohet, M. Casado, and D. Smith, 2017: A
1974 warm path to Gulf Stream–troposphere interactions. *Tellus*, **69**, 1–13.
1975 Sen Gupta, A., A. Stellema, G. M Pontes, *et al.,* 2021: Future changes to the upper ocean
1976 Western Boundary Currents across two generations of climate models. *Sci. Rep.,*
1977 **11,** 9538.
1978 Shi, Q., and M. A. Bourassa, 2019: Coupling Ocean Currents and Waves with Wind Stress over
1979 the Gulf Stream. *Remote Sens*., **11**, 1476.
1980 Shinoda, T., S. Pei, W. Wang, J. X. Fu. R.-C. Lien, H. Seo, and A. Soloviev, 2021: Climate
1981 Process Team: improvement of ocean component of NOAA Climate Forecast System
1982 relevant to Madden-Julian Oscillation simulations. *J. Adv. Model. Earth Syst.,* **13**,
1983 e2021MS002658.

1984 Shroyer, E., and Coauthors, 2021: Bay of Bengal Intraseasonal Oscillation and the 2018
1985 Monsoon Onset. *Bull. Amer. Meteo. Soc.,* **102**, E1936-E1951.
1986 Singleton, A. T., and C. J. C. Reason, 2006: Numerical simulations of a severe rainfall event
1987 over the Eastern Cape coast of South Africa: Sensitivity to sea surface temperature and
1988 topography. *Tellus*, **58A**, 335–367.
1989 Siqueira, L., and B. P. Kirtman, 2016: Atlantic near-term climate variability and the role of a
1990 resolved Gulf Stream. *Geophys. Res. Lett*., **43**, 3964–3972.
1991 Siqueira, L., B. P. Kirtman, and L. C. Laurindo, 2021: Forecasting Remote Atmospheric
1992 Responses to Decadal Kuroshio Stability Transitions. *J. Climate,* **34**, 379–395.
1993 Skyllingstad, E. D., D. Vickers, L. Mahrt, and R. Samelson, 2007: Effects of mesoscale sea-
1994 surface temperature fronts on the marine atmospheric boundary layer. *Boundary-Layer*
1995 *Meteorol,* **123,** 219–237.
1996 Skyllingstad, E. D., and J. B. Edson, 2009: Large-eddy simulation of moist convection during a
1997 cold-air outbreak over the Gulf Stream. *J. Atmos. Sci.,* **66**(5), 1274-1293.
1998 Skyllingstad, E. D., S. P. de Szoeke, and L. W. O'Neill, 2019: Modeling the Transient Response
1999 of Tropical Convection to Mesoscale SST Variations. *J. Atmos. Sci.*, **76**, 1227-1244.
2000 Small, R. J., S.-P. Xie, Y. Wang, S. K. Esbensen, and D. Vickers, 2005a: Numerical Simulation
2001 of Boundary Layer Structure and Cross-Equatorial Flow in the Eastern Pacific. *J. Atmos.*
2002 *Sci.*, **62**(6), 1812-1830.
2003 Small, R. J., S.-P. Xie, and J. Hafner, 2005b: Satellite observations of mesoscale ocean features
2004 and copropagating atmospheric surface fields in the tropical belt. *J. Geophys. Res*., **110**,
2005 C02021.
2006 Small, R. J., S. de Szoeke, S.-P. Xie, L. O'Neill, H. Seo, Q. Song, P. Cornillon, M. Spall, and S.
2007 Minobe, 2008: Air-Sea Interaction over Ocean Fronts and Eddies. *Dyn. Atmos. Oceans*,
2008 **45**, 274-319.
2009 Small, R. J., R. Msadek, Y. Kwon, J. F. Booth, and C. Zarzycki, 2019: Atmosphere surface
2010 storm track response to resolved ocean mesoscale in two sets of global climate model
2011 experiments. *Clim. Dyn.*, **52**, 2067–2089.
2012 Small, R. J, V. Rousseau, R. Parfitt, L. Laurindo, L. O'Neill, R. Masunaga, N. Schneider, and P.
2013 Chang, 2022. Near-surface wind convergence over the Gulf Stream – the role of SST
2014 revisited. Submitted to *J. Climate*.

Smirnov, D., M. Newman, M. A. Alexander, Y.-O. Kwon, and C. Frankignoul, 2015: Investigating the local atmospheric response to a realistic shift in the Oyashio sea surface temperature front. *J. Climate*, **28**, 1126–1147.

Song, H., J. Marshall, P. Gaube, and D. J. McGillicuddy, 2015: Anomalous chlorofluorocarbon uptake by mesoscale eddies in the Drake Passage region. *J. Geophys. Res. Oceans*, **120**, 1065-1078.

Song, H., J. Marshall, M. J. Follows, S. Dutkiewicz and G. Forget, 2016: Source waters for the highly productive Patagonian shelf in the southwestern Atlantic. *J. Mar. Syst*., **158**, 120-128.

Song, Q., P. Cornillon, and T. Hara, 2006: Surface wind response to oceanic fronts. *J. Geophys. Res*., **111**, C12006.

Song, Q., D. B. Chelton, S. K. Esbensen, N. Thum, and L. W. O'Neill, 2009: Coupling between Sea Surface Temperature and Low-Level Winds in Mesoscale Numerical Models. *J. Climate*, **22**, 146-164.

Song, Q., D. B. Chelton, S. K. Esbensen, and A. R. Brown, 2017: An Investigation of the Stability Dependence of SST-Induced Vertical Mixing over the Ocean in the Operational Met Office Model. *J. Climate*, **30**, 91-107.

Song, H., J. Marshall, D. J. McGillicuddy Jr., and H. Seo, 2020: The impact of the current-wind interaction on the vertical processes in the Southern Ocean. *J. Geophys. Res.-Oceans*, **125**, e2020JC016046.

Souza, R., L. Pezzi, S. Swart, F. Oliveira, and M. Santini, 2021: Air-Sea Interactions over Eddies in the Brazil-Malvinas Confluence. *Remote Sens.*, **13**, 1335.

Spall, M. A., 2007a: Midlatitude wind stress-sea surface temperature coupling in the vicinity of oceanic fronts, *J. Climate*, **20**, 3785-3801.

Spall, M. A., 2007b: Effect of sea surface temperature-wind stress coupling on baroclinic instability in the ocean. *J. Phys. Oceanogr*., **37**, 1092-1097.

Sprintall, J., V. J. Coles, K. A. Reed, A. H. Butler, G. R. Foltz, S. G. Penny, and H. Seo, 2020: Best practice strategies for process studies designed to improve climate modeling. *Bull. Amer. Meteor. Soc.*, **101**, E1842–1850.

Stevens, B., and Coauthors, 2003: Dynamics and Chemistry of Marine Stratocumulus – DYCOMS-II. *Bull. Amer. Meteor. Soc*., **84**, 579–594.

2046 Stevens, B., and Coauthors, 2019: DYAMOND: the DYnamics of the Atmospheric general
2047 circulation modeled on non-hydrostatic domains. *Prog. Earth Planet Sci*., **6,** 61.
2048 Stevens, B., and Coauthors, 2021: EUREC4A. *Earth System Science Data*, **13**, 4067-4119.
2049 Stoffelen, A., R. Kumar, J. Zou, V. Karaev, P. S. Chang, and E. Rodriguez, 2019: Ocean Surface
2050 Vector Wind Observations. In: Barale V., Gade M. (eds) Remote Sensing of the Asian
2051 Seas. Springer, Cham. https://doi.org/10.1007/978-3-319-94067-0_24.
2052 Su, Z., and Coauthors, 2018: Ocean submesoscales as a key component of the global heat
2053 budget. *Nat. Commun.,* **9**, 775.
2054 Sugimoto, S., B. Qiu, and N. Schneider, 2021: Local Atmospheric Response to the Kuroshio
2055 Large Meander Path in Summer and Its Remote Influence on the Climate of Japan. *J.*
2056 *Climate*, **34**, 3571-3589. Sullivan, P. P. and J. C. McWilliams, 2010: Dynamics of Winds
2057 and Currents Coupled to Surface Waves. *Annu. Rev. Fluid Mech*., **42**, 19–42.
2058 Sullivan, P., and J. C. McWilliams, 2019: Langmuir turbulence and filament frontogenesis in the
2059 oceanic surface boundary layer. *J. Fluid Mech*., **879**, 512-553.
2060 Sullivan, P. P., J. C. McWilliams, J. C. Weil, E. G. Patton, and H. J. S. Fernando, 2020: Marine
2061 Boundary Layers above Heterogeneous SST: Across-Front Winds. *J. Atmos. Sci*., **77**,
2062 4251-4275.
2063 Sullivan, P. P., J. C. McWilliams, J. C. Weil, E. G. Patton, and H. J. S. Fernando, 2021: Marine
2064 Boundary Layers above Heterogeneous SST: Alongfront Winds. *J. Atmos. Sci*., **78**, 3297-
2065 3315.
2066 Sutton, R. and P. P. Mathieu, 2002: Response of the atmosphere–ocean mixed-layer system to
2067 anomalous ocean heat-flux convergence. Quart. J. Roy. Met. Soc., **128**, 1259-127
2068 Sun, X., and R. Wu, 2022: Spatial scale dependence of the relationship between turbulent surface
2069 heat flux and SST. *Clim. Dyn.,* **58**, 1127-1145.
2070 Suzuki, N., B. Fox-Kemper, P. E. Hamlington, and L. P. Van Roekel, 2016: Surface waves affect
2071 frontogenesis. *J. Geophys. Res. Oceans*, **121**, 1-28.
2072 Sweet, W., R. Fett, J. Kerling, and P. La Violette, 1981: Air-sea interaction effects in the lower
2073 troposphere across the north wall of the Gulf Stream. *Mon. Wea. Rev*., **109**, 1042–1052.
2074 Taguchi, B., S.-P. Xie, N. Schneider, M. Nonaka, H. Sasaki, and Y. Sasai, 2007: Decadal
2075 variability of the Kuroshio Extension: Observations and an eddy-resolving model
2076 hindcast. *J. Climate*, **20**, 2357–2377.

2077 Taguchi, B., H. Nakamura, M. Nonaka, and S.-P. Xie, 2009: Influences of the Kuroshio/Oyashio
2078 Extensions on air–sea heat exchanges and storm-track activity as revealed in regional
2079 atmospheric model simulations for the 2003/04 cold season. *J. Climate*, **22**, 6536–6560.
2080 Taguchi, B., H. Nakamura, M., Nonaka, K. Komori, A. Kuwano-Yoshida, K. Takaya, and A.
2081 Goto, 2012: Seasonal evolutions of atmospheric response to decadal SST anomalies in
2082 the North Pacific subarctic frontal zone: observations and a coupled model simulation. *J.*
2083 *Climate*, **25**, 111–139.
2084 Takahashi, N., T. Hayasaka, B. Qiu, and R. Yamaguchi, 2021, Observed response of marine
2085 boundary layer cloud to the interannual variations of summertime Oyashio extension SST
2086 front, *Clim. Dyn*., **56**, 3511-3526.
2087 Takahashi, N., T. Hayasaka, A. Manda, N. Schneider, 2020: Impact of the Oyashio extension
2088 SST front on synoptic variability of oceanic low-level cloud in summertime based on
2089 WRF numerical simulation. *J. Geophys. Res. Atmos*., **125**, e2020JD032518
2090 Takatama, K., S. Minobe, M. Inatsu, and R. J. Small, 2012: Diagnostics for near-surface wind
2091 convergence/divergence response to the Gulf Stream in a regional atmospheric model.
2092 *Atmos. Sci. Lett*., **13**, 16–21.
2093 Takatama, K., S. Minobe, M. Inatsu, and R. J. Small, 2015: Diagnostics for near-surface wind
2094 response to the Gulf Stream in a regional atmospheric model. *J. Climate*, **28**, 238–255.
2095 Takatama, K., and N. Schneider, 2017: The Role of Back Pressure in the Atmospheric Response
2096 to Surface Stress Induced by the Kuroshio. *J. Atmos. Sci.*, **74**, 597–615.
2097 Thompson, D. W. J., and J. M. Wallace 2000: Annular Modes in the Extratropical Circulation.
2098 Part I: Month-to-Month Variability*, J. Climate*, **13**, 1000-1016.
2099 Thomson, J., 2012: Wave Breaking Dissipation Observed with "SWIFT" Drifters. *J. Atmos.*
2100 *Oceanic Technol*., **29**, 1866-1882.
2101 Thomson, J., and J. Girton, 2017: Sustained measurements of Southern Ocean air-sea coupling
2102 from a Wave Glider autonomous surface vehicle. *Oceanogr.*, **30**, 104–109.
2103 Thum, N., S. K. Esbensen, D. B. Chelton, and M. J. McPhaden, 2002: Air-sea heat exchange
2104 along the northern sea surface temperature front in the eastern tropical Pacific. *J.*
2105 *Climate*, **15**, 3361–3378.

2106 Tokinaga, H., Y. Tanimoto, and S.-P. Xie, 2005: SST-Induced Surface Wind Variations over the
2107 Brazil–Malvinas Confluence: Satellite and In Situ Observations. *J. Climate*, **18**, 3470-
2108 3482.
2109 Tokinaga, H., Y. Tanimoto, S.-P. Xie, T. Sampe, H. Tomita, and H. Ichikawa, 2009: Ocean
2110 Frontal Effects on the Vertical Development of Clouds over the Western North Pacific:
2111 In Situ and Satellite Observations. *J. Climate*, **22**, 4241-4260.
2112 Tozuka T, M. F. Cronin, and H. Tomita, 2017: Surface frontogenesis by surface heat fluxes in
2113 the upstream Kuroshio Extension region. *Sci Rep*., **7**, 10258.
2114 Tozuka, T., S. Ohishi, and M. F. Cronin, 2018: A metric for surface heat flux effect on horizontal
2115 sea surface temperature gradients. *Clim. Dyn*., **51**, 547–561.
2116 Trenberth, K. E., and D. J. Shea, 2005: Relationships between precipitation and surface
2117 temperature. *Geophys. Res. Lett*., **32**, L14703.
2118 Trindade, A., M. Portabella, A. Stoffelen, W. Lin, and A. Verhoef, 2020: ERAstar: A High-
2119 Resolution Ocean Forcing Product. *IEEE Transactions on Geoscience and Remote*
2120 *Sensing*, **58**, 1337–1347.
2121 Trowbridge, J., R. Weller, D. Kelley, E. Dever, A. Plueddemann, J. A. Barth, and O. Kawka,
2122 2019: The Ocean Observatories Initiative. *Front. Mar. Sci.,* **6**, 74.
2123 Tsopouridis, L., C. Spensberger, and T. Spengler, 2021: Cyclone intensification in the Kuroshio
2124 region and its relation to the sea surface temperature front and upper-level forcing. *Quart.*
2125 *J. Roy. Met. Soc*., **147**, 485-500.
2126 Vannière, B., A. C. H. Dacre, and T. Woollings, 2017: A “cold path” for the Gulf Stream–
2127 troposphere connection. *J. Climate*, **30**, 1363–1379.
2128 Vecchi, G. A., S.-P. Xie, and A. S. Fischer, 2004: Ocean-atmosphere covariability in the western
2129 Arabian Sea. *J. Climate*, **17**, 1213-1224.
2130 Verdy, A., and M. R. Mazloff, 2017: A data assimilating model for estimating Southern Ocean
2131 biogeochemistry. *J. Geophys. Res. Oceans*, **122**, 6968– 6988.
2132 Villas Bôas, A. B., O. T. Sato, A. Chaigneau, and G. P. Castelão, 2015: The signature of
2133 mesoscale eddies on the air-sea turbulent heat fluxes in the South Atlantic Ocean.
2134 *Geophys. Res. Lett.*, **42**, 1856–1862.

Villas Bôas, A. B., and Coauthors, 2019: Integrated Observations of Global Surface Winds, Currents, and Waves: Requirements and Challenges for the Next Decade. *Front. Mar. Sci*., **6**, 425.

Villas Bôas, A. B., and W. Young, 2020: Directional diffusion of surface gravity wave action by ocean macroturbulence. *J. Fluid Mech*., **890**, R3.

Villas Bôas, A. B., B. D. Cornuelle, M. R. Mazloff, S. T. Gille, and F. Ardhuin, 2020: Wave–Current Interactions at Meso- and Submesoscales: Insights from Idealized Numerical Simulations. *J. Phys. Oceanogr*., **50**, 3483-3500.

Villas Bôas, A. B., and N. Pizzo, 2021: The geometry, kinematics, and dynamics of the two-way coupling between wind, waves, and currents. *US CLIVAR Variations*, **19**, 18-26.

Wai, M. M., and S. A. Stage, 1989: Dynamical analyses of marine atmospheric boundary layer structure near the Gulf Stream oceanic front. *Quart. J. Roy. Met. Soc.,* **115**, 29–44.

Wallace, J. M., T. P. Mitchell, and C. Deser, 1989: The influence of sea surface temperature on sea surface wind in the eastern equatorial Pacific. Seasonal and interannual variability. *J. Climate*, **2**, 1492–1499.

Wang, Q., J. A. Kalogiros, S. R. Ramp, J. D. Paduan, G. Buzorius, and H. Jonsson, 2011: Wind Stress Curl and Coastal Upwelling in the Area of Monterey Bay Observed during AOSN-II. *J. Phys. Oceanogr*., **41**, 857–877.

Wang, Q., and Coauthors, 2018: CASPER: Coupled Air-Sea Processes and Electromagnetic (EM) ducting Research. *Bull. Amer. Meteor. Soc*., **99**, 1449–1471.

Wanninkhof, R., 1992: Relationship between wind speed and gas exchange over the ocean. *J. Geophys. Res.*, **97**, 7373–7382.

Wanninkhof, R., W. E. Asher, D. T. Ho, C. Sweeney, and W. R. McGillis, 2009: Advances in quantifying air-sea gas exchange and environmental forcing. *Ann. Rev. Mar. Sci.*, **1**, 213–44.

Wanninkhof, R., G. Park, D. B. Chelton, and C. M. Risien, 2011: Impact of Small-Scale Variability on Air-Sea CO_2 Fluxes. In Gas Transfer at Water Surfaces, 2010, edited by S. Komori, W. McGillis, and R. Kurose, 431–44. Kyoto University Press, Kyoto.

Warner, T. T., M. N. Lakhtakia, J. D. Doyle, and R. A. Pearson, 1990: Marine atmospheric boundary layer circulations forced by Gulf Stream sea surface temperature gradients. *Mon. Wea. Rev*., **118**, 309–323.

2166 Weaver, A. J., Coauthors, 2012: Stability of the Atlantic meridional overturning circulation: A
2167 model intercomparison. *Geophys. Res. Lett.*, **39**, L20709.
2168 Wenegrat, J. O., and R. S. Arthur, 2018: Response of the atmospheric boundary layer to
2169 submesoscale sea surface temperature fronts. *Geophys. Res. Lett.*, **45***,* 13,505– 13,512.
2170 Wengel, C., and Coauthors, 2021: Future high-resolution El Niño/Southern Oscillation
2171 dynamics. *Nat. Clim. Chang.* **11**, 758–765.
2172 Willison, J., W. A. Robinson, and G. M. Lackmann, 2013: The Importance of Resolving
2173 Mesoscale Latent Heating in the North Atlantic Storm Track. *J. Atmos. Sci.*, **70**, 2234-
2174 2250.
2175 Wills, S. M., D. W. J. Thompson, and L. M. Ciasto, 2016: On the Observed Relationships
2176 between Variability in Gulf Stream Sea Surface Temperatures and the Atmospheric
2177 Circulation over the North Atlantic. *J. Climate*, **29**, 3719-3730.
2178 Wills, S. M., and D. W. J. Thompson, 2018: On the Observed Relationships between Wintertime
2179 Variability in Kuroshio–Oyashio Extension Sea Surface Temperatures and the
2180 Atmospheric Circulation over the North Pacific. *J. Climate*, **31**, 4669-468.
2181 Wineteer, A., H. S. Torres, and E. Rodriguez, 2020: On the surface current measurement
2182 capabilities of spaceborne Doppler scatterometry. *Geophys. Res. Lett*., **47**,
2183 e2020GL090116.
2184 Winton, M., S. M. Griffies, B. L. Samuels, J. L. Sarmiento, and T. L. Frölicher, 2013:
2185 Connecting Changing Ocean Circulation with Changing Climate. *J. Climate*, **26**, 2268-
2186 2278.
2187 Woolf, D. K., 1993: Bubbles and the air-sea transfer velocity of gases. *Atmosphere-Ocean*, **31**,
2188 517–540.
2189 Woollings, T., J. M. Gregory, J. G. Pinto, M. Reyers, and D. J. Brayshaw, 2012: Response of the
2190 North Atlantic storm track to climate change shaped by ocean-atmosphere coupling. *Nat.*
2191 *Geosci.*, **5**, 313–317.
2192 Wu, L., et al., 2012: Enhanced warming over the global subtropical western boundary currents,
2193 *Nat. Clim. Change*, **2**(3), 161–166.
2194 Wu., R., B. P. Kirtman, and K. Pegion, 2006: Local Air-Sea Relationship in Observations and
2195 Model Simulations. *J. Climate*, **19**, 4914-4932.

Xie, S.-P. 2004: Satellite observations of cool ocean-atmosphere interaction. *Bull. Amer. Meteor. Soc.,* **85**, 195–209.

Xie, T., W. Perrie, and W. Chen, 2010: Gulf Stream thermal fronts detected by synthetic aperture radar. *Geophys. Res. Lett.*, **37**, L06601.

Yang, H., G. Lohmann, W. Wei, M. Dima, M. Ionita, and J. Liu, 2016: Intensification and poleward shift of subtropical western boundary currents in a warming climate. *J. Geophys. Res. Oceans,* **121**, 4928–4945.

Yang, H., and Coauthors, 2020: Poleward shift of the major ocean gyres detected in a warming climate. *Geophys. Res. Lett.,* **47**, e2019GL085868.

Yoda, K., K. Shiomi, and K. Sato, 2014: Foraging spots of streaked shearwaters in relation to ocean surface currents as identified using their drift movements. *Prog. Oceanogr*., **122**, 54–64.

Yu, L., 2019: Global air-sea fluxes of heat, fresh water, and momentum: energy budget closure and unanswered questions. *Ann. Rev. Mar. Sci.*, **11**, 227-248.

Zanna, L., P. G. Porta Mana, J. Anstey, T. David, and T. Bolton, 2017: Scale-Aware Deterministic and Stochastic Parametrizations of Eddy-Mean Flow Interaction. *Ocean Modell.*, **111**, 66-80.